PACIFIC EARTHQUAKE ENGINEERING
RESEARCH CENTER

PEER NGA-East Database

Christine A. Goulet
Tadahiro Kishida
Pacific Earthquake Engineering Research Center

Timothy D. Ancheta
Risk Management Solutions, Newark, California

Chris H. Cramer
Center for Earthquake Research and Information
University of Memphis

Robert B. Darragh
Walter J. Silva
Pacific Engineering and Analysis, Inc.
El Cerrito, California

Youssef M. A. Hashash
Joseph Harmon
University of Illinois, Urbana-Champaign

Jonathan P. Stewart
University of California, Los Angeles

Katie E. Wooddell
Pacific Gas & Electric Company

Robert R. Youngs
AMEC Environment and Infrastructure
Oakland, California

PEER 2014/17
OCTOBER 2014

PEER NGA-East Database

Christine A. Goulet
Tadahiro Kishida
Pacific Earthquake Engineering Research Center

Timothy D. Ancheta
Risk Management Solutions, Newark, California

Chris H. Cramer
Center for Earthquake Research and Information
University of Memphis

Robert B. Darragh
Walter J. Silva
Pacific Engineering and Analysis, Inc.
El Cerrito, California

Youssef M. A. Hashash
Joseph Harmon
University of Illinois, Urbana-Champaign

Jonathan P. Stewart
University of California, Los Angeles

Katie E. Wooddell
Pacific Gas & Electric Company

Robert R. Youngs
AMEC Environment and Infrastructure
Oakland, California

PEER Report 2014/17
Pacific Earthquake Engineering Research Center
Headquarters at the University of California, Berkeley
October 2014

ABSTRACT

This report serves as a documentation of the ground motion database development for the NGA-East Project. The ground motion database includes the two- and three-component ground-motion recordings from numerous selected events (**M** > 2.5, distances up to 1500 km) recorded in the Central and Eastern North America (CENA) region since 1988. The final database contains over 29,000 records from 81 earthquake events and 1379 recording stations. The time series and metadata collected went through numerous rounds of quality assurance and review. The NGA-East database constitutes the largest database of processed recorded ground motions in Stable Continental Regions (SRCs).

The motivation behind the development of the empirical database is the same as for other NGA projects (NGA-West1 and NGA-West2), which is to be used, along with other information and data, for the development of ground motion prediction equations (GMPEs). The NGA-East ground motion database, similar to those from the NGA-West projects, includes pseudo-spectral acceleration (PSA) for the 5%-damped elastic oscillators with periods ranging from 0.01 to 10 sec. The preferred PSA measure used for the NGA-East GMPE development is RotD50, which is also provided for the same period range. Additionally, the NGA-East database includes Fourier amplitude spectral (FAS) of the processed ground motions. The NGA-East database therefore consists of three groups of complementary products: the summary file referred to as the flatfile, which contains metadata, ground motion information and intensity measures on a record-per-record basis, the time series (acceleration, velocity, and displacement), and the corresponding Fourier spectra files.

The primary objective of the database task was to provide the time series, response spectra, and Fourier spectra to the NGA-East GMPE developers. However, the NGA-East time series database will also be made available to the public through the PEER online ground motion tool. This report documents the data collection, processing, and development of data products for the NGA-East database.

ACKNOWLEDGMENTS

This study was sponsored by the Pacific Earthquake Engineering Research center (PEER), as part of the NGA-East research project, and was funded by the U.S. Nuclear Regulatory Commission (NRC), the U.S. Department of Energy (DOE), and the Electric Power Research Institute (EPRI), with the participation of the U.S. Geological Survey (USGS).

Any opinions, findings, and conclusions or recommendations expressed in this material are those of the authors and do not necessarily reflect those of the sponsoring agencies.

In addition to the co-authors of this report, numerous other researchers and practitioners contributed to the development of the NGA-East database. Specific acknowledgements are provided in Section 1.2 for the key sub-tasks documented in the current report.

CONTENTS

ABSTRACT iii

ACKNOWLEDGMENTS v

TABLE OF CONTENTS vii

LIST OF TABLES ix

LIST OF FIGURES xi

1 OVERVIEW OF THE NGA-EAST DATABASE 1

1.1 Motivation for the NGA-East Ground Motion Dataset 1

1.2 Database Team and Report Organization 2

1.2.1 Database Design, Data Selection and Collection (Chapter 2) 2

1.2.2 Time Series Processing (Chapter 3) 3

1.2.3 Development of Earthquake Source Table (Chapter 4) 3

1.2.4 Development of the Station Database (Chapter 5) 3

1.2.5 Development of Final Database Products (Chapter 6) 4

2 DATA COLLECTION 5

2.1 Selection Criteria 5

2.2 Earthquake Events 5

2.3 Time Series 8

3 TIME SERIES PROCESSING 17

3.1 Introduction and Overview 17

3.2 Time Series Pre-Processing 17

3.2.1 Initial Processing Approach 17

3.2.2 Quality Assurance and Updating of Metadata and Time Series 18

3.3 NGA-East Instrument Correction and Alignment 19

3.4 Time Series Processing 21

3.4.1 Inspection for Time Series Acceptance 21

3.4.2 Determination of Time Windows for Data Processing 22

3.4.3 DC (Mean) Removal, Taper, and Fourier Amplitude Spectra 29

3.4.4 Filtering Methodology 32

3.4.5 Baseline Correction 36

3.4.6 Treatment of Microseisms 39

3.4.7 Processing Information Table 40

4 EARTHQUAKE SOURCE TABLE 41
4.1 Organization and Objectives of Earthquake Source Table 41
4.2 Finite Fault Models 41
4.3 Earthquake Source Parameters 43
4.4 Method of Simulating a Finite Fault Geometry 44
4.5 Event Classification: Class 1 versus Class 2 45
4.5.1 Methodology 46
4.6 Event Classification: Potentially-Induced Events 47
5 NGA-EAST STATION DATABASE, V_{S30} ASSIGNMENT 49
5.1 Introduction and Scope of Station Database (STDB) 49
5.2 Station Metadata 50
5.3 Data Sources and Distribution of V_{S30} 50
5.4 Proxy-Based Estimation of V_{S30} 52
5.4.1 Available Proxies 52
5.4.2 Proxy Evaluation 52
5.5 Preferred V_{S30} and Its Uncertainty 54
5.5.1 Method of Selecting Preferred V_{S30} 54
5.5.2 V_{S30} Uncertainty 57
5.5.2.1 Code 0 sites (sites with geophysical measurement of V_{S30}) 57
5.5.2.2 Code 1 sites 57
5.5.2.3 Code 2 and 3 sites 58
5.5.2.4 Code 4 and 5 sites 58
6 DATABASE FLATFILE AND GROUND MOTION PRODUCTS 59
6.1 Overview of Flatfile Components and Organization 59
6.2 Summary of Selected Intensity Measures 60
6.2.1 Rotdnn 60
6.2.2 Duration 61
7 REFERENCES 63
APPENDIX A: EARTHQUAKE SOURCE TABLE 67
APPENDIX B: STATION DATABASE 83
APPENDIX C: FLATFILE FOR 5%-DAMPED PSA 85

LIST OF TABLES

Table 2.1 Earthquakes considered for inclusion in the NGA-East ground motion database. 6

Table 2.2 Data per network. 13

Table 3.1 Table of record quality codes used in the initial NGA-East flat files. 19

Table 3.2 Source duration ($T_{d\text{-}source}$) versus moment magnitude. 26

Table 3.3 Cosine taper length applied to windowed accelerations. 29

Table 3.4 Minimum frequency for FAS calculation. 30

Table 4.1 Available finite fault models for earthquakes in NGA-East. 42

Table 4.2 Earthquakes in NGA-East with M estimated using relationships from NUREG-2115. 43

Table 4.3 Summary of assumed probabilistic distributions of parameters used in finite fault simulation procedure. 45

Table 5.1 Sources of geophysical data for CENA stations. 51

Table 5.2 Relative proxy weights by region and applied weights for estimation of V_{S30} when all estimates are available (Code 4). 56

Table 5.3 Relative proxy weights by region and applied weights for estimation of V_{S30} when no estimate by *P*-wave proxy is available (Code 5). 56

LIST OF FIGURES

Figure 2.1 Central and Eastern North America earthquakes selected for inclusion in the NGA-East ground motion database. The 1929 Grand Banks and 1985 Nahanni earthquakes are off this map and hence not shown. 9

Figure 2.2 Seismograph and accelerograph stations with at least one record in the NGA-East ground motion database. Some station coverage extends beyond the borders of this map. 10

Figure 2.3 Magnitude versus distance coverage of recordings in the NGA-East ground motion database. 11

Figure 3.1 Example of time-aligned three component time series that had been truncated during original processing. The top plot shows the as-is, instrument-corrected acceleration trace and the bottom plot shows the time-aligned components. Colored vertical lines with symbols show the origin time (black), first arrival (magenta) and the end of each time series (horizontals are blue and red, vertical is green). In the example above, the pre-event noise for the vertical and the East components had been cut short relative to the North component (top plot). This is corrected in the bottom plot. 21

Figure 3.2 Example of time series rejected based on visual inspection. 22

Figure 3.3 Schematic drawing of the six time windows used. 23

Figure 3.4 Selection of P-wave arrival time. 24

Figure 3.5 Acceleration and displacement time series and calculated arrival times (horizontal axis is time, in seconds). 25

Figure 3.6 Relationship between *Lg*-wave travel time and distance [Chapman 2013]. 27

Figure 3.7 Relationship between *Lg*-wave travel time and distance, selected model. The lower line corresponds to the mean model from Chapman [2013] and the top line is the model used for NGA-East (twice the lower line). 27

Figure 3.8 Determination of Coda time window. 28

Figure 3.9 Example Fourier amplitude spectra from acceleration time series for different windows. 31

Figure 3.10 Time domain response of acausally filtered impulse signal. 33

Figure 3.11 Fourier Amplitude Spectra for acausally filtered impulse signal. 33

Figure 3.12 Fourier Phase Spectra for acausally filtered impulse signal. 34

Figure 3.13 Time domain response of causally filtered impulse signal. 35

Figure 3.14 Fourier Amplitude Spectra for causally filtered impulse signal. 35

Figure 3.15 Fourier Phase Spectra for causally filtered impulse signal. 35

Figure 3.16 Time series of acausally filtered pad-stripped record. Shown are (a) acceleration (b) velocity, and (c) displacement time series. The initial velocity and displacement are assumed to be zero in the integration. 37
Figure 3.17 Time series of acausally filtered record with zero padding. Shown are the (a) acceleration and (b) velocity time series. 37
Figure 3.18 Acausally filtered time series with baseline correction. Shown are (a) acceleration, (b) velocity, and (c) displacement time series 38
Figure 3.19 Effect of baseline correction on PSA for acausally filtered time series. 38
Figure 3.20 FAS affected by microseisms. 39
Figure 3.21 Acceleration, velocity, and displacement time series 40

Figure 4.1 Schematic representation of strike, dip, rake, depth to top of rupture (Z_{TOR}), down dip width (W), and length (L).....42
Figure 4.2 Definitions of the CRJB distance metrics. 46

Figure 5.1 Histogram of V_{S30} measurements in the NGA-East station database.....51
Figure 5.2 Residual of proxy-based estimations at sites where available for (a) geology [Kottke et al. 2012], (b) terrain [Yong et al. 2012], (c) slope [Wald and Allen 2007, (d) *P*-wave seismogram with multiple estimates [Kim et al. 2014], and (e) hybrid slope-geology [Thompson and Silva 2013]. 53
Figure 5.3 Average residual and standard deviation on the residual for Geology [Kottke et al. 2012], Terrain [Yong et al. 2012], Slope [Wald and Allen 2007], Hybrid [Thompson and Silva 2013] and *P*-wave [Kim et al. 2014], of V_{S30} estimates by proxy at recording stations. Circles represent the residual on the V_{S30} at the 34 recording stations that have estimates of V_{S30} by all proxy methods. Triangles represent the residual on the V_{S30} over all stations where the proxy-based estimate is available. 54
Figure 5.4 Distribution of code assignment for recommendation of V_{S30}. 56
Figure 5.5 Recommended V_{S30} and $\sigma \ln_V$ by from Codes 0–5 assignment at all stations.....57

1 Overview of the NGA-East Database

1.1 MOTIVATION FOR THE NGA-EAST GROUND MOTION DATASET

As part of its Next Generation Attenuation (NGA) research program, the Pacific Earthquake Engineering Research Center (PEER) has been leading the development of multiple ground motion prediction equations (GMPEs). The first NGA project was initiated in 2003 and led to the development of the first set of GMPEs for active tectonic regions (ATRs) [Power et al. 2008. That project, now referred to as NGA-West1, was followed by NGA-West2, which was completed in early 2014 [Bozorgnia et al. 2014]. A major component of these two projects was the development of large, high-quality datasets of recorded earthquake ground motions. The databases also include very rich metadata associated with the ground motions. This combination of carefully processed, high-quality records with metadata into a single repository serves as an essential building block for GMPE development.

The NGA-East Project was initiated in 2010, building on the experience of the previous two NGA-West Projects. NGA-East is focused on development of GMPEs for the large region referred to as Central and Eastern North America (CENA), a region that includes most of the U.S. and Canada, from the Rockies to the Atlantic Ocean. As was done for the other NGA projects, one of the first key tasks was to develop a high-quality empirical ground motion database. The main objective for NGA-East was to develop GMPEs and associated logic trees for horizontal ground motions. Therefore, the current database report focuses on recordings that have at least two horizontal components. If a third vertical component was available, it was also processed, but single vertical records are currently not included in the initial release of database products.

Data challenges for stable continental regions (SCRs) such as CENA are different from those of ATRs. The data are more sparse, both in magnitude and distance, compared to those of ATRs and are generally of lower amplitudes, requiring different thresholds for an acceptable range of signal-to-noise ratio. The low attenuation rate in SCRs also requires longer durations to fully capture the motions until the end of the Coda waves. Under the auspices of the Pacific Earthquake Engineering Research Center (PEER) and its long established history of collecting and processing data, the NGA-East Project addressed those issues early on and made the required adjustments to develop the database.

The NGA-East Project is also unique in that GMPEs were developed using two different approaches, which required additional data products. The first approach, consistent with what was carried out in the NGA-West Projects, was to develop models mostly based on recorded pseudo-spectral acceleration (PSA). The second approach involved the initial development of

GMPEs in the Fourier amplitude spectral (FAS) space. A discussion of this approach is beyond the scope of the current report, but is mentioned here to justify the choice of database products developed for the project. A more detailed discussion of this methodology will be published next year.

The NGA-East database consists of three groups of complementary products: the summary file referred to as the flatfile, which contains metadata, ground motion information, and intensity measures on a record-per-record basis, the time series (acceleration, velocity, and displacement), and the corresponding Fourier spectra files. This report documents the data collection, processing, and development of data products for the NGA-East database.

1.2 DATABASE TEAM AND REPORT ORGANIZATION

The development of the NGA-East ground motion database involved a number of complementary tasks completed by various groups of researchers and contributors. The extensive list of authors for this report reflects the considerable effort that the development of such a database requires. Key tasks are summarized below with a list of their key contributors:

1.2.1 Database Design, Data Selection, and Collection (Chapter 2)

A team led by Professor Chris Cramer from the Center for Earthquake Research and Information (CERI) at the University of Memphis was in charge of the initial database development. As part of a pre-NGA-East effort in 2007–2009, the U.S. Nuclear Regulatory Commission (NRC) funded a two-year initial development of a CENA database of ground motions similar to the NGA-West-1 strong-motion database. This initial effort focused on database design and collection of appropriate CENA broadband and accelerograph records from earthquakes of moment magnitude (**M**) 4 and larger to populate the database. An additional two-year effort was funded as part of NGA-East to complete the data collection and pre-processing of the database. Data selection criteria were developed under the leadership of the NGA-East Database Working Group. Extensive quality assurance measures and reviews were conducted both during and after the assembling of the database. The design and formats of the database products are discussed in Cramer [2008] and Cramer et al. [2011]. The design of the NGA-East file system employed at CERI for data collection and processing is hierarchical and based on earthquake, station, and record table; see Cramer et al. [2013] for details. Four key products from the group form the basis of the NGA-East database: the earthquake source table, the station table and the record table (referred-to as the initial flatfile), and the recorded time series. All those products were initially developed by the CERI team and further modified by several NGA-East contributors, as summarized in the following sections.

- CERI team: Jerome R. Kutliroff, Donny T. Dangkua, and Md. Nayeem Al Noman.
- NGA-East Database Working Group: Charles Mueller (Chair) and David Boore (USGS), Kenneth Campbell (EQECAT, Inc.), Chris Cramer (University of Memphis, CERI), Robert Herrmann (Saint Louis University) and Walt Silva (Pacific Engineering and Analysis, Inc.). John Adams (Geological Survey of Canada), and Gabriel Toro (Lettis Consultants International, Inc.) were also members of the

Working Group in the 2009–2011 period and provided essential contributions and support.

1.2.2 Time Series Processing (Chapter 3)

Time series were initially processed by the CERI team (above), as documented in Cramer et al. [2013]. However, the NGA-East project required additional products, necessitating the re-processing of the time series. For example the FAS for specific windows (for noise, *P*-, *S*-, *Lg*- and Coda wave) need to be extracted at the processing stage. The collection of these data is optimal when working with instrument-corrected time series rather than with raw time series. The CERI team shared the collected raw time series and their processing package (codes and workflow) for computing instrument-corrected time series. Christine Goulet (PEER) produced the instrument-corrected time series in ASCII format for use by the NGA-East processing team.

A team led by Tadahiro Kishida (PEER) was in charge of reprocessing the instrument-corrected time series. The team built on software developed for the NGA-West2 database [Ancheta et al. 2014] and included additional computational capabilities to address NGA-East's specific data needs. Numerous contributors were instrumental in the success of this task: Robert Darragh and Walt Silva (Pacific Engineering and Analysis, Inc.), Tim Ancheta (RMS), Olga-Joan Ktenidou (PEER and ISTerre, Grenoble), Albert Kottke (Bechtel), David Boore (USGS), Brian Chiou (CalTrans), as well as Dan Assouline, Claudia Bongiovanni, Sahar Derakhshan, Tomoyuki Inoue, Imad El Khoury, and Sifat Muin (PEER).

1.2.3 Development of Earthquake Source Table (Chapter 4)

The initial earthquake source table developed by the CERI team was reviewed and modified by the EPRI [2013] project team. The final NGA-East source table includes those modifications, but it was further developed and documented by Robert Youngs (AMEC). The earthquake source table contains alternative moment tensor solutions along with a set of preferred ones if such a judgment could be made from the literature review. Annemarie Baltay (USGS) completed an independent review of the source parameters and provided feedback and comments to NGA-East. Additional information on potentially induced events was provided by Justin Rubinstein and Charles Mueller (USGS), and included the source table.

1.2.4 Development of the Station Database (Chapter 5)

The initial station information table developed by the CERI team was used as the basis for the station database (version 2013-02-28). While the Geotechnical Working Group (GWG) gathered site condition information, Charles Mueller (USGS) and Christine Goulet (PEER) reviewed the existing metadata and collected additional information on instruments location and housing/foundation. The new information came from various sources, including reports, papers, and personal communications with numerous individuals (see Appendix B). John Adams and Maurice Lamontagne (Geological Survey of Canada) and Gail Atkinson (Western University) were also instrumental in collecting supplemental information for the Canadian stations. The station information was then merged for co-located instruments (Section 5.1) and combined with

the site conditions collected by the GWG. This new station database was shared within the project in April 2014.

The members of the NGA-East Geotechnical Working Group include: Youssef Hashash (Chair) and Joseph Harmon (University of Illinois Urbana-Champaign, UIUC), Jonathan Stewart (UCLA), Albert Kottke (formerly with PEER and now with Bechtel), Byungmin Kim (formerly with UIUC and currently with RMS), Walt Silva (Pacific Engineering and Analysis, Inc.), Ellen Rathje (U. Texas, Austin), and Kenneth Campbell (EQECAT, Inc.).

Alan Yong, David Wald, and Vince Quitoriano (USGS), Eric Thompson (UCSD), and Lian Fan (UIUC) also helped substantially at various stages in the station database development.

1.2.5 Development of Final Database Products (Chapter 6)

The final NGA-East database products were developed by the same group of people involved in data collection and time series processing (Sections 1.2.1 and 1.2.2). One key product is a flatfile gathering source, site, and path metadata, relevant processing information, and ground motion intensity measures. Additional products include individual files for processed time series of acceleration, velocity, and displacement, as well as acceleration Fourier spectral information. The latter is a new product relative to previous NGA-West and NGA-West2 database releases.

2 Data Collection

2.1 SELECTION CRITERIA

Data selection criteria were developed by the NGA-East Database Working Group documented in Cramer [2008] and Cramer et al. [2011]. The criteria are to include all **M**4+ earthquakes and add selected well-recorded **M** ≥ ~2.5 earthquakes with five or more records within 100 km. The five or more records within 100 km rule for **M** < 4 earthquakes is to avoid selecting smaller earthquakes with too few records for GMPE development and to focus on selecting earthquakes with more important records at distances less than 100 km. Due to recording station coverage, effectively these criteria apply to CENA earthquakes from 1988 onwards, with the bulk of the records comprising earthquakes since 2000.

2.2 EARTHQUAKE EVENTS

Table 2.1 lists the earthquakes selected for inclusion in the NGA-East ground motion database. The 1982 Miramichi and 1985 Nahanni strong-motion records have also been included, in addition to those meeting the selection criteria since 1988. Also, key large magnitude data from CENA and analogous regions have been included, namely the 1925 Charlevoix, 1929 Grand Banks, 1935 Timiskaming, 1944 Cornwall-Massena, 1976 Gazli, and 2001 Bhuj earthquakes. All earthquakes were assigned a unique integer number (EQID). Fortunately, recording station density has increased significantly in the last decade, and several recent **M**>4 earthquakes have been better recorded. The EarthScope USArray (TA) has significantly contributed to the better recording of these recent earthquakes. However, not all the all **M**4+ CENA earthquakes have been included due to poor station coverage (the Teresa, Mexico, earthquake, for example), leading to gaps in the EQID sequence after events were rejected. It is believed that the NGA-East ground motion database represents well the source regions in CENA. Event names that include the event location (or a short-hand of it) and the date have been used to organize all the data into event-specific folders (e.g., CapRouge97-11-06).

Table 2.1 Earthquakes considered for inclusion in the NGA-East ground motion database.

EQID	Earthquake	Location	M
1	Charlevoix_1925-03-01	Charlevoix QC	6.43
2	GrandBanks_1929-11-18	Grand Banks NL	7.25
3	Temiskaming_1935-11-01	Timiskaming QC	6.21
4	CornwallMassena_1944-09-05	Cornwall Massena ON	5.79
5	Saguenay_1988-11-25	Saguenay QC	5.85
6	LaMalbaie_1997-08-20	La Malbaie QC	3.27
7	LaMalbaie_1997-10-28	La Malbaie QC	4.29
8	CapRouge_1997-11-06	Cap-Rouge QC	4.45
9	CoteNord_1999-03-16	Cote-Nord QC	4.43
10	Kipawa_2000-01-01	Kipawa QC	4.62
11	LaMalbaie_2000-06-15	La Malbaie QC	3.29
12	Laurentide_2000-07-12	Laurentide QC	3.65
13	Laurentide_2000-07-12A	Laurentide QC	3.11
14	Ashtabula_2001-01-26	Ashtabula OH	3.85
15	Enola_2001-05-04	Enola AR	4.37
16	AuSableForks_2002-04-20	Au Sable Forks NY	4.99
17	LacLaratelle_2002-06-05	Lac Laratelle QC	3.81
18	Caborn_2002-06-18	Caborn IN	4.55
19	Boyd_2002-11-03	Boyd NE	4.18
20	Charleston_2002-11-11	Charleston SC	4.03
21	FtPayne_2003-04-29	Ft Payne AL	4.62
22	Blytheville_2003-04-30	Blytheville AR	3.60
23	Bardwell_2003-06-06	Bardwell KY	4.05
24	LaMalbaie_2003-06-13	La Malbaie QC	3.53
25	BarkLake_2003-10-12	Bark Lake QC	3.82
26	Jefferson_2003-12-09	Jefferson VA	4.25
27	StTeresa_2004-04-06	St Teresa MX	4.31
28	LaBaie_2004-05-04	La Baie QC	2.87
29	PrairieCntr_2004-06-28	Prairie Center IL	4.18
30	PortHope_2004-08-04	Port Hope ON	3.12
31	MilliganRdg_2005-02-10	Milligan Ridge AR	4.14
32	RiviereDuLoup_2005-03-06	Riviere Du Loup QC	4.65
33	ShadyGrove_2005-05-01	Shady Grove AR	4.25
34	Miston_2005-06-02	Miston TN	4.01
35	Thurso_2006-02-25	Thurso ON	3.70
36	Hawkesbury_2006-02-26	Hawkesbury ON	2.59
37	BaieStPaul_2006-04-07	Baie Saint Paul QC	3.72
38	Ridgely_2006-09-07	Ridgely TN	3.35
39	GulfMexico_2006-09-10	Gulf of Mexico	5.85

EQID	Earthquake	Location	M
40	Acadia_2006-10-03	Acadia ME	3.87
41	Marston_2006-10-18	Marston MO	3.41
42	Marvin_2006-11-02	Marvin VA	4.00
43	Skeggs_2006-11-23	Skeggs VA	4.00
44	Cobourg_2007-07-19	Cobourg ON	2.80
45	BaieStPaul_2008-01-03	Baie Saint Paul QC	2.77
46	MtCarmel_2008-04-18	Mt Carmel IL	5.30
47	MtCarmel_2008-04-18a	Mt Carmel IL	4.64
48	MtCarmel_2008-04-21	Mt Carmel IL	4.03
49	MtCarmel_2008-04-25	Mt Carmel IL	3.75
50	Buckingham_2008-06-11	Buckingham QC	2.97
51	RiviereDuLoup_2008-11-15	Riviere Du Loup QC	3.57
52	PineForest_2008-12-16	Pine Forest SC	3.16
53	RoseHill_2009-01-29	Rosehill SC	2.77
54	Palmetto_2009-05-06	Palmetto SC	2.18
55	ConstanceBay_2009-05-08	Constance Bay ON	2.57
56	Jones_2010-01-15	Jones OK	3.84
57	Lincoln_2010-02-27	Lincoln OK	4.18
58	Whiting_2010-03-02	Whiting MO	3.40
59	Lebanon_2010-05-21	Lebanon IL	2.62
60	ValDesBois_2010-06-23	Val-des-Bois QC	5.10
61	StFlavien_2010-07-23	St. Flavien QC	3.51
62	Buhj_2001-01-26	Bhuj India	7.60
63	MontLaurier_1990-10-19	Mont Laurier QC	4.47
64	Montgomery_2010-07-16	Montgomery MD	3.42
65	Gazli_1976-05-17	Gazli USSR	6.80
66	Slaughterville_2010-10-13	Slaughterville OK	4.36
67	Guy_2010-10-15	Guy AR	3.86
68	Concord_2010-09-26	Concord NH	3.05
69	Nahanni_1985-11-09	Nahanni NWT	4.40
70	Nahanni_1985-12-23	Nahanni NWT	6.76
71	Nahanni_1985-12-23a	Nahanni NWT	5.10
72	Nahanni_1985-12-25	Nahanni NWT	5.15
73	Arcadia_2010-11-24	Arcadia OK	3.96
74	BethelAcres_2010-12-12	Bethel Acres OK	3.23
75	Greentown_2010-12-30	Greentown IN	3.85
76	Guy_2010-11-20	Guy AR	3.90
77	Greenbrier_2011-02-17	Greenbrier AR	3.83
78	Greenbrier_2011-02-18	Greenbrier AR	3.91
79	Greenbrier_2011-02-18a	Greenbrier AR	4.10
80	Greenbrier_2011-02-28	Greenbrier AR	4.68

EQID	Earthquake	Location	M
81	Sullivan_2011-06-07	Sullivan MO	3.89
82	EagleLake_2006-07-14	Eagle Lake ME	3.46
83	ValDesBois_2010-06-24	Val-des-Bois QC	2.57
84	ValDesBois_2010-07-22	Val-des-Bois QC	2.37
85	Hawkesbury_2011-03-16	Hawkesbury ON	3.59
86	Charlevoix_2001-05-22	Charlevoix QC	3.60
87	BaieStPaul_2002-08-17	Baie Saint Paul QC	3.24
88	Mineral_2011-08-23	Mineral VA	5.74
89	Mineral_2011-08-25	Mineral VA	3.97
90	Sparks_2011-11-05	Sparks OK	4.73
91	Sparks_2011-11-06	Sparks OK	5.68
92	Comal_2011-10-20	Comal TX	4.71
93	Miramichi_1982-03-31	Miramichi NB	4.46
94	Miramichi_1982-05-06	Miramichi NB	3.55
116	Saguenay_1988-11-23	Saguenay	4.19
117	Saguenay_1988-11-26	Saguenay	3.53

2.3 TIME SERIES

A total of 30,167 horizontal (H) and vertical (V) component records (19,817 H, 10,358 V) from 89 CENA **M** $\geq$2.5 earthquakes (Figure 1.1) from 1925 through 2011 were collected and prepared (instrument response removed, initial filtering to acceptable-signal band, quality assurance, etc.) for the database. This includes records from the April 18, 2008, **M**5.2 Mt. Carmel, Illinois, mainshock and three **M**4 aftershocks, the February 28, 2011, **M**4.7 Greenbrier, Arkansas, earthquake, the August 23, 2011, **M**5.7 Mineral, Virginia, mainshock and largest aftershock, and the November 6, 2011, **M**5.6 Sparks, Oklahoma, mainshock and foreshock. Also an accelerograph recording of the May 17, 1976, **M**6.8 Gazli, USSR, earthquake and engineering seismoscope observations for the January 26, 2001 **M**7.6 Bhuj, India, earthquake have been included in the NGA-East ground motion database. The Geologic Survey of Canada (GSC) strong-motion recordings, previously not available, have also been added as they became available through funding from the NGA-East project. In particular, broadband station coverage has improved greatly in the last decade and, more recently, the EarthScope Transportable USArray traversing the U.S. has added significantly to the density of observations in CENA (Figure 1.2). The additional earthquakes since 2000 increase the number of ground motion recordings in the 10–100 km range (Figure 1.3), particularly from the Mt. Carmel events, the 2005 **M**5.0 Rivière-du-Loup, Québec, Canada, earthquake, and the Arkansas and Virginia events. Records from soil sites (V_{S30} < 1500 m/sec) have also been added to the database, which are needed for developing V_{S30} scaling term in NGA-East GMPEs. Available source (location, magnitude, focal mechanism, etc.) and site (geology, V_S profile, V_{S30}, etc.) information has been gathered as part of this effort and included in the ground motion database. The information was grouped into three tables: the initial record catalog, the earthquake source database, and the station database. The record table is used as the basis for the development of the final project

flatfile. The other two tables have been revised over time and are discussed in detail in Chapters 4 and 5.

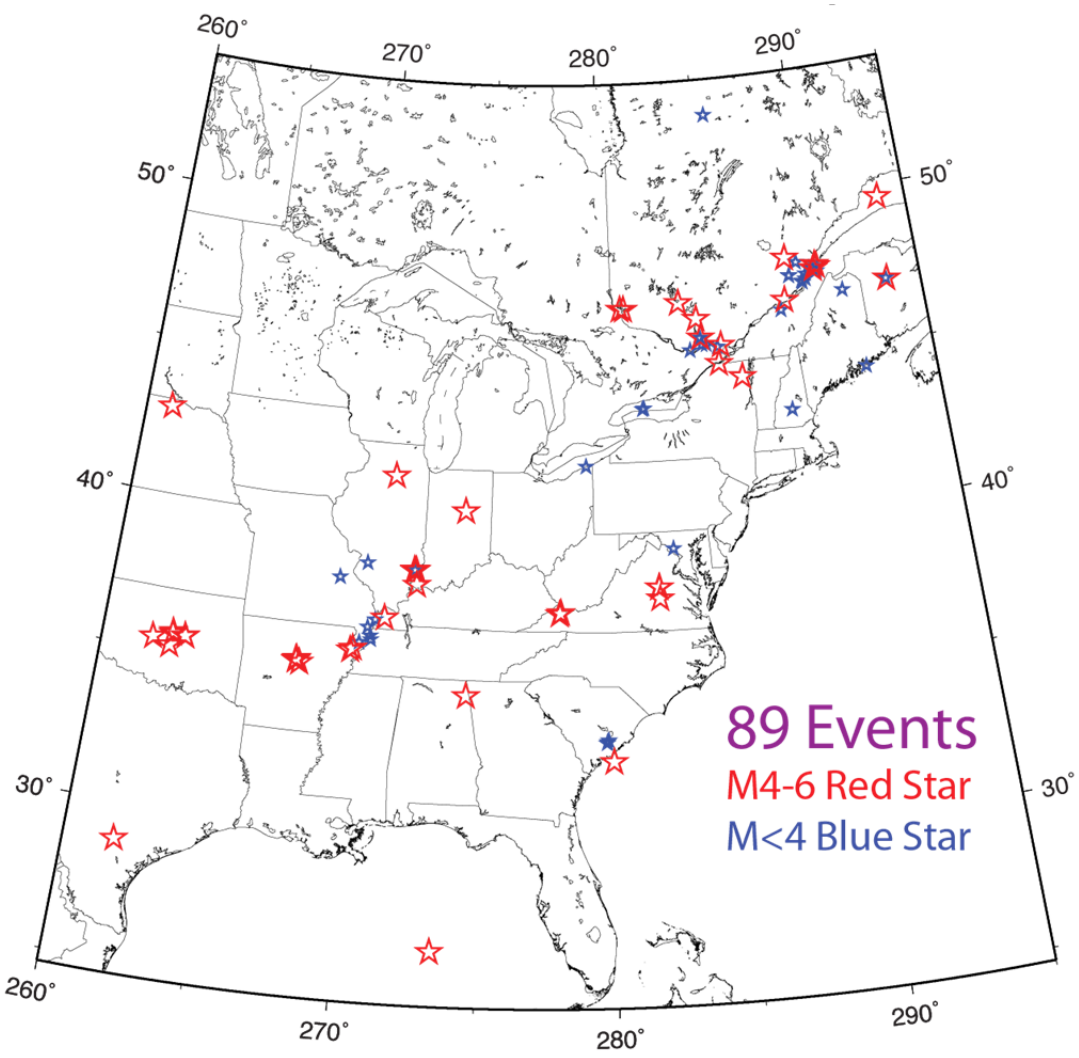

Figure 2.1 **Central and Eastern North America earthquakes selected for inclusion in the NGA-East ground motion database. The 1929 Grand Banks and 1985 Nahanni earthquakes are off this map and hence not shown.**

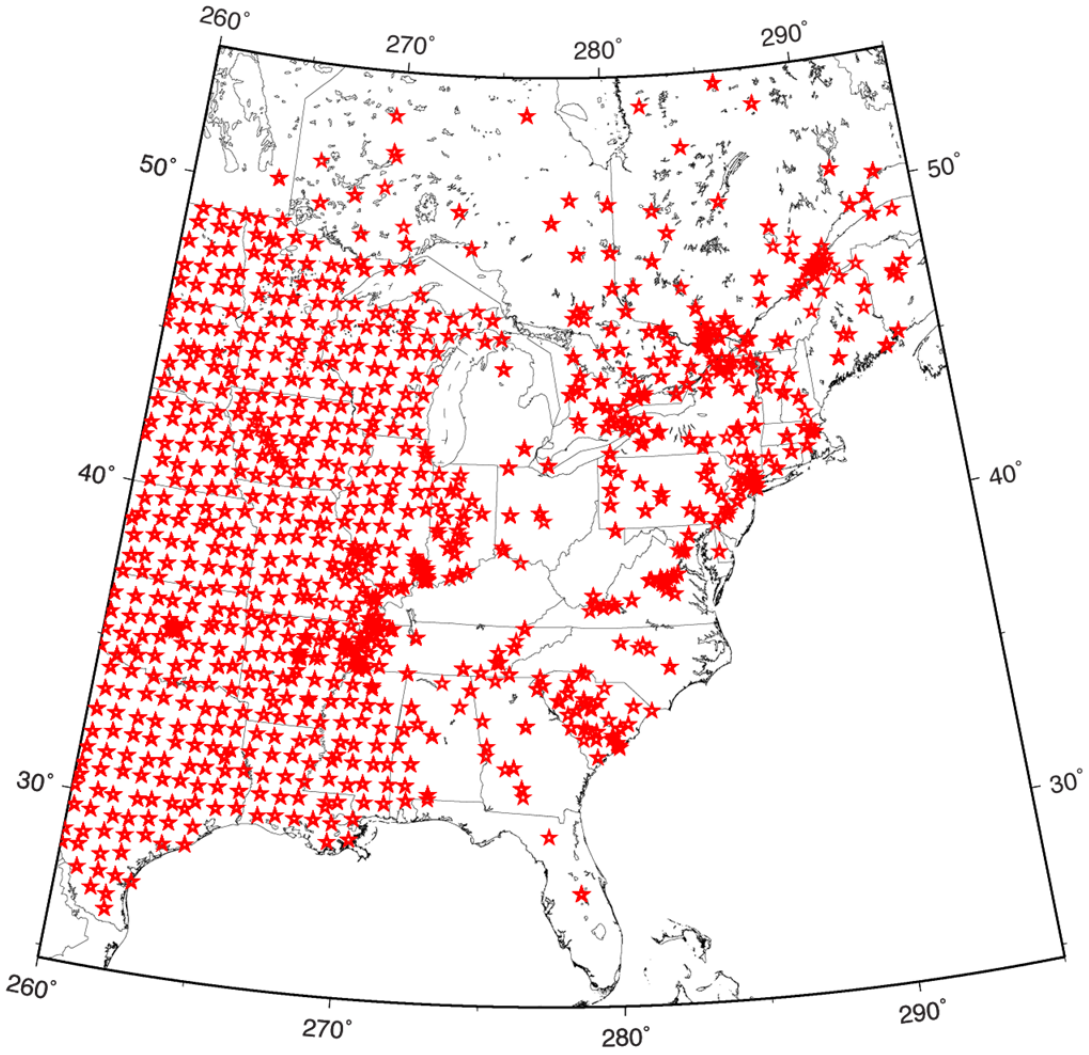

Figure 2.2 **Seismograph and accelerograph stations with at least one record in the NGA-East ground motion database. Some station coverage extends beyond the borders of this map.**

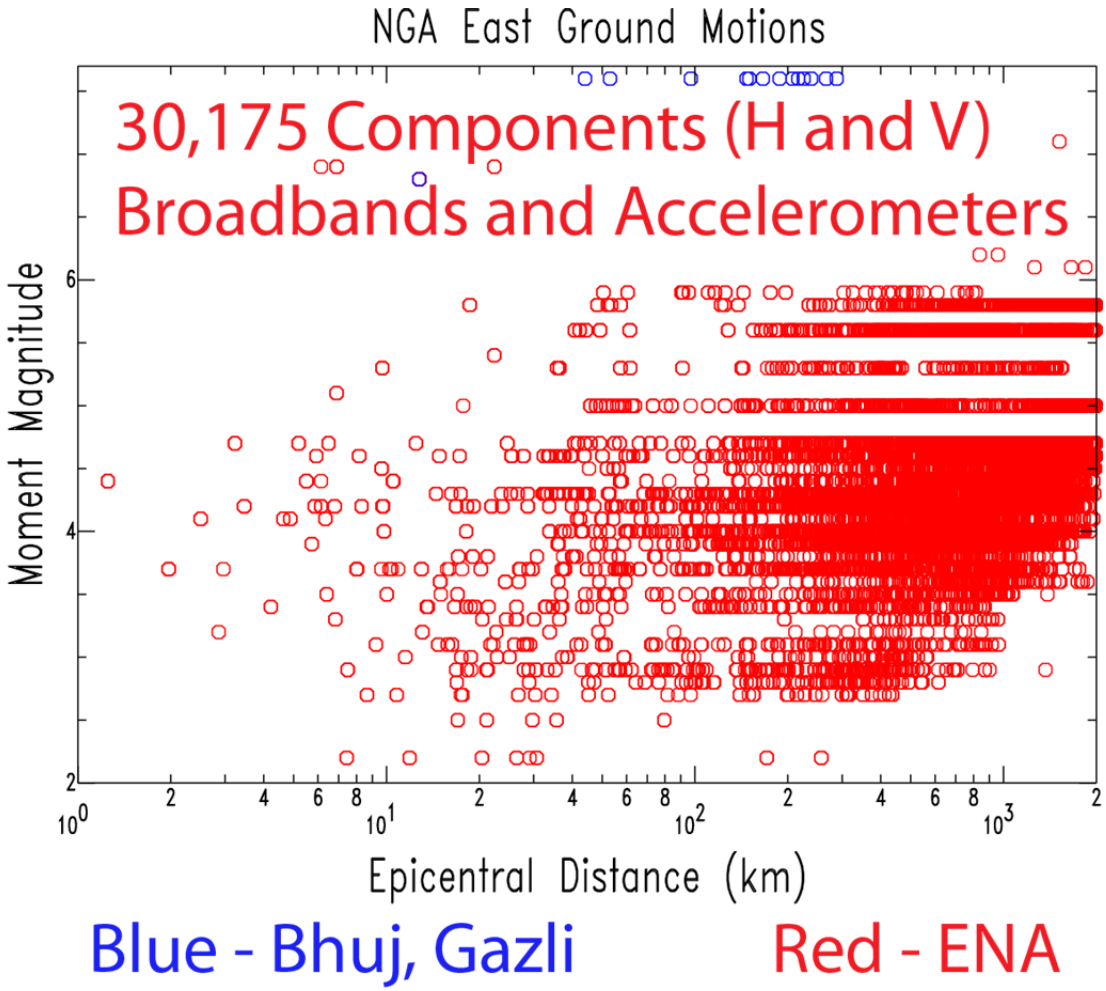

Figure 2.3 **Magnitude versus distance coverage of recordings in the NGA-East ground motion database.**

The broadband and accelerometer records were assembled from several sources: IRIS Data Center (IRIS), Canadian National Data Center (CNDC), the Geological Survey of Canada (GSC), the Center for Earthquake Research and Information (CERI), St. Louis University Earthquake Center (SLU), the U.S. Geological Survey's Advanced National Seismic System (USGS ANSS), Lamont Doherty Cooperative Network (LDCN), Virginia Polytechnic Institute's Southeast Network, Weston Observatory's Northeast Network, Hydro Québec (HQ), NetQuakes, and Quake Catchers. Also included in the database are hand-digitized records for long period only from four pre-1950 large magnitude CENA earthquakes [Atkinson and Chen 1997, spectral acceleration data from the 2001 **M**7.6 Bhuj, India earthquake [Cramer and Kumar 2003, and a close-in accelerometer record from the 1976 **M**6.8 Gazli, USSR earthquake.

The naming convention for files in the NGA-East database follows the IRIS convention, which is based on the station identifier of the downloaded data. The form of the station identifier is NN.SSS.IIO.AA. NN is the network identifier (see Table 1.2), SSS is a 3–5 character unique station id for that network, and II is a two-letter code for the instrument type. O is the instrument orientation (generally E, N, or Z for East, North, and Vertical). And AA is a two-character designator among different instruments at the same station (which is sometimes optional if only

one recording instrument is present; these usually comprise datasets from older earthquakes). An AA of 00 (zero zero) is usually the same instrument as earlier records from a given station without the optional designation.

Table 2.1 lists details of the data sources by network. Included are network name, network owner/manager, data source, data type, and instrumentation information. The table is organized alphabetically by two-letter network code associated with the data files. The network name and owner/manager columns list this information as provided by the IRIS Network Codes website. The actual source (data source) we accessed to receive the data files for each network is also listed, as some data did not come directly from the owner/manager with the most common acronyms defined in Section 2.3. The other sources are spelled out. Under the Data Type column, V is for velocity (broadband or short period), and A is for acceleration (strong motion). As to data format, SAC is for SAC files, SEED for SEED files (read using RDSEED from IRIS), MiniSeed for MiniSeed files, and ASCII files for text format files (specific to the provider). Instrument Type codes are the standard codes from the IRIS SEED manual. The first letter is the band code (B – broadband, H – high-gain broadband, E – Extremely Short Period, and S – Short Period). The second letter is an instrument code (H – high-gain seismometer, L – low-gain seismometer, and N – accelerometer). The third symbol or letter is the orientation code (Z – vertical, N – north, E – East, and dash for all three). The last two columns are Time Interval and Sampling Frequency, and are related (one the inverse of the other). Records that were already instrument corrected are flagged with an asterisk after the instrument type under the Instrument Type column.

Table 2.2 Data per network.

Network Code	Network Name	Network Owner/Manager	Data Source	Data type	Data Format	Instrument Type	Time Interval (sec)	Sampling Frequency (Hz)
AG	Arkansas Seismic Network	Arkansas Geological Survey/CERI	CERI, IRIS	V,A	SAC, SEED	HH-/HN-	0.01	100
AO	Arkansas Seismic Observatory	University of Arkansas at Little Rock	CERI	V,A	SAC	HH-.00, HN-.10	0.01	100
CN	Canadian National Seismic Network	Geological Survey of Canada	CNDC, IRIS, GSC	V,A	SEED, ASCII Files	BH-, HH-, HN- *, EHZ, SHZ	0.025, 0.01, 0.005, 0.01, 0.0166	40, 100, 200, 100, 60
CO	South Carolina Seismic Network	University of South Carolina, Columbia	IRIS	V	SEED	BH-/HH-	0.01	100
EP	UTEP Seismic Network	University of Texas, El Paso	IRIS	V	SEED	BH-	0.025	40
ET	CERI Southern Appalachian Seismic Network	CERI, University of Memphis	CERI, IRIS	V,A	SEED, SAC	HH-/HN-	0.01	100
GS	US Geological Survey Networks	USGS NEIC/NetQuakes	IRIS	V/A	SEED/ MiniSeed	BH-/HN-	0.025/ 0.005	40/200
HQ	Hydro Québec Network (unofficial designation)	Hydro Québec	Hydro Québec	A	ASCII Files	HN-	0.005	200
II	IRIS/IDA Network	Scripts Institute of Oceanography, UC San Diego	IRIS	V	SEED	BH-	0.05	20
IU	IRIS/USGS Global Seismograph Network (GSN)	USGS Albuquerque Seismological Laboratory	IRIS	V	SEED	BH-	0.05/ 0.025	20/40
IU	IRIS/USGS Global Seismograph Network (GSN)	USGS Albuquerque Seismological Laboratory	IRIS	V	SEED	HH	0.01	100
IW	Intermountain West Seismic Network	USGS/ANSS Golden, CO	IRIS	V	SEED	BH-	0.025	40
LD	Lamont-Doherty Cooperative Seismographic Network	Lamont-Doherty Earth Observatory of Columbia University	IRIS	V	SEED	BH-	0.025	40

Network Code	Network Name	Network Owner/Manager	Data Source	Data type	Data Format	Instrument Type	Time Interval (sec)	Sampling Frequency (Hz)
LD	Lamont-Doherty Cooperative Seismographic Network	Lamont-Doherty Earth Observatory of Columbia University	IRIS	V	SEED	HH-	0.01	100
LI	Laser Interferometer Gravitational-Wave Experiment	Caltech/USGS, Southern California Seismic Network	IRIS	V	SEED	BH-/HH-	0.05/ 0.01	20/100
NE	New England Seismic Network	Weston Observatory, Boston College/MIT	IRIS, Weston Obs.	V	SEED, SAC	BH-	0.025	40
NM	Cooperative New Madrid Seismic Network	St. Louis University/ University of Memphis	CERI, SLU, IRIS	V,A	SAC, SEED	BH-	0.05, 0.025, 0.02	20/40/50
NM	Cooperative New Madrid Seismic Network	St. Louis University/ University of Memphis	CERI, SLU, IRIS	V,A	SAC, SEED	HH-/HN-	0.01/ 0.005	100/200
NP	United State National Strong-Motion Network	USGS National Strong-Motion Program, Menlo Park	IRIS	V	SEED	HN-	0.005	200
NQ	NetQuakes	USGS Menlo Park	IRIS, CERI	A	SEED, SAC	HN-.01	0.005	200
OK	Oklahoma Seismic Network	Oklahoma Geological Survey	IRIS	V	SEED	HH-	0.01	100
PE	Penn State Network	Penn State University	IRIS	V	SEED	BH-	0.02, 0.01	50, 100
PO	POLARIS	Geological Survey of Canada and Canadian Universities	IRIS	V	SEED	HH-	0.01	100
QC	Quake Catcher Network	Stanford University	Stanford	A	SAC	BN- *	0.1 to 0.02	10 to 50
RU	USSR Strong Motion Station (unofficial designation)	Unknown	Vladimir Graizier	A	ASCII files	HN- *	0.005	200
SC	New Mexico Tech Seismic Network	New Mexico Tech, Socorro	IRIS	V	SEED	BH-	0.025	40
SE	Southeastern Appalachian Cooperative Seismic Network	Virginia Tech	CERI, Virginia Tech	V	SAC	HH-, EH-	0.01	100

Network Code	Network Name	Network Owner/Manager	Data Source	Data type	Data Format	Instrument Type	Time Interval (sec)	Sampling Frequency (Hz)
SP	South Carolina Earthq Physics Project	University of South Carolina, Columbia	IRIS	V	SEED	BH-	0.05	20
TA	USArray Transportable Array	EarthScope Project, IRIS	IRIS	V	SEED	BH-	0.025	40
US	US National Seismic Network	USGS/NEIC, USGS/ASL, EarthScope Project of IRIS	IRIS	V	SEED	BH-/HN-	0.05, 0.025 /0.005	20, 40 /200
UU	University of Utah Regional Network	University of Utah, Salt Lake City	IRIS	V	SEED	BH-/HH-	0.025/ 0.01	40/100
XC	IRIS Temporary Network	IRIS	IRIS	V	SEED	BH-	0.1	10
XF	IRIS Temporary Network	IRIS	IRIS	V	SEED	BH-	0.025	40
XK	IRIS Temporary Network	IRIS	IRIS	V	SEED	BH-	0.05	20
XM	IRIS Temporary Network	IRIS	IRIS	V	SEED	BH-	0.05	20
XO	IRIS Temporary Network	IRIS	IRIS	V	SEED	BH-	0.025	40
XR	IRIS Temporary Network	IRIS	IRIS	V	SEED	BH-	0.025	40
Y8	IRIS Temporary Network	IRIS	IRIS	V	SEED	HH-	0.01	100
YC	IRIS Temporary Network	IRIS	IRIS	V	SEED	HH-	0.01	100
Z3	IRIS Temporary Network	IRIS	IRIS	V	SEED	BHZ, HH-	0.05, 0.01	20, 100
Z9	Temporary Network	IRIS	IRIS	V	SEED	BH-	0.02	50

3 Time Series Processing

3.1 INTRODUCTION AND OVERVIEW

All the time series collected were initially processed by the CERI team, as documented in Cramer et al. [2013]. However, the NGA-East team required additional products necessitating the re-processing of the time series. For example the FAS for specific windows (for noise, *P*-, *S*-, *Lg*- and Coda-wave), need to be extracted at the processing stage. The collection of these data is optimal when working with instrument-corrected time series rather than with raw time series. The CERI team shared the collected raw time series and their processing package (codes and workflow) for computing instrument-corrected time series. Christine Goulet (PEER) produced the instrument-corrected time series in ASCII format, which were then used by the NGA-East processing team to generate the products required by the project.

This chapter summarizes the steps and methods used to process earthquake recordings (also called "time series" or "time histories") for use in the NGA-East project. These steps are grouped into two main categories: pre-processing and processing. The pre-processing phase includes the initial data screening, processing and quality assurance review completed by the CERI team, the development of the initial flatfile, and the preparation of files for processing. The NGA-East processing steps include the time window selection and tapering, FAS computation, signal filtering, and the application of baseline corrections. A summary of this methodology is available in Chiou et al. [2008] and Ancheta et al. [2013].

3.2 TIME SERIES PRE-PROCESSING

3.2.1 Initial Processing Approach

Data processing procedures are documented in Cramer [2008], and Cramer et al. [2009, 2011] and have been reviewed and approved by the NGA-East ground-motion-database working group. The general flow of data processing for NGA-East is to download uncorrected waveforms and their poles and zeros files, review the wave forms for obvious problems, instrument correct and general filtering of original waveforms, generation of signal and pre-event noise Fourier spectra and selection of initial filtering corners, and initial bandpass filtering. The data processing was accomplished using SAC (Seismic Analysis Code) [Goldstein and Snoke 2005; Goldstein et al. 2003]. Instrument correction was accomplished using poles and zeros representing the instrument response to displacement (in meters). The instrument correction procedure involved

removing the mean, linear detrending, and applying a 2% cosine taper prior to instrument correction. The SAC TRANSFER command was used to affect instrument correction using appropriate poles and zeros files. Filtering was accomplished using the frequency domain, acausal, cosine-tapered, bandpass filter in the SAC TRANSFER function when correcting the waveforms. As a check on the validity of the bandpass filtering by SAC TRANSFER, selected records were processed and filtered using a Butterworth filter by Dave Boore and compared to both the SAC TRANSFER filtered and SAC BANDPASS Butterworth filtered records. The results from these three alternative filtering approaches are identical in the time domain [Cramer 2008].

Most waveforms were downloaded as uncorrected data files and instrument corrected using poles and zeros files provided by the data source or, in special cases, developed by the CERI team from detailed instrumentation information (seismometer and digitizer). In some cases the waveforms were only available as instrument-corrected files. Mainly, the Canadian strong-motion records and Gazli strong motion record were provided in instrument-corrected and processed files, which are simply passed through the instrument correction task as is. Similarly, the broad band records for the 1990 Mont Laurier and 1988 Saguenay earthquakes were retrieved from the National Center for Earthquake Engineering Research (NCEER) StrongMo database (which is now defunct). These records were already instrument-corrected and hence were passed through (like the Canadian strong-motion records). Data files from the IRIS Data Center and the Canadian National Data Center were downloaded from their websites using the tools provided. Data files from CERI were copied from their data achieve system to which we had access. Many of the CERI data files are available now via the IRIS Data Center. The remaining data files were provided in electronic format by the network operators as a result of a direct request to them from the NGA-East database developers.

3.2.2 Quality Assurance and Updating of Metadata and Time Series

Quality assurance (QA) has been an important aspect of developing the NGA-East ground motion database. During the initial processing of the waveforms at CERI, quality assurance measures included the following:

- A review of the waveform after download for obvious problems such as clipping, distortion, missing data, noise spikes, etc.
- A comparison of record component signal and pre-event noise Fourier spectra for selecting initial bandpass filtering limits and identifying spectral response problems and shape.
- A review of final acceleration and displacement time series after initial filtering for problems associated with the initial bandpass filter corner selections and the possible revision of the filter corners or cutting of the final waveform to avoid large acceleration spikes, long-period displacement noise, and noise contaminated portions of the recordings.

- The plotting and review of component (as is) ground motions, such as PGA, PGV, and 0.2 sec and 1.0 sec Sa, to identify poles and zeros (PZ) or gain problems causing outliers and to help flag possible clipping, radiation, directivity, and other issues with individual records.

All identified problems have been documented in a waveform quality table (quality.dat file) for each earthquake and the information included in flat file entries in the quality column (summary) and at the end (full report), plus in time series file headers (full report). Only high-quality waveforms or those with minor quality issues were included in the initial NGA-East ground motion database flat files and time series files. Table 3.1 lists the record quality codes found in the flat files.

Post processing quality assurance measures have also been applied, discovered problems corrected and, where appropriate, processing for ground motion values redone or metadata corrected. In mid-2011 a check was conducted on the horizontal alignment of record time series, particularly for older records. Generally, most downloaded waveform records are properly aligned. Cross correlation of horizontal traces in SAC was used to identify possible uncorrelated horizontal components in a record. Experience showed that cross-correlation values exceeding a 30-sec separation for the correlation peak corresponded to records needing review while those not exceeding a 30-sec separation were properly aligned. Unaligned pairs (of which there were very few) were identified and eliminated as appropriate. Many seemingly unaligned pairs were actually uncorrelated local noise instead of earthquake signals (and hence discarded).

Quality assurance on the PZ files was conducted beyond the simple looking for outliers on ground motion parameter plots with distance. In June 2011, a systematic review of the GSC online station book documentation was completed on station PZ files, leading to updates as needed. A similar exercise was completed in July 2012 to update mid-2010 and earlier PZ files for ten Lamont Doherty Cooperative Network (LDCN) stations with documented changes in PZ information. Several GSC and LDCN PZ files were corrected and affected records reprocessed and QA checked for proper ground motion levels.

Table 3.1 Table of record quality codes used in the initial NGA-East flat files.

Code	Meaning
A	Good
?	Accepted, but might have problem
D	Directivity or source effect
N	Radiation effect

3.3 NGA-EAST INSTRUMENT CORRECTION AND ALIGNMENT

As mentioned earlier, NGA-East required additional products (namely FAS for various windows) that were not obtained through the first round of processing by the CERI team. Another critical issue requiring re-processing was the choice of using RotD50 for NGA-East. Contrary to other average PSA metrics such as the geometrical mean, RotD50 requires proper phasing and adequate alignment of the horizontal components in time. The original processing at CERI included removing noise or spikes in time domain on a per-component basis, sometimes

leading to different phase start times in the time series. During this process, the timing information was saved in miniSEED or SEED formats, but not in the ASCII files generated by the CERI team. NGA-East elected to start from the miniSEED time series that had already been through the QA checks to pre-process the data, as summarized below. This allowed the NGA-East project to benefit from the extensive QA work and ensuing improvements in data quality conducted at CERI (see discussion above).

The data and a suite of scripts and software were obtained from the CERI team. Key components of the software package included IRIS rdseed and SAC software, used in combination with the time series, event data files, and PZ files. The first step was to read the data with rdseed to convert all miniSEED data into binary SAC format. A shell script was then run to update the event information (source location, date and time, etc.). Finally, SAC was used to perform the instrument correction. Additional scripts were developed in MatLab to read the binary SAC files and to extract the time series and the required different times (event origin time "O", beginning and end value of the independent variable "B' and "E," and the first arrival time relative to the reference time "A"). A series of checks were performed to make sure the start times matched between the components. In cases where a component had been truncated in the original processing (either at the beginning or end of the record), the longer time series was truncated to the match the shorter component and aligned in time. An example of time-aligned three-component time series is shown in Figure 3.1.

The time-aligned time series were saved into ASCII files that included the origin and first arrival times, and the distance estimates (directly from SAC headers) to be used in the subsequent processing steps. A final verification was performed consisting in reading the ASCII files and generating acceleration plots for all of the available components. A manual review of each plot was completed to evaluate suitability for processing. Records that had obvious problems such as late trigger, very short Coda waves, clipping, or large ringing (recurring spikes in time) were discarded. Noise-dominated records were usually not discarded at this step.

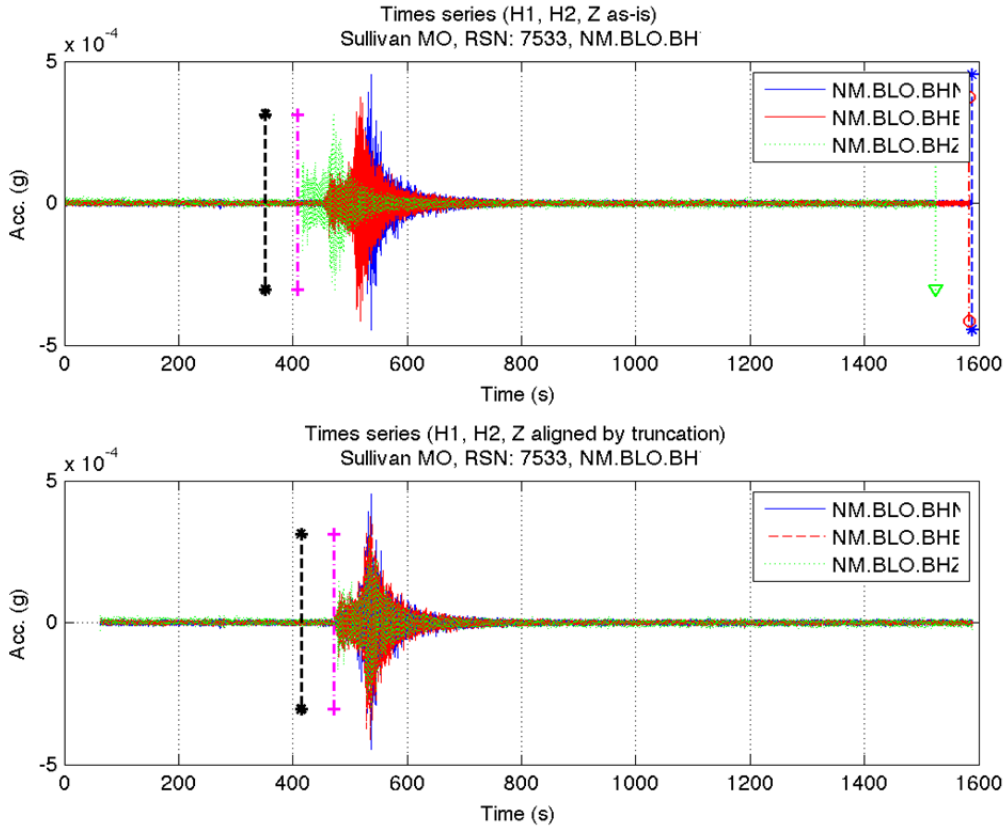

Figure 3.1 **Example of time-aligned three component time series that had been truncated during original processing. The top plot shows the as-is, instrument-corrected acceleration trace and the bottom plot shows the time-aligned components. Colored vertical lines with symbols show the origin time (black), first arrival (magenta) and the end of each time series (horizontals are blue and red, vertical is green). In the example above, the pre-event noise for the vertical and the East components had been cut short relative to the North component (top plot). This is corrected in the bottom plot.**

3.4 TIME SERIES PROCESSING

An extensive software package was developed in R [R Development Team 2011] for the processing of the time series. The code was originally developed for the NGA-West2 project [Ancheta et al., 2013] and additional developments were implemented to address NGA-East's specific needs. This chapter summarizes the time series processing completed with this software package and the products generated for the project. Key products include acceleration, velocity and displacement time series, PSA metrics, and Fourier spectra for several time series windows.

3.4.1 Inspection for Time Series Acceptance

The first step in the process involved determining the acceptability of time-aligned, instrument-corrected time series that were not otherwise processed or filtered, as described in the previous section. An initial visual inspection of the time series and a trial-and-error approach was used to

consider the potential for successfully retrieving the time series. At this stage, each potential recording was either accepted or rejected. This approach is consistent with that applied in the NGA-West1 [Chiou et al. 2008] and NGA-West2 [Ancheta et al., 2013] projects. Figure 3.2 shows an example of a recording that was rejected during this process. In this recording, the long-period noise is dominant compared to the ground motion signal of interest, and the recording was rejected.

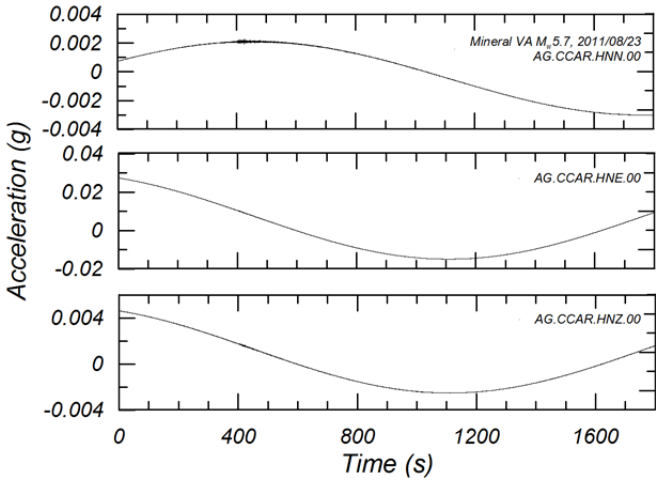

Figure 3.2 Example of time series rejected based on visual inspection.

3.4.2 Determination of Time Windows for Data Processing

Six distinct time windows were then determined for each of the accepted acceleration time series. Figure 3.3 shows these six windows schematically. The first time window contains only pre-event noise (magenta box). The second time window contains *P*-waves (yellow box) and includes a small buffer prior to the first arrival. The third time window contains *S*- and *Lg*-waves (green box) and is hereafter termed the "*SLg*-wave window". The fourth time window contains the Coda waves (gray box). The fifth and sixth time windows are combinations of these first four windows. The fifth time window contains the *P*-, *S*- and *Lg*-waves and represents the combined second and third time windows (orange box). The sixth time window encompasses the entire recording (blue box); FAS were computed for all the time windows for each of the recordings. The method for definition of each the six windows is presented in more detail in the following sub-sections.

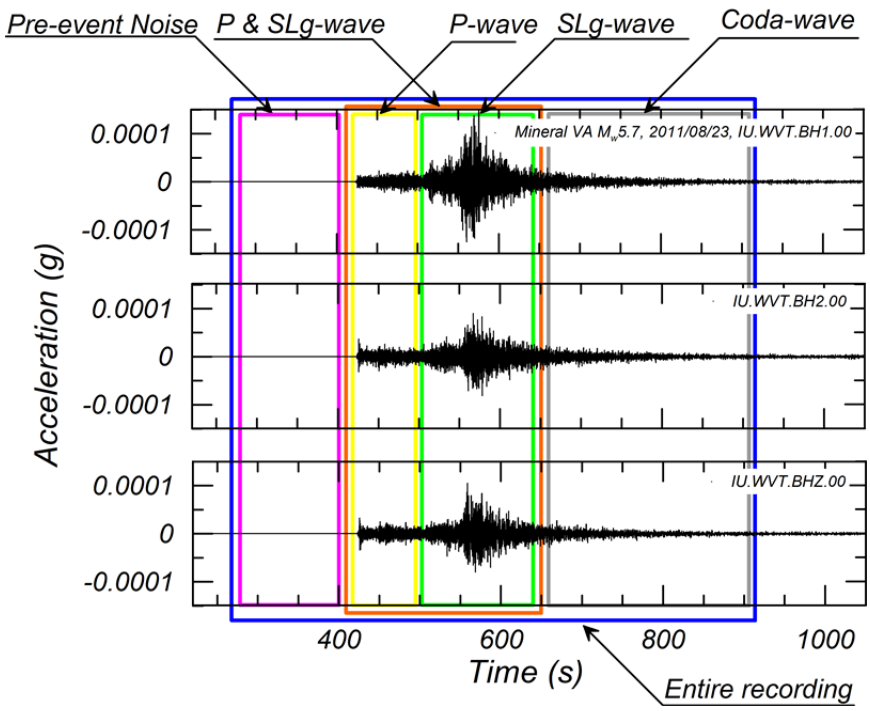

Figure 3.3 Schematic drawing of the six time windows used.

Entire Recording Time Window

The time window for the entire recording includes the windows for pre-event noise, *P*-waves, *SLg*-waves, and Coda waves. Its duration is determined by the following formula:

$$T_{d-entire} = T_{d-noise} + T_{d-P} + T_{d-SLg} + T_{d-Coda} \tag{3.1}$$

where T_d denotes the duration for each of the time windows described in the following sections.

Pre-Event Noise Time Window

The acceleration values recorded in the pre-event noise time window are used to calculate the noise FAS. The noise FAS is used as a guide in selecting the filter corner frequencies. The start and the end times of the pre-event noise window are selected based on the *P*-wave arrival time using the following formulas:

$$t_{noise-start} = t_{noise-end} - T_{d-SLg} \tag{3.2}$$

$$t_{noise-end} = t_{P-arrival} - 2.0 \tag{3.3}$$

Where possible, the preferred duration of the noise–time window ($T_{d-noise}$) is equal to the duration of the *SLg*-wave time window (T_{d-SLg}); however, the noise–time window can be shorter if not enough pre-event signal was recorded. The 2.0 sec before the *P*-wave arrival ($t_{P-arrival}$) are included in the *P*-wave time window, rather than the noise–time window, to ensure that an emergent *P*-wave arrival is contained within the *P*-wave window. The *P*-wave arrival time is

visually determined by examining the three-component acceleration time series (see Figure 3.4). The vertical recording is usually used to determine the *P*-wave arrival because the *P*-wave tends to be more prominent in the vertical direction. The software used for data processing has an option to zoom in on the acceleration trace near *P*-wave arrival, thereby allowing for a more accurate selection. The manual selection of window start and end points is completed by clicking directly on the plots shown on the screen.

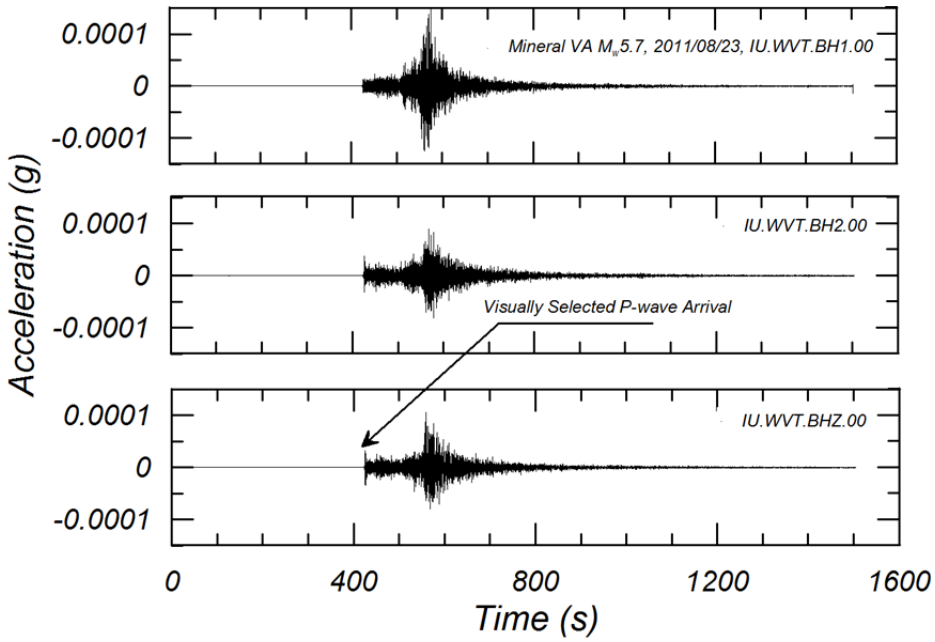

Figure 3.4 Selection of P-wave arrival time.

P-wave Time Window

The *P*-wave time window starts at the end of the pre-event noise time window. As such, the start time of the *P*-wave window is noted as $t_{noise\text{-}end}$ and defined in Equation (3.3). The end of the *P*-wave time window is calculated based on the arrival of the *S*-wave as defined by following equation:

$$t_{P-end} = t_{S-arrival} - 0.5 \tag{3.4}$$

The reduction of the *P*-wave time window by 0.5 sec is necessary to accommodate the FAS taper at the start of the *SLg*-wave time window. The *S*-wave arrival time ($t_{S-arrival}$) is visually selected based on a change in amplitude and frequency content of the acceleration and displacement time series, as shown in Figure 3.5. The displacement time series in Figure 3.5 are calculated after applying a high-pass causal filter with a corner at 0.2 Hz (5 sec) along with a baseline correction. As a guide for the analyst, the theoretical *S*-wave arrival time is also plotted in the figure using the following equation:

$$t_{S-arrival} = t_0 + R_h / 4.5 \tag{3.5}$$

where t_0 is the origin time, R_h is the hypocentral distance in km, both provided in the ASCII file headers, and 4.5 is the assumed crustal shear wave velocity in km/sec. Using this information, an

estimate of the *S*-wave arrival times were determined. Figure 3.4 shows the *P*-wave window determined for the example recording in Figure 3.3.

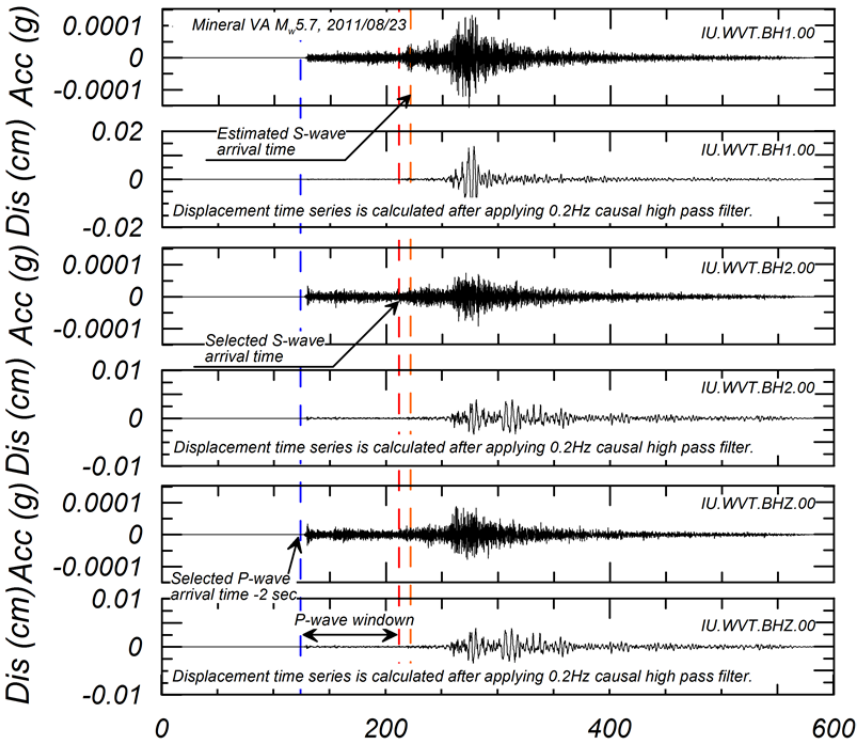

Figure 3.5 Acceleration and displacement time series and calculated arrival times (horizontal axis is time, in seconds).

SLg-wave Time Window

The start time of *SLg*-wave time window is the end time of the *P*-wave window ($t_{P\text{-}end}$), which is defined by Equation (3.4). The end time of the *SLg*-wave window is defined by the following equation:

$$t_{SLg-end} = t_{Lg-arrival} + T_{d-Lg} + T_{d-source} \tag{3.6}$$

where $T_{d\text{-}Lg}$ and $T_{d\text{-}source}$ are *Lg*-wave and source durations, respectively. The parameter $t_{Lg\text{-}arrival}$ in Equation (3.6) was calculated using the relationship in Figure 3.6 [Chapman 2013] between *Lg*-wave travel time and hypocentral distance, as follows:

$$t_{Lg-arrival} = t_0 + R_h/3.53 \tag{3.7}$$

The parameter $T_{d\text{-}Lg}$ in Equation (3.6) can be calculated using the relationship in Figure 3.6 [Chapman 2013] between *Lg*-wave duration and hypocentral distance, as follows:

$$T_{d-Lg} = 8.71 + 0.026R_h \tag{3.8}$$

However, for data processing purposes, this project used the following estimate of $T_{d\text{-}Lg}$ to provide a conservative upper bound for Lg-wave window duration:

$$T_{d-Lg} = 17.4 + 0.052R_h \tag{3.9}$$

Equation (3.9) provides duration estimates that are double those calculated by Equation (3.8), as can be seen in Figure 3.7. This longer time window may result in some Coda waves being captured in the *SLg* window. However, this conservative duration estimate ensures that late arriving *Lg* waves are analyzed within the time same window. The parameter $T_{d\text{-}source}$ in Equation (3.6) is estimated based on the corner frequency (f_c) of a Fourier spectrum source model [Brune 1970; Aki 1967; and Boore 1983], as follows:

$$f_c = 4.9 \cdot 10^6 \beta \left(\frac{\Delta\sigma}{M_0} \right)^{\frac{1}{3}} \tag{3.10}$$

where

$$M_0 = 10^{1.5M + 16.05} \tag{3.11}$$

where the parameter β is the shear wave velocity at the source. The parameter $\Delta\sigma$ is the stress drop of the earthquake. Taking into account these theoretical f_c values for each magnitude bin, Table 3.2 was calculated to provide $1/f_c$ for data processing purposes. Because most of the earthquakes in the NGA-East database have magnitudes of less than 6.5, the effect of $T_{d\text{-}source}$ on *SLg* window size is relatively small. For example, Figure 3.8 shows the *SLg* window as having a duration of 130 sec. By contrast, the contribution of $T_{d\text{-}source}$ to the *SLg* window duration is 3 seconds according to Table 3.2.

Table 3.2 Source duration ($T_{d\text{-}source}$) versus moment magnitude.

Magnitude	Source Duration (sec)
M< 5	1
5≤ **M** < 6.5	3
6.5 ≤ **M** < 7.5	10
7.5 ≤ **M** 8.25	30

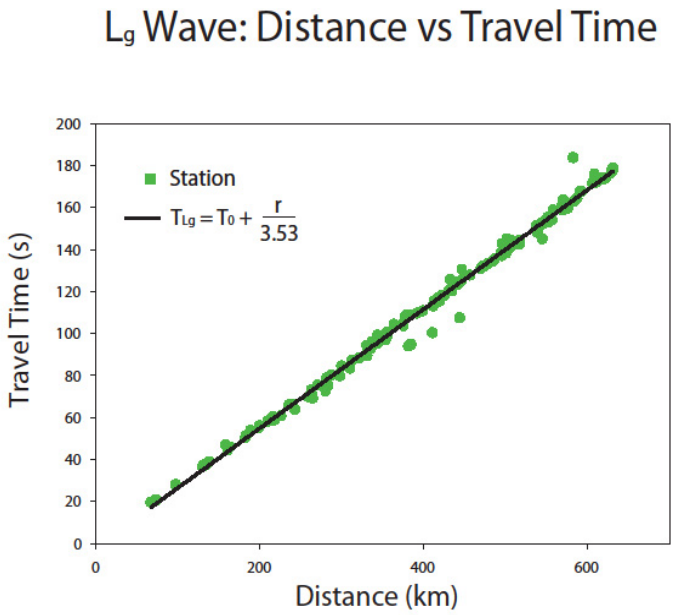

Figure 3.6 **Relationship between *Lg*-wave travel time and distance [Chapman 2013].**

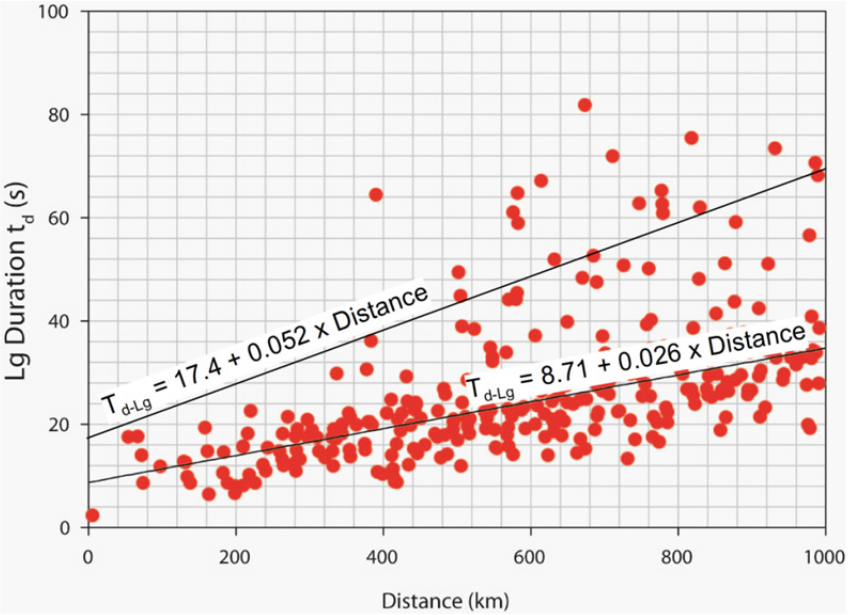

Figure 3.7 **Relationship between *Lg*-wave travel time and distance, selected model. The lower line corresponds to the mean model from Chapman [2013] and the top line is the model used for NGA-East (twice the lower line).**

Coda Time Window

The start time of the Coda window is the end of the *SLg*-wave time window ($t_{SLg-end}$), which is defined by Equation (3.6). The preferred Coda window duration is set to twice the *SLg*-window duration, whenever possible. The end time of the Coda window is defined by the following equation.

$$t_{Coda-end} = t_{SLg-end} + 2 \cdot T_{d-SLg} \tag{3.12}$$

Figure 3.7 shows the Coda window for the example recording shown in Figure 3.4. The Coda time window excludes the large amplitude *S*- and *Lg*-waves, and only contains the small amplitude Coda waves.

There are several alternative methods that can be used for Coda window selection. One approach calculates the start of the Coda window by taking twice the S-wave travel time and adding it to the S-wave arrival time [Aki 1969; Philips and Aki 1986; and Kato et al. 1995]. This approach defines a window that captures the non-directional Coda wave after the *S*-wave energy has passed. This definition also provides a theoretically consistent assessment of Coda wave onset. However, it may lead to *S*-waves being captured into the Coda time window for cases where there is a long source duration and short hypocentral distance. This definition was tested for this project. The analysis confirmed that the approach works adequately well for intermediate epicentral distances (e.g., 30–100 km) and relatively small magnitudes (near 4 or less).

Another approach to defining the start of the Coda window is to use the time immediately following the S-wave window, such as defined by Novelo-Casanova and Lee [1991] and Wong et al. [2001]. However, some of these definitions may cause the Coda window to contain late arriving *S*-waves or surface waves. Based on analysis of CENA data, this study found that the most appropriate approach is that shown in Figure 3.8.

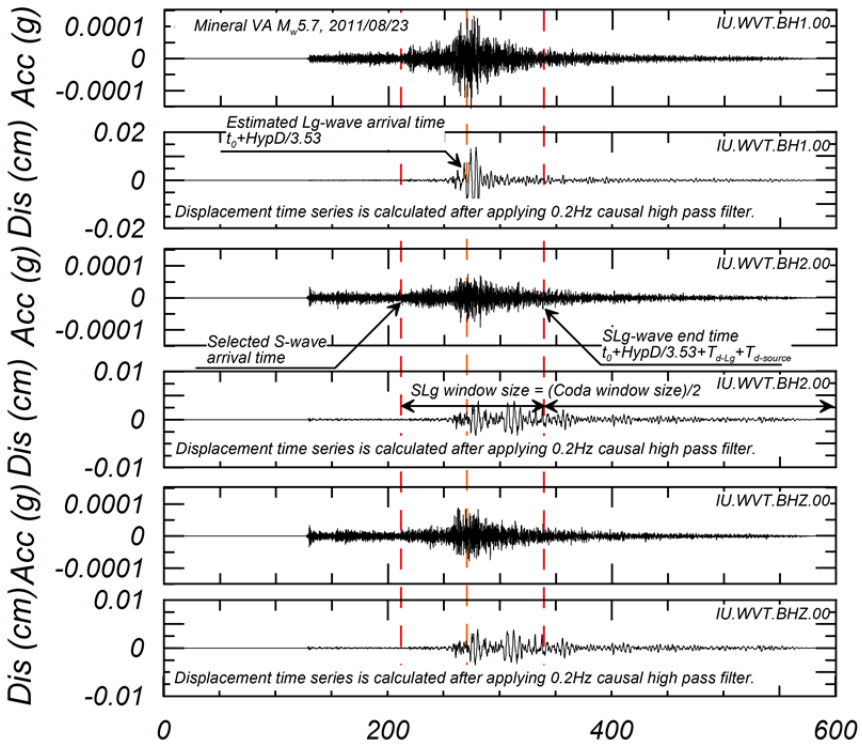

Figure 3.8 Determination of Coda time window.

Recordings with Late Triggering

For recordings with late triggering, the above-mentioned methodology cannot be applied. For recordings with late *P*-wave triggering, the pre-event noise time window is excluded. Recordings

with late *S*-wave triggering were not processed. An exception was made for recordings from a few critical events, such as the Saguenay 1988 earthquake. These late *P*- and *S*-wave triggered ground motions have been flagged at the time of processing to be documented as such in the flatfile.

3.4.3 DC (Mean) Removal, Taper, and Fourier Amplitude Spectra

DC (Mean) Removal and Taper

In the context of signal processing, removal of the mean from waveforms is often referred to "DC removal". The term originally comes from electronic signal processing (DC standing for direct current), but has since been extended to any waveform. DC (mean) removal and tapers are applied to the various windowed time series before calculation of the FAS. DC removal is defined by the following equation:

$$\mathbf{a}' = \mathbf{a} - \overline{a} \tag{3.13}$$

where **a'** denotes the acceleration time series after DC removal; **a** and $\overline{a}$ denote the windowed acceleration time series and the mean offset which is often called DC coefficient. After DC removal, cosine tapers are applied at the beginning and end of each window. The cosine tapers are defined by the following equations (e.g., Kanasewich [1981]).

At the beginning of window,

$$w_i = \frac{1}{2}\left[1 + \cos\left(\pi \frac{n_b + i - 1}{n_b}\right)\right], \text{i} = 1, .., n_b \tag{3.14}$$

At the end of window

$$w_i = \frac{1}{2}\left[1 + \cos\left(\pi \frac{i - 1}{n_e}\right)\right], \text{i} = 1, \ldots, n_e \tag{3.15}$$

where n_b and n_e are the numbers of points from the beginning and the end of the time series, respectively. These functions produce a weight of zero at the first and last data points in the time series for beginning and end tapers, and gradually increase to 1.0 outward. Table 3.3 lists the length of cosine tapers applied to the accelerations.

Table 3.3 Cosine taper length applied to windowed accelerations.

Windowed Time Histories	Cosine Taper Length	
	Start Time	End Time
Entire	1% of Total Length	1% of Total Length
Pre-event noise	0.5 sec	0.5 sec
P-wave	0.5 sec	0.5 sec
SL_g-Waves	0.5 sec	0.5 sec
Coda	0.5 sec	0.5 sec

Fourier Amplitude Spectra

Fourier spectra were calculated from the windowed time series after DC removal and tapering. FAS and Fourier phase spectra (FPS) were saved as output files. Before calculating Fourier spectra, a series of zeroes was added at the end of recordings to increase the number of data points to a power of two. The entire length may increase to approximately 50 min for a causal filter, depending on the sampling frequency, as shown in Table 3.4. This window length was selected based on the longest recording in NGA-East dataset so that all the recordings become at least twice their original duration. This extended duration avoids the possible wrap-around effects that can occur in the time domain after applying acausal filters. The lengths of pre-event noise, *P*-, *SLg*, and Coda wave windows were all increased to 50 min with zeroes. This process provides a consistent frequency step (*df*) among the different windows and recordings, making the FAS usable directly for many applications, without the need for users to decimate or interpolate each record individually.

Table 3.4 Minimum frequency for FAS calculation.

Samplingfrequency (Hz)	*dt* (sec)	Duration (sec)	Power of 2	*df*
10	0.1	3276.80	15	0.00030518
20	0.05	3276.80	16	0.00030518
40	0.025	3276.80	17	0.00030518
50	0.02	2621.44	17	0.00038147
100	0.01	2621.44	18	0.00038147
200	0.005	2621.44	19	0.00038147

The FAS and FPS are computed as follows:

$$FAS_k = T\left|C_k\right| \tag{3.16}$$

where

$$C_k = \frac{1}{N}\sum_{j=1}^{N} x(j)\omega_N^{(j-1)(k-1)} \tag{3.17}$$

$$\omega_N = e^{(-2\pi i)/N} \tag{3.18}$$

$$T = Ndt \tag{3.19}$$

C_k is the Fourier coefficient for each frequency *df(k-1)*, where *df* is the frequency step. The term *x(j)* represents a time series, *N* represents the number of data points in the time series and *dt* is the time step of the series. Equations (3.16) and (3.17) show that C_k decreases, although FAS does not change, as a result of adding terminal zeros to the time series. The FPS is calculated from the real and imaginary values of Fourier spectra as follows.

$$FPS = \tan^{-1}\left[\mathrm{Im}(C)/\mathrm{Re}(C)\right] \tag{3.20}$$

where the phase ranges from $-\pi$ to π in the output file. Figure 3.9 shows the FAS for the H1 component of the time series shown in Figure 3.8.

The FAS shown in Figure 3.9 are smoothed to facilitate the selection of the low-pass corner frequency where the details of filtering are described in the following section. Several smoothing methods were reviewed for this project. The methods included the linear-scale rectangular window, linear-scale triangular window, log-scale rectangular window, and the log-scale Konno-Ohmachi window [1998]. The appropriate FAS smoothing method for any application depends on the objective [see Konno and Ohmachi, 1998; Boore, 2010a]. For this project a log-scale rectangular window was selected because it provides adequate smoothing and is computationally efficient. This smoothing window is expressed by the following function.

$$W(f, f_o) = \begin{cases} 1, & 10^{-d/2} \le f/f_o \le 10^{d/2} \\ 0, & otherwise \end{cases} \tag{3.21}$$

where d is the window size in log scale, and f and f_o are the frequency of interest and the central frequency, respectively. The default window size is d = 0.05 in log-scale, which provides smoothing within a range of ±6% around a given frequency. Using this method, the smoothed FAS value is calculated at the central frequency of interest using the following formula. An equal weight is used for each FAS.

$$\ln(FAS_o) = \sum_{i=1}^{n} w_i \ln(FAS_i) \tag{3.22}$$

$$w_i = 1/n \tag{3.23}$$

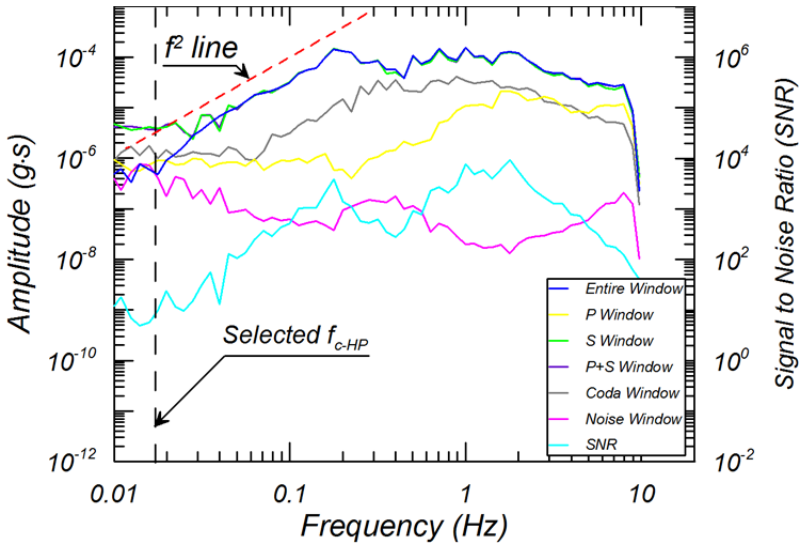

Figure 3.9 **Example Fourier amplitude spectra from acceleration time series for different windows.**

where FAS_o is the smoothed *FAS* value at the central frequency, and n is a number of points in the window. Because the rectangular window has a constant width on a log scale, the value of the parameter n increases from low frequency to high frequency. For example, if the common *df* of 0.000763 is used, n is 8 when f_o = 0.05 Hz and is 1510 when f_o = 10 Hz. Therefore, smoothing at a higher f_o will average more points of the *FAS* within a given log-scale rectangular window.

3.4.4 Filtering Methodology

High-pass (low-cut) and low-pass (high-cut) filters are applied to only the window encompassing the entire record. The other four time windows discussed above are not filtered. The filtering is done in the frequency domain. Causal and acausal Butterworth filters are applied in which five and four poles are used for the high-pass and low-pass filters, respectively. Corner frequencies were selected based on the theoretical acceleration decay at low frequencies consistent with the f^2 model [Brune 1970; Boore and Bommer 2005]. A line consistent with the f^2 assumption is shown on Figure 3.9, as an example. The FAS calculated from the accelerations in the pre-event noise window also helps in the selection of corner frequencies.

Figure 3.9 shows the selected high-pass corner frequency ($f_{c\text{-}HP}$) for an example recording. This frequency was chosen based on the smoothed FAS as described in the previous section. In the figure, the selected $f_{c\text{-}HP}$ is shown by the vertical line at 0.018 Hz, which is the frequency at which the spectrum deviates from an f^2 model. It is also the intercept with the increasing noise spectrum as decreasing the frequency below 0.1 Hz. A low-pass corner frequency ($f_{c\text{-}LP}$) was not selected for this record because no additional filtering was needed. All the records in NGA-East database were processed following this method of determining $f_{c\text{-}HP}$ and $f_{c\text{-}LP}$. The usable frequency is also calculated with a multiplicative factor of 1.25 inward, as is PEER standard practice [Ancheta et al. 2013].

Characteristics of causal and acausal Butterworth filters have been reviewed previously by several researchers (e.g., see Boore and Akkar [2003] and Bazzurro et al. [2005]). The filters have the same transfer function amplitudes, but different phase spectra. The following sections provide an overview of these filters based on the previous studies with an emphasis on information most relevant to the NGA-East Strong Motion Database. The discussion focuses on the analysis of results obtained when an impulse signal is filtered using each of the approaches.

Acausal Butterworth Filter

An acausal Butterworth filter is expressed by the following formula;

$$Y = \sqrt{\frac{\left(f/f_c\right)^{2n}}{1+\left(f/f_c\right)^{2n}}} \tag{3.24}$$

where n is the number of poles and f_c is corner frequency. Acausally filtered time series were used for computation of the RotDxx (see Boore [2010b) provided in the flatfile, as described in Chapter 6. Figure 3.10 shows the time-domain response of an impulse signal analyzed using Equation (3.24) for different corner frequencies. The input time series was an impulse signal occurring at a time equal to 20 sec with the amplitude of *1/dt*. The figure shows that Equation

(3.24) applied to an impulse signal produces a response in the time domain before the impulse occurs. As a result, acausal filters produce a displacement (calculated by integration) in the pre-event motions [Bazzurro et al. 2005]. Figures 3.11 and 3.12 show the FAS and FPS for different corner frequencies obtained from the filtered results shown in Figure 3.2. Figure 3.11 shows that the amplitude rapidly decreases as frequencies become increasingly lower than $f_{c\text{-}HP}$. Figure 3.12 shows that FPS are maintained after filtering; hence, the resulting PSA of acausally filtered records are not dependent on the selected $f_{c\text{-}HP}$ [Boore and Akkar 2003]. As a result, acausal filtering is the preferred technique when computing the PSA.

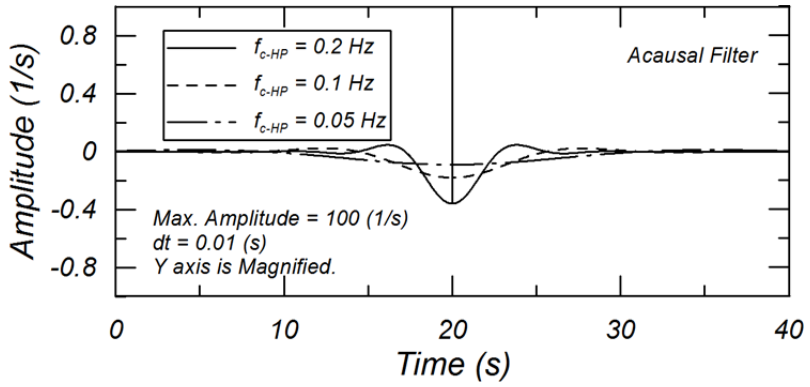

Figure 3.10 Time domain response of acausally filtered impulse signal.

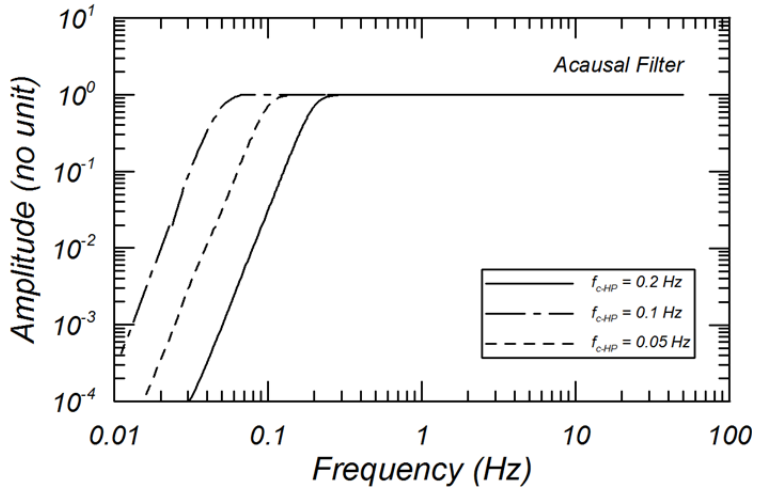

Figure 3.11 Fourier Amplitude Spectra for acausally filtered impulse signal.

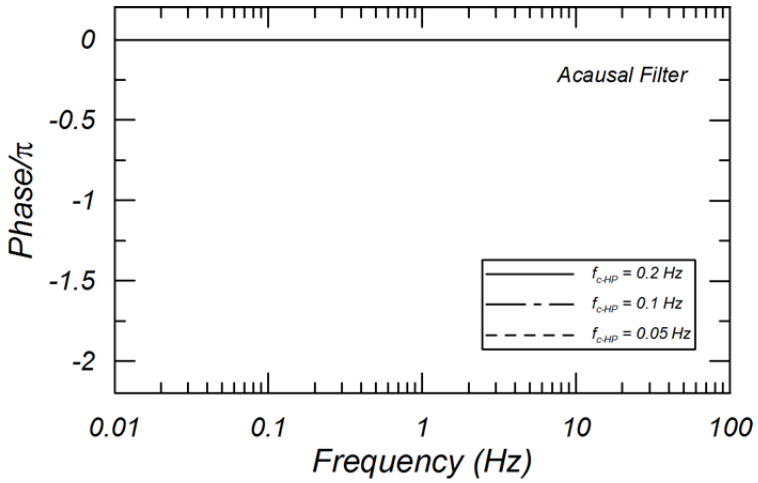

Figure 3.12 Fourier Phase Spectra for acausally filtered impulse signal.

Causal Butterworth Filter

Causal Butterworth filters were also used for data processing. A causal filter is expressed by the following functional form:

$$Y = \frac{1}{\prod_{j=1}^{n}\left\{ i\left(f_c / f\right) - \exp\left[\frac{i\pi}{2n}\left(2j - 1 + n\right)\right]\right\}} \tag{3.25}$$

where n is the number of poles, and f_c is corner frequency. Figure 3.13 shows the time domain response of an impulse signal filtered using Equation (3.25) with different corner frequencies. The impulse signal was again applied at 20 sec with the amplitude of *1/dt*. Figure 3.13 shows that applying Equation 3.25 to the impulse signal leads to a time domain response of zero before the signal occurs; hence, it maintains the correct arrival time for each frequency component. Figures 3.13 and 3.14 show the FAS and FPS for different corner frequencies obtained from the filtered results shown in Figure 3.13. Figure 3.14 shows that the amplitude rapidly decreases as frequencies become increasingly lower than $f_{c\text{-}HP}$, which is similar to the acausal filter (see Figure 3.11). Figure 3.15 shows that applying Equation (3.25) to an impulse signal produces distortions of phase affecting a wide frequency band above the selected $f_{c\text{-}HP}$. Thus, the PSA calculated is highly sensitive to the $f_{c\text{-}HP}$ used in filtering, even though the periods of interest are much shorter than the selected $f_{c\text{-}HP}$ [Boore and Akkar, 2003].

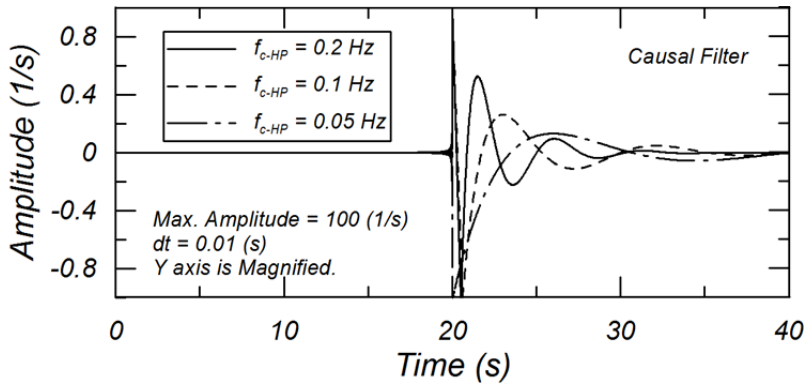

Figure 3.13 Time domain response of causally filtered impulse signal.

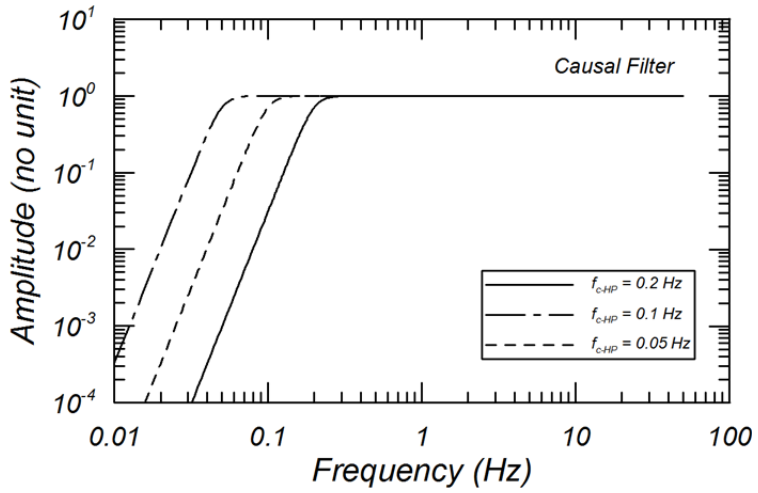

Figure 3.14 Fourier Amplitude Spectra for causally filtered impulse signal.

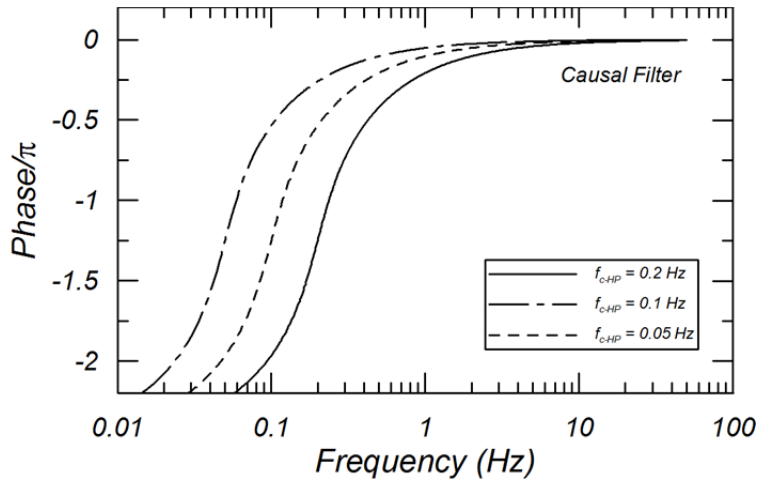

Figure 3.15 Fourier Phase Spectra for causally filtered impulse signal.

3.4.5 Baseline Correction

After filtering was completed, the zero pads were removed from the series (hereafter called "pad-stripped" time series). The acceleration time series is then double integrated in the time domain to compute the displacement time series.

Figure 3.16(a) shows the pad-stripped acceleration time series after applying an acausal filter. Figures 3.16(b) and 3.16(c) the show velocity and displacement time series calculated by integrating the acceleration time series shown in Figure 3.16(a). In performing the integrations, the initial velocity and displacement were assumed to be zero. The displacement time series in Figure 3.16(c) shows a linear trend of baseline drift, which indicates that the velocity time series includes a constant offset throughout the recording. This drift occurred because an initial velocity (prior to the start of the actual signal) was added to the pad-stripped recording as a result of applying an acausal filter (refer to the example in Figure 3.10).

Figure 3.16 shows the acausally filtered time series, in which zeros were padded at the beginning of recording. The figure shows that there is a small velocity at the start time of the original record. Therefore, the velocity time series has a positive bias if the initial velocity is assumed to be zero for a pad-stripped time series. As a result, this positive bias in velocity time series appears as a ramp in the displacement time series in Figure 3.15c. Boore et al. [2012] showed that this drift does not occur if the correct initial velocity and displacement are used in integrating acceleration time series. They also discussed that this does not occur if zero-padded filtered time series are provided as the final product, as it was the case for another study [Akkar et al. 2010]. Therefore, baseline correction is not required if the time series are provided with the zero-pads, as described in Boore et al. [2012].

However, records from PEER databases are often used by engineers in response history analyses of various systems and for this application, very long time series are considered impractical. To address this issue, a baseline correction as described by Boore et al. [2012] is applied. The NGA-East project decided to produce pad-stripped, baseline-corrected acceleration time series, such that initial velocity and displacement can be assumed to be zero.

To process the pad-stripped time series, first a beginning taper is added to the acceleration series, which are then integrated to displacement. A sixth order polynomial fit to the trend is computed as the baseline correction that is removed from the displacement time series. The time series is then differentiated back to acceleration. Figure 3.18 shows the baseline corrected, pad-stripped acceleration, velocity, and displacement time series corresponding to Figure 3.16. The process of baseline correction also ensures compatibility of the processed acceleration, velocity and displacement time series as discussed in Chiou et al. [2008] and Boore et al. [2012]. Figure 3.19 provides a comparison of PSA before and after applying baseline corrections. The figure shows that the effect of baseline correction on PSA is negligible.

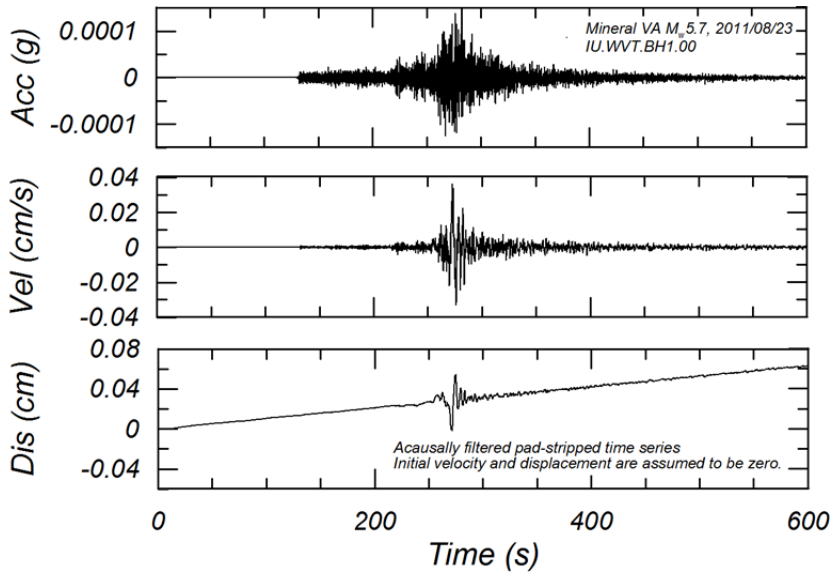

Figure 3.16 **Time series of acausally filtered pad-stripped record. Shown are (a) acceleration (b) velocity, and (c) displacement time series. The initial velocity and displacement are assumed to be zero in the integration.**

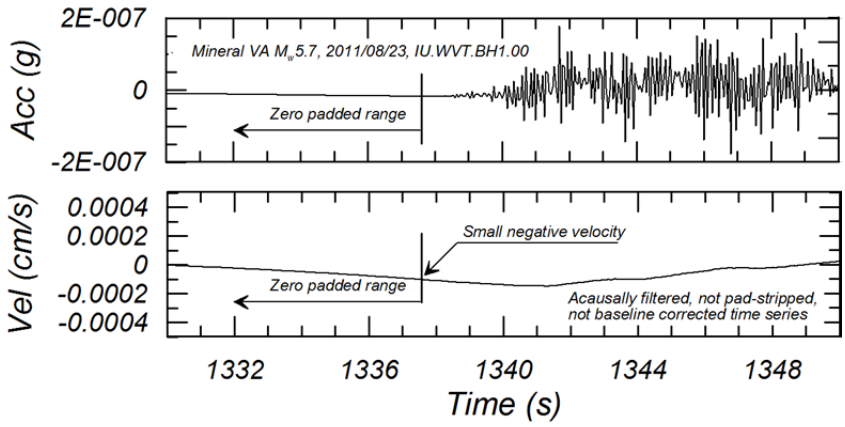

Figure 3.17 **Time series of acausally filtered record with zero padding. Shown are the (a) acceleration and (b) velocity time series.**

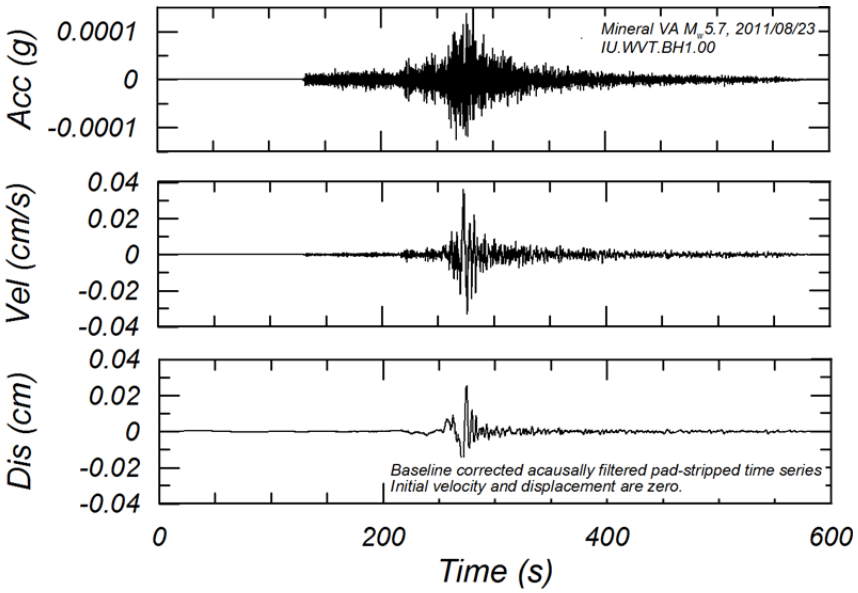

Figure 3.18 **Acausally filtered time series with baseline correction. Shown are (a) acceleration, (b) velocity, and (c) displacement time series**

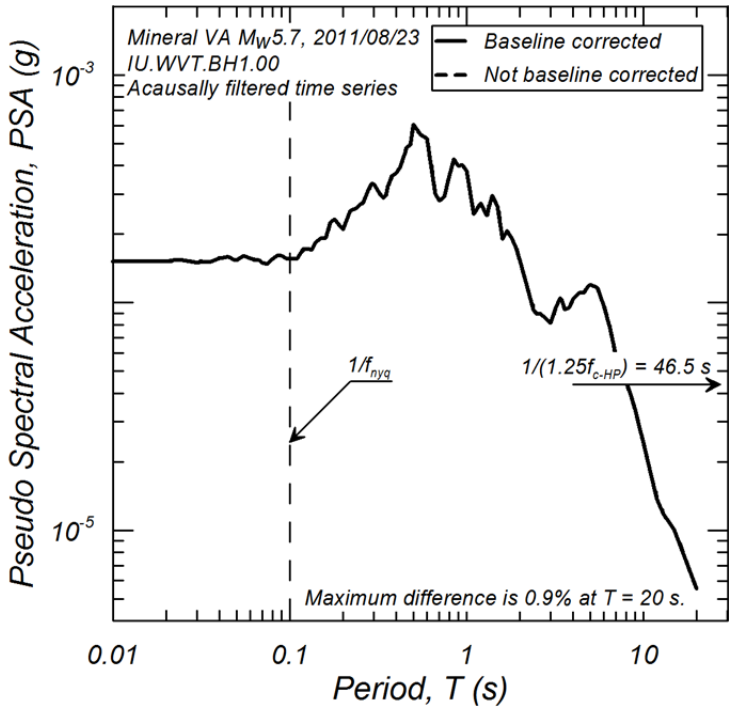

Figure 3.19 **Effect of baseline correction on PSA for acausally filtered time series.**

3.4.6 Treatment of Microseisms

Microseisms not related to earthquake processes can sometimes dominate in time series when these are recorded from small magnitudes events at large distances. Figure 3.20 shows example FAS from a record affected by microseisms. Note that by comparing the FAS for the entire window to the noise window that the time series is affected by microseisms for frequency ranges between 0.13–0.23 Hz (magenta line). Outside of that frequency range, the noise FAS is mostly flat. If the $f_{c\text{-}HP}$ is selected at 0.23 Hz, the processed records lose usable frequencies from 0.055–0.15 Hz, below the microseisms range. On the other hand, if the $f_{c\text{-}HP}$ is selected at 0.055 Hz, the processed record includes the microseisms. For NGA-East, we decided to keep the entire range usable frequencies by selecting the lower bound of $f_{c\text{-}HP}$ (i.e., $f_{c\text{-}HP}$ = 0.055 Hz in the example record). However, the frequency ranges affected by microseisms are also provided in the flatfile, allowing users to bypass that range of frequencies in their analyses, depending on their specific application. Figure 3.21 shows the acceleration, velocity and displacement time series for the example record in Figure 3.20 after applying the high-pass filter with $f_{c\text{-}HP}$ of 0.055 Hz. The figure shows that microseisms can be visible in the velocity and displacement waveforms in the pre-event noise and Coda. This feature therefore comes for a deliberate choice at the project level, and not from a mistake or oversight in processing.

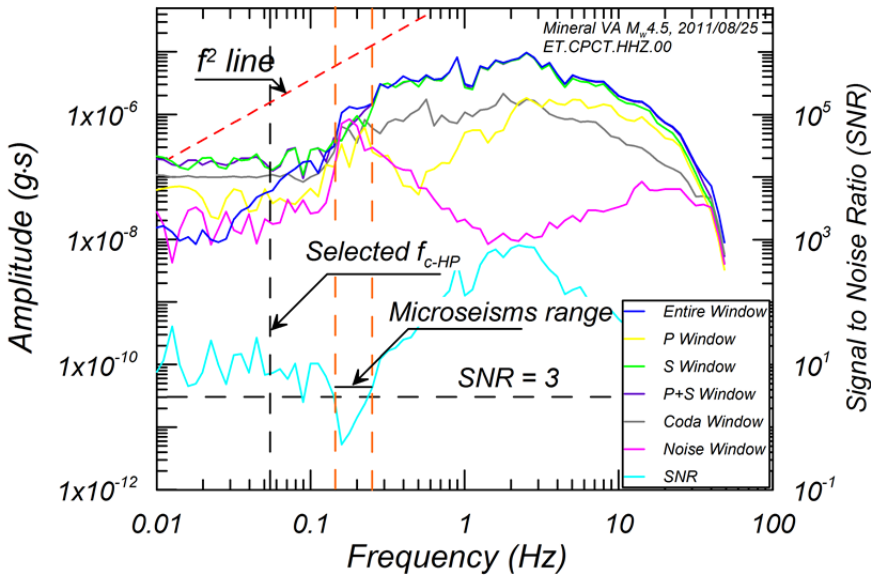

Figure 3.20 FAS affected by microseisms.

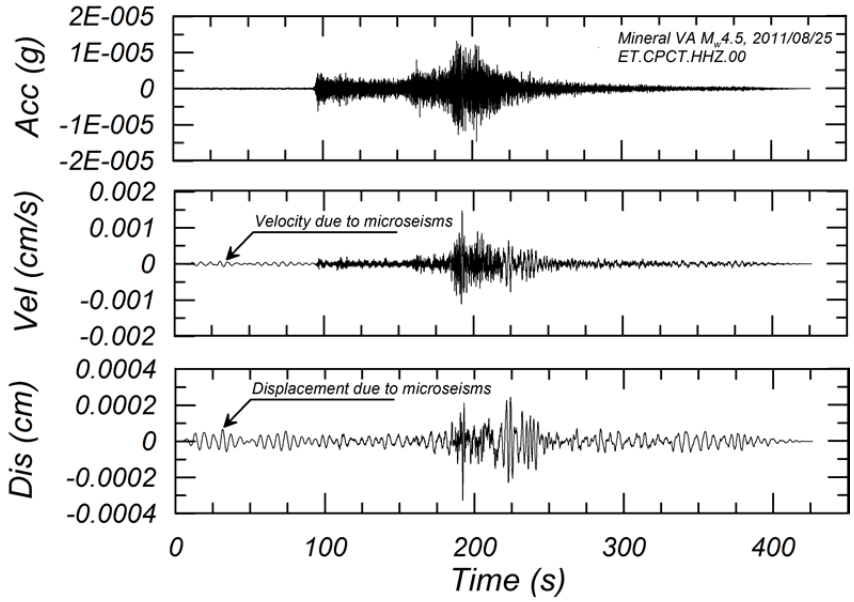

Figure 3.21 Acceleration, velocity, and displacement time series

3.4.7 Processing Information Table

As the time series are processed, the processing information is saved into a table for each record, using the record sequence number as the reference. Relevant information saved in the table includes the various windows start and end points, the corner frequencies, the microseisms bandwidths as well as additional quantities to be merged with the final project flatfile (Chapter 6).

4 Earthquake Source Table

4.1 ORGANIZATION AND OBJECTIVES OF EARTHQUAKE SOURCE TABLE

The earthquake source table contains basic information about the seismic source, including earthquake origin date and time, moment magnitude, hypocenter location, focal mechanism, among other metadata. As discussed in Chapter 2, the initial collection of data led to a list of 94 candidate earthquakes for the NGA-East database. Finite fault models for three CENA earthquakes were collected and systematically evaluated while one was taken from the PEER NGA-West1 project. The finite fault model provided additional information such as the dimension of fault rupture and depth to the top of rupture.

The key contents of the source table that are merged into the flatfile include the event name, time, magnitude, location, mechanism, and finite fault geometry (strike, dip, length, width, top of rupture, etc.). This information provides the GMPE developers with consistent source parameters and classifications for all the earthquakes in the NGA-East dataset. The complete source table contains additional detailed information that is provided as part of the documentation. Section 4.2 details the finite fault review methodology and the selected finite fault models included in the earthquake source table. Selection of the source parameters including event magnitude, hypocenter location, and focal mechanism for other events are detailed in Section 4.3. Distance metrics are then computed for known finite-fault geometries. When a finite fault geometry was not available, an updated version of the methodology used by Chiou and Youngs [2008] for simulating unavailable source parameters was applied. A description of method is included in Section 4.4. An event classification (aftershock/mainshock) developed by Wooddell and Abrahamson [2014] and utilized in the NGA-West2 project is also used for the NGA-East events. The classification method detailed in Section 4.5 is intended to reduce inconsistent event selection between the GMPE developer groups. Finally, Section 4.6 documents the adoption of the potentially induced events (PIE) flag provided by the USGS National Seismic Hazard Mapping Program (NSHMP).

4.2 FINITE FAULT MODELS

An earthquake's finite fault model is a critical piece of information from which numerous other source and path data were derived. The finite fault geometry can be defined by the end points of the top edge of rupture, the depth to the bottom edge of rupture, the fault dip angle, and the strike direction (Figure 4.1). The finite fault geometry is typically obtained, in the order of preference,

from field observation of primary surface rupture, co-seismic slip distribution obtained by inversions of waveform and geodetic data, and observation of aftershock distribution.

The available finite fault models for events in the NGA-East database are summarized in Table 4.1. One out of the four models was taken from the NGA-West1 project. The NGA-West1 finite fault models were built on three model collections previously used in ground-motion studies: PEER-NEAR [Silva et al. 1999], USGS-Yucca Mountain (YM) [Spudich et al. 1996], and Chiou et al. [2000].

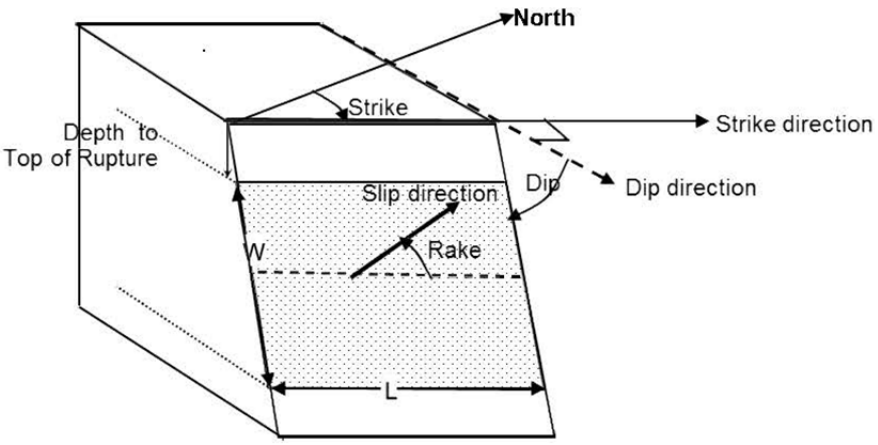

Figure 4.1 Schematic representation of strike, dip, rake, depth to top of rupture (Z_{TOR}), down dip width (W), and length (L).

Information about each finite fault model was extracted from the available publications and converted to a uniform format and to a latitude/longitude coordinate system. The areal extent of the rupture was a main issue in evaluating the finite fault model. When a model included regions of zero or low level of slip near the edges, the model area was reduced or trimmed back. For example, the model selected by PEER-NEAR for the **M**6.9 Nahanni earthquake was trimmed using the 70-cm slip contour. The trimmed model reduces the fault length from 48 km to 33.6 km, fault width from 20 km to 17.57 km.

Table 4.1 Available finite fault models for earthquakes in NGA-East.

EQID	Earthquake Name	Year	M	Reference
70	Nahanni, Northwest Territories	1985	6.76	Hartzell et al. [1994]
5	Saguenay, Québec	1988	5.85	Hartzell et al. [1994]
32	Rivière-du-Loup, Québec	2005	4.65	SLU [2014]
88	Mineral, Virginia	2011	5.74	Chapman [2013]

4.3 EARTHQUAKE SOURCE PARAMETERS

Finite fault inversions are typically not available for events with moment magnitude less than about five. As most events in the NGA-East database have a magnitude less than five, the source parameters were chosen from earthquake and moment tensor catalogs or publications as available. Parameters that are typically available in the catalogs or in the literature included the event time, magnitude, strike, dip, rake, hypocenter location, and hypocenter depth. Appendix B documents the assessments for each earthquake in the NGA-East database.

Magnitude assignments for each event were based on data collection and magnitude estimates from both the NGA-East and EPRI [2013] database working groups. Both working groups collected magnitude estimates from the literature and the final comprehensive list is contained in the source table.

The earthquake size measure selected for use in the NGA-East project is moment magnitude (**M**) related to seismic moment, M_0, by the Hanks and Kanamori [1979] relationship:

$$\mathbf{M} = 2/3log(M_0\ in\ dyne - cm) - 10.7 \tag{4.1}$$

When multiple estimates of M_0 were available, each was converted to **M** using Equation (4.1) and the resulting values averaged. If estimates of M_0 were not available for an earthquake, then **M** was estimated from other magnitude scales using the relationships developed in Chapter 3 of NUREG-2115 [EPRI/DOE/NRC 2012]. The earthquakes with magnitude estimated from other size measures are listed Table 4.2.

Table 4.2 Earthquakes in NGA-East with M estimated using relationships from NUREG-2115.

EQID	Earthquake	Date	M
27	St Teresa, MX	4/6/2004	4.31
28	La Baie, QC	5/4/2004	2.87
36	Hawkesbury, ON	2/26/2006	2.59
44	Cobourg, ON	7/19/2007	2.80
45	Baie Saint Paul, QC	1/3/2008	2.77
50	Buckingham, QC	6/11/2008	2.97
52	Pine Forest, SC	12/16/2008	3.16
53	Rosehill, SC	1/29/2009	2.77
54	Palmetto, SC	5/6/2009	2.18
55	Constance Bay, ON	5/8/2009	2.57
59	Lebanon, IL	5/21/2010	2.62
61	St. Flavien, QC	7/23/2010	3.51
68	Concord, NH	9/26/2010	3.05
69	Nahanni, NWT foreshock	11/9/1985	4.4
71	Nahanni, NWT aftershock	12/23/1985	5.1
83	Val-des-Bois, QC aftershock	6/24/2010	2.57
84	Val-des-Bois, QC aftershock	7/22/2010	2.37

Epicentral locations were selected from special studies of individual earthquakes published in the literature, if available. Otherwise, the location was taken from online catalogs (the ANSS catalog for earthquakes located in the U.S. or the NRCAN catalog for earthquakes located in Canada).

Two types of depth data are available. The standard catalog depths are the reported hypocentral depths. However, for many earthquakes, a moment centroid depth is reported as part of the central moment tensor solution. In most cases, the difference between these two depths is larger than the typical dimensions of rupture for the reported earthquakes. Where available, the moment centroid depth was selected as it is consistent with the calculated seismic moment used to define the magnitude. The hypocentral depths from on seismic network location reporting typically have significant uncertainty because of sparse station density. Both depths are reported in the source table when available. When multiple depths are reported based on different moment tensor solutions, the average depth was selected, consistent with the averaging of the magnitude estimates.

Focal mechanisms are taken from the SLU website or published literature. If a preferred plane is indicated by the source, it is selected as the only focal plane. Otherwise, both planes are used in estimating distances. Where multiple focal mechanisms are reported, a single focal mechanism solution is selected for use in estimating distance measures. It is expected that minor differences in focal mechanism parameters will produce only small differences in estimated distances. Unresolved fault planes are treated as a source of uncertainty in the calculation of distance measures (Section 4.4).

If a high-quality moment tensor solution (or fault plane solution) is not available for an earthquake, then its strike and dip are estimated from other associated events in the same region. Unknown fault strike is treated in the calculation of distance measures as a uniformly distributed random variable between -180° and 180°. The selected unknown fault strike is based on the methodology described in Section 4.4.

4.4 METHOD OF SIMULATING A FINITE FAULT GEOMETRY

In the interim NGA-East flatfile reviewed by the EPRI [2013] study, distance metrics such as the closest distance to the surface projection of the fault rupture plane, Joyner-Boore distance (R_{JB}), and the closest distance to the fault rupture plane (R_{RUP}) were missing. Similar to NGA-West2, a decision was made by the NGA-East project to adopt a method to simulate finite fault planes for events without a finite fault model but with minimal information of hypocenter, magnitude, and fault plane solution (or style of faulting). The goal of the simulation routine is to obtain an approximate fault rupture geometry that may be used to compute distance metrics and a few other path data (such as, the fault rupture width W, and the depth to the top of the rupture, Z_{TOR}) that require knowledge of finite fault geometry.

The simulation methodology described here is a modified procedure from Chiou and Youngs [2008] Appendix B. During the NGA-West2 project the methodology was modified to provide a more stable simulated finite fault when recordings are removed or added to the event. In this methodology, the missing fault plane information is filled in by random sampling of pertinent probabilistic distributions of fault ruptured area, aspect ratio of ruptured area, and hypocenter position on the fault plane, as summarized in Table 4.3. The simulation routine

generates a set of 101 random fault ruptures that are rotated and translated in space but fixed on the given hypocenter location. The strike and dip is fixed if reported. The routine computes the median R_{RUP} value of the 101 simulated ruptures using a grid of pseudo stations (700 spaced around the epicenter at epicentral distances from 0 to 300 km). A simulated rupture is selected based on a minimization of the squared difference between each pseudo-station median R_{RUP} value for all ruptures and that rupture.

Table 4.3 Summary of assumed probabilistic distributions of parameters used in finite fault simulation procedure.

Parameter	Distribution/reference
Rupture area	Somerville et al. [2001]
Aspect ratio	Chiou and Youngs [2008]
Hypocenter location down dip	Chiou and Youngs [2008]
Hypocenter location along strike	Chiou and Youngs [2008]

4.5 EVENT CLASSIFICATION: CLASS 1 VERSUS CLASS 2

Over the past twenty years, it has been observed that median ground motions from aftershocks are systematically lower than median ground motions from mainshocks by about 20–40% at short spectral periods [Boore and Atkinson 1989; Boore and Atkinson 1992; and Abrahamson and Silva 2008]. One possible explanation for this is that the mainshock rupture has reduced the stress on the fault surface and surrounding rocks. Aftershocks then may have lower stress drops and correspondingly reduced short-period source spectra. In contrast, seismic moment controls the long period spectral levels and hence no difference is observed. Given these observations, ground motion model developers have accounted for this difference either by removing aftershocks from the dataset [Boore and Atkinson 2008; Campbell and Bozorgnia 2008], or by including a term to account for a constant scale factor between mainshocks and aftershocks [Abrahamson and Silva 2008; Chiou and Youngs 2008].

However, classifying an earthquake as a mainshock or aftershock is not a straightforward problem. In terms of ground motion, not all of these aftershock types systematically produce similar median ground motions. Based on observations reported in Wooddell and Abrahamson [2014], triggered events that occur at some distance from the mainshock rupture plane, which are often called aftershocks, may have median ground motions that are similar to mainshocks of similar magnitude (presumably because the mainshock rupture did not significantly reduce the stress on these other faults). However, events closer to the rupture plane were found to exhibit smaller median short-period ground motions than mainshocks, as had been found previously. Given these observations, earthquakes in the NGA-East database are grouped into two classes based on their distance to the rupture plane of the main event and their time with respect to the main event. Following Wooddell and Abrahamson [2014], Class 1 earthquakes are mainshocks, triggered events, or foreshocks that occur off the surface projection of the mainshock rupture plane, and Class 2 earthquakes are the earthquakes that occur within or near the surface projection of the mainshock rupture plane and within a time window for aftershocks. The hypothesis is that the earthquakes occurring within the fault plane or damaged region of the main

event have a systematic bias toward lower median ground motion due to the lower stress drops from these earthquakes that re-rupture the fault plane. This is consistent with the results of Baltay et al. [2013], which showed that, on average, the stress drops for the mainshocks (Class 1 earthquakes) in the NGA-West2 dataset are about 1.6 times higher than the stress drops for the aftershocks (Class 2 earthquakes).

4.5.1 Methodology

The mainshock flag in the NGA-East database is used to select earthquakes for use in the attenuation model development. A MatLab script is used to distinguish Class 1 events (mainshocks, foreshocks, triggered events, and off-plane aftershocks) from Class 2 events (aftershocks that re-rupture the mainshock fault plane or occur within the damaged zone within a time window for aftershocks). This procedure is based on a windowing method that designates an event as a Class 2 event if it occurred inside the spatial and temporal windows of a larger Class 1 earthquake. The windowing approach used for the classifications in the NGA-West2 database uses the Gardner and Knopoff [1974] time window and a distance window based on the shortest distance between the centroid of Joyner-Boore rupture surface of the potential Class 2 earthquakes and the closest point on the edge of the Joyner-Boore rupture surface of the Class 1 mainshock. We call this the centroid Joyner-Boore distance CRJB. Justification of the new CRJB distance can be found in Wooddell and Abrahamson [2014]. Figure 4.2 shows examples of how the CRJB distance metric is defined. In Figure 4.2 the red lines are the surface projections of the top of the rupture planes, the dashed lines are the surface projections of the rupture planes, the yellow star is the epicenter of the Class 1 mainshock, and the orange stars are the epicenters of the aftershocks (potential Class 2 earthquakes).

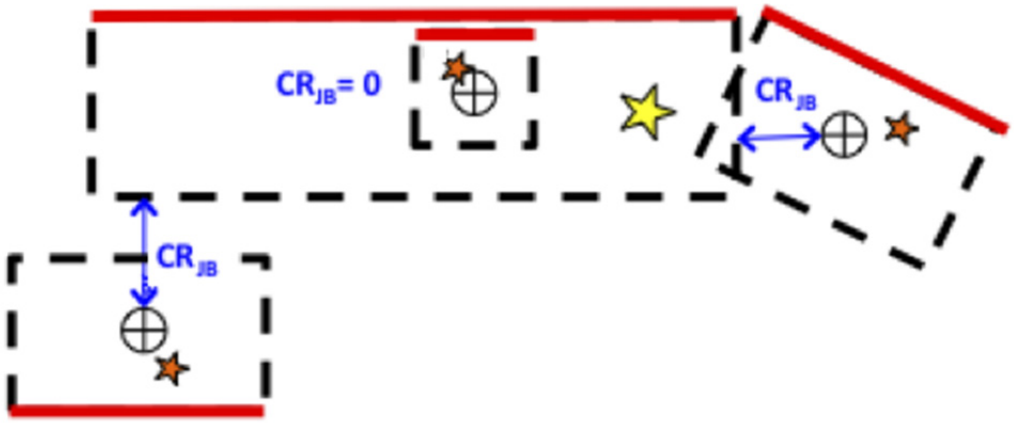

Figure 4.2 Definitions of the CRJB distance metrics.

Rupture plane geometries associated with earthquakes in the NGA-East database were used to estimate the CRJB distance metric and the Gardner and Knopoff time. The distance and time windows were used to classify the NGA-East earthquakes. Currently, the database includes sets of columns for the results of the classification algorithm because the results can change as different values of the cutoff CRJB are used. For example, if the algorithm is run using a cutoff

CRJB of zero, then only earthquakes that have a fault plane centroid within the surface projection of the Class 1 rupture plane are Class 2 earthquake candidates. If, however, a cutoff CRJB of 20 km is used, the algorithm will allow earthquakes with rupture plane centroids up to 20 km from the surface projection of the Class 1 rupture plane to be considered Class 2, as long as they are within the time window for aftershocks.

4.6 EVENT CLASSIFICATION: POTENTIALLY INDUCED EVENTS

The CENA region has seen a sharp increase in earthquake activity rates since the mid-2000s [Ellsworth 2013], and it has been suggested that much of the upsurge is related to underground fluid injection. Research is currently on-going to better understand and characterize those earthquake events relative to those traditionally associated with natural processes. There is currently no clear method for discriminating between induced and natural (or tectonic) events. In addition, it is still unclear at this point if (or how) ground motions from this type of events are different than for naturally occurring events. The study of this issue will continue well beyond the NGA-East project completion date. The NGA-East approach is to provide a flag for those Potentially Induced Events (PIEs), which were identified as such by the USGS National Seismic Hazard Mapping Program (NSHMP) 2014 development team, as described below.

Because the USGS maps underpin long-term engineering and public-policy guidelines like building codes, the NSHMP concluded it was undesirable for the seismic hazard to be conditional on unpredictable industrial activity that can start or stop for commercial or policy reasons. On this basis, the USGS identified and deleted these earthquakes from the catalogs that were used for the building-code hazard maps. Sequences were identified using information from the literature, and their extents are estimated by looking for suspicious activity within local sub-catalogs, parameterized by simple time windows and spatial polygons [Petersen et al. 2014]. The USGS PIE flags were added to the NGA-East earthquake source table, but contrary to the 2014 NHSMP, NGA-East did not exclude records from these events from the final database, leaving this choice to the database user.

5 NGA-East Station Database, V_{S30} Assignment

5.1 INTRODUCTION AND SCOPE OF STATION DATABASE (STDB)

The NGA-East flatfile contains ground motion intensity measures and supporting distance, path, and site parameters for use in the development of GMPEs for CENA. Site parameters for the stations in the flatfile are taken from the station database (StDB), which contains information on site condition and housing for the 1379 stations with recordings in the project flatfile. The site information was originally compiled from the station table developed by CERI team and dated 2013-02-28. That table was merged with the updated station metadata table released within NGA-East on 2014-04-15. The site parameter investigated is the time-averaged shear wave velocity in the upper 30 m (V_{S30}).

Values of V_{S30} have been measured for 84 of the 1379 stations (6%). For the other 1295 stations, V_{S30} is estimated from various sources. Values of V_{S30} are estimated for a majority of sites using proxies, which is also common practice for active crustal regions [Chiou et al. 2008; Seyhan et al., 2014]. The most commonly available proxies for the stations in the database are geology, terrain, and slope, which are available for 1375 (99.7%), 1367 (99.1%), and 1375 (99.7%) of the sites, respectively. Section 5.4 describes proxy-based methods for estimating $V_{S30}$from this data, which use geology only, slope only, terrain only, and a hybrid of slope and geology. In addition to proxies, the StDB also contains estimates of V_{S30} using a *P*-wave seismogram method [Kim et al. 2014], which is based on recorded ground motions and increases in accuracy as more ground motions are available for a site. The StDB contains p-wave estimates derived from single recordings for 42 sites and from multiple recordings for 81 sites (6%).

The categories of information contained in the StDB are as follows:

- Station metadata including name, location, and housing
- V_{S30} values derived from measurements
- Available proxies for the site, including geology, terrain category, and slope
- Inferred values of $V_{S30}$from known geology and local conditions (site visited)
- Proxy-based estimates of V_{S30} using ground slope, surface geology, terrain, and hybrid slope-geology methods.
- Estimates of V_{S30}derived from *P*-wave methods (utilizing ground motion data)
- Recommended values of V_{S30} with identification of the basis for the recommendation
- Recommended values of V_{S30} dispersion

The objectives of this chapter are to: (1) document key changes relative to the original CERI-developed station table; (2) describe principal sources of V_{S30} measurements; (3) identify proxy-based methods for estimating V_{S30}, and (4) explain the protocols developed for assigning preferred V_{S30} values and their uncertainties to a site conditioned on the amount of information available from proxies and measurements in CENA. The methods and formulations are modified only slightly from those developed during the NGA-West2 Project as presented in Seyhan et al. [2014] and in Ancheta et al. [2014]. Appendix B contains the complete StDB in Excel format and an explanation of column headings.

5.2 STATION METADATA

Considerable effort was dedicated to updating the station metadata assembled by the CERI team. The original station table was developed on an instrument-specific basis, which can be impractical for GMPE development, as briefly discussed below. The organization of the station metadata data was therefore modified to location-specific basis.

In the CENA region, including parts of Canada and the U.S., there are often several seismic instruments at a single location (such as broadband or high-gain seismometers and/or strong-motion accelerometers). Some instruments were permanently removed at some point. The evolution of the specific instrumentation layout is continuous, involving changes such as sensor type, gain level settings, and/or digitizers over time, but the location of these instruments tends to remain essentially fixed, which we refer to as a *station*. In addition, a single instrument can also have different names depending on the network operator responsible for distributing the data at a given time. This is especially true for stations shared by Canada and the U.S. or, for example, when data is distributed from the GSC, IRIS, and/or SLU data centers (see Chapter 1 for details).

In the context of NGA-East GMPE development, each record is processed individually and its specific bandwidth is reported in the project flatfile. Keeping instruments separate in the station flatfile is not only unnecessary but can lead to incorrect statistics during model development. That would be the case, for example, if recordings of a single event from co-located instruments are treated as independent measurements. One key change relative to the original station file was therefore to designate a unique station ID number to each "station," independently of the number of instruments installed at that location. This station ID was selected from those available in the original station table. Alternate station IDs and names for stations shared between networks are also provided in the current version of the StDB and alternate instrument designations were also collected and documented whenever possible. Keeping the alternate station IDs for each station allows cross-referencing between the older station files and the officially released ones. The different V_{S30} estimates discussed below are therefore associated with a single site (station) at which one or more instrument(s) recorded earthquake ground motions.

5.3 DATA SOURCES AND DISTRIBUTION OF V_{S30}

The V_{S30} values in the NGA-East StDB are from a variety of sources and are summarized in Table 5.1. Many sources of V_{S30} values are available in the open literature. The distribution of V_{S30} values derived from measurements are shown in Figure 5.1. The small number of strong

motion sites with geophysical measurements is in contrast to the situation for active crustal regions, where approximately 50% of recordings stations have V_{S30} from measurements [Seyhan et al. 2014].

Table 5.1 Sources of geophysical data for CENA stations.

Measurement Source	Count
Beresnev and Atkinson [1997]	9
Paul Mayne [*personal communication, 2011*]	9
Dames and Moore [1974]	1
EPRI [2013]	33
Ghofrani and Atkinson [2014]	1
GCS CNSN online station book [2014]	1
Herrmann and Crossey [2008]	1
Jaume [2006)	5
Lin and Adams [2010]	1
Karen Assatourians [*personal communication, 2011*]	2
Chris Cramer [*personal communication, 2013*]	2
Odum et al. [2010]; USGS NGMD	5
Read et al [2008]	2
Saint Louis University Earthquake Center [2014]	4
USGS ANSS [2013]	2
Kayen et al. [2014]: in preparation	1
Williams et al. [2003]	5

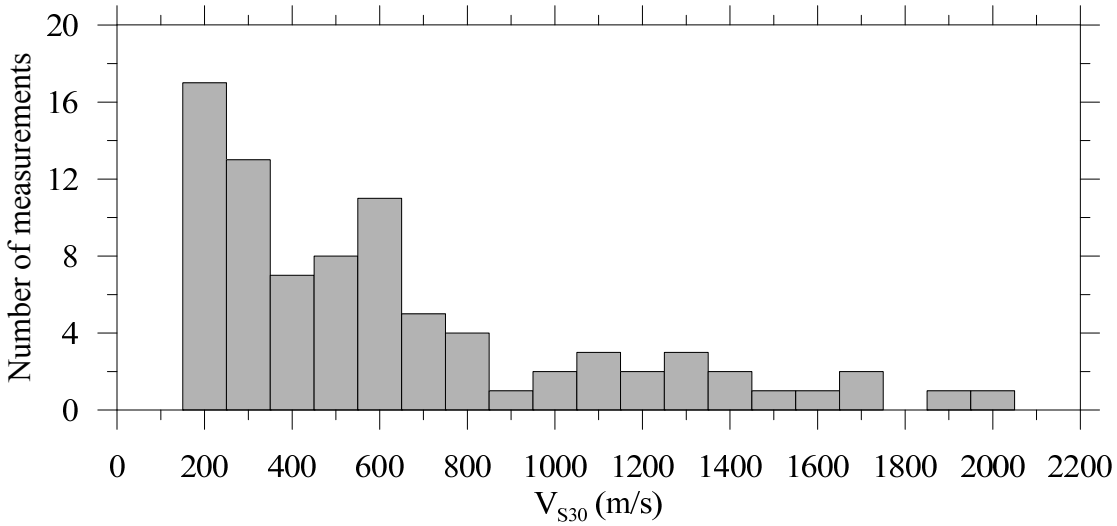

Figure 5.1 Histogram of V_{S30} measurements in the NGA-East station database.

5.4 PROXY-BASED ESTIMATION OF V_{S30}

5.4.1 Available Proxies

Various descriptors or quantitative metrics of site conditions have been proposed to develop estimates of V_{S30} in the absence of measurement. In the NGA-East project, the development of these estimates is critical because only 6% of considered recording stations have measurements. The methods and proxies considered in this study are: (1) V_{S30} estimation using ground slope at 30 arc-sec resolution [Wald and Allen 2007; Allen and Wald 2009]; (2) V_{S30} estimation using a geomorphological terrain proxy [Yong et al. 2012]; (3) V_{S30} estimation based on surface geology [Kottke et al. 2012]; (4) V_{S30} estimation by a hybrid slope-geology proxy [Thompson and Silva 2013]; and (5) V_{S30} estimation by *P*-wave seismogram method [Kim et al. 2014].

Kottke et al. [2012] developed a procedure to estimate V_{S30} from surface geology. We utilize relatively small-scale (1:2,000,000) digital maps for the U.S. [Fullerton et al. 2003] and 1:5,000,000 scale maps for Canada [Fulton 1986]. There are two potential issues with these maps: (1) in some cases the maps represent true surface geology, whereas in other they are bedrock geology maps (soil not included); and (2) due in part to the small scale, there are occasions where sites of interest (strong-motion stations) plot in bodies of water. The issue of variable meaning of the mapped geology has not been resolved as of this writing, and the current applications are based on the mapped geologic unit regardless of map type. When geologic unit is not available (typically because a site plots in a body of water), a global average value of V_{S30} is assigned based on the database compiled by Kottke et al. [2012]. For the stations in this database, 1083 (79%) have estimates based on mapped geology and 292 (21%) use the global estimate.

The hybrid slope-geology proxy by Thompson and Silva [2013] provides two estimates for V_{S30}, which are referred to as 'actual' and 'effective'. The 'actual' value is based on a V_{S30} measurement that is in the vicinity of the station. The 'effective' value is adjusted from the 'actual' based on inferences of different surface geology at the measurement location and the instrument location (typically, shallow soil at measurement and inferred rock at surface for instrument). We use the 'actual' V_{S30} over the 'effective' V_{S30} to allow for comparison to V_{S30} measurements that may not have been corrected. The electronic supplement of this document provides both 'effective' and 'actual' V_{S30} estimates by hybrid slope-geology, but only the 'actual' estimates are considered here.

The *P*-wave seismogram method [Kim et al. 2014] allows for a V_{S30} estimate to be made at a location if a ground motion recording is available. The accuracy of this approach improves when more than one ground motion recording is available at a site. The electronic supplement of this document provides all available V_{S30} estimates by the *P*-wave seismogram method, but only estimates derived from more than one ground motion recording are evaluated.

5.4.2 Proxy Evaluation

The reliability of proxy-based estimations of V_{S30} in CENA is evaluated by comparing predictions of V_{S30} to values derived from geophysical testing. For each site i where a value of V_{S30} is available from geophysical measurements, the residual, R_i is calculated as:

$$R_i = \ln\left(V_{S30}\right)_i - \overline{\ln\left(V_{S30}\right)}_{(proxy,i)} \tag{5.1}$$

where $\ln(V_{S30})_i$ is the measurement-based V_{S30} for a site, *i,* and $\overline{\ln\left(V_{S30}\right)}_{(proxy,i)}$ is the proxy-based estimate of V_{S30} for site *i*. Model bias is estimated as the mean of the residuals (μ_{lnV}), and the standard deviation of the residuals is represented as (σ_{lnV}). This analysis of residuals is based on the small dataset of 84 strong motion sites having geophysical data. The much larger profile database compiled by Kottke et al. [2012] will be used in future work for residuals analysis Figure 5.2 shows the distribution of residuals for each proxy-based estimation method considered in this study.

The relative efficacy of the different proxy-based estimation techniques can be judged on the basis of bias and standard deviation of the residuals (μ_{lnV} and σ_{lnV}). Figure 5.3 shows these quantities at sites distinguished by proxy availability. Only 34 stations in the NGA-East StDB have all considered V_{S30} estimates and measured V_{S30} values available. The most substantial limitation is for sites for which multiple estimates by the *P*-wave seismogram method are available. Note that estimates by the terrain, slope, and geology-hybrid techniques have substantial bias, whereas geology and *P*-wave methods are relatively unbiased. Standard deviations of the proxy-based estimates are much higher than is typical in active crustal regions (0.35–0.45) [Seyhan et al. 2014]. Among the methods considered, the *P*-wave seismogram estimates of V_{S30} have the smallest dispersion.

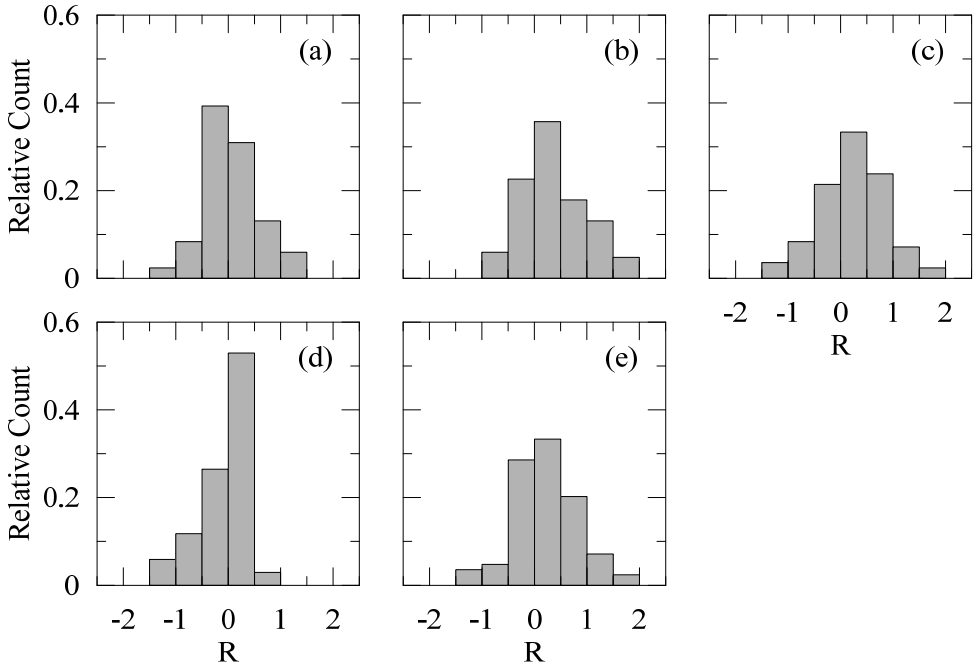

Figure 5.2 **Residual of proxy-based estimations at sites where available for (a) geology [Kottke et al. 2012], (b) terrain [Yong et al. 2012], (c) slope [Wald and Allen 2007, (d) *P*-wave seismogram with multiple estimates [Kim et al. 2014], and (e) hybrid slope-geology [Thompson and Silva 2013].**

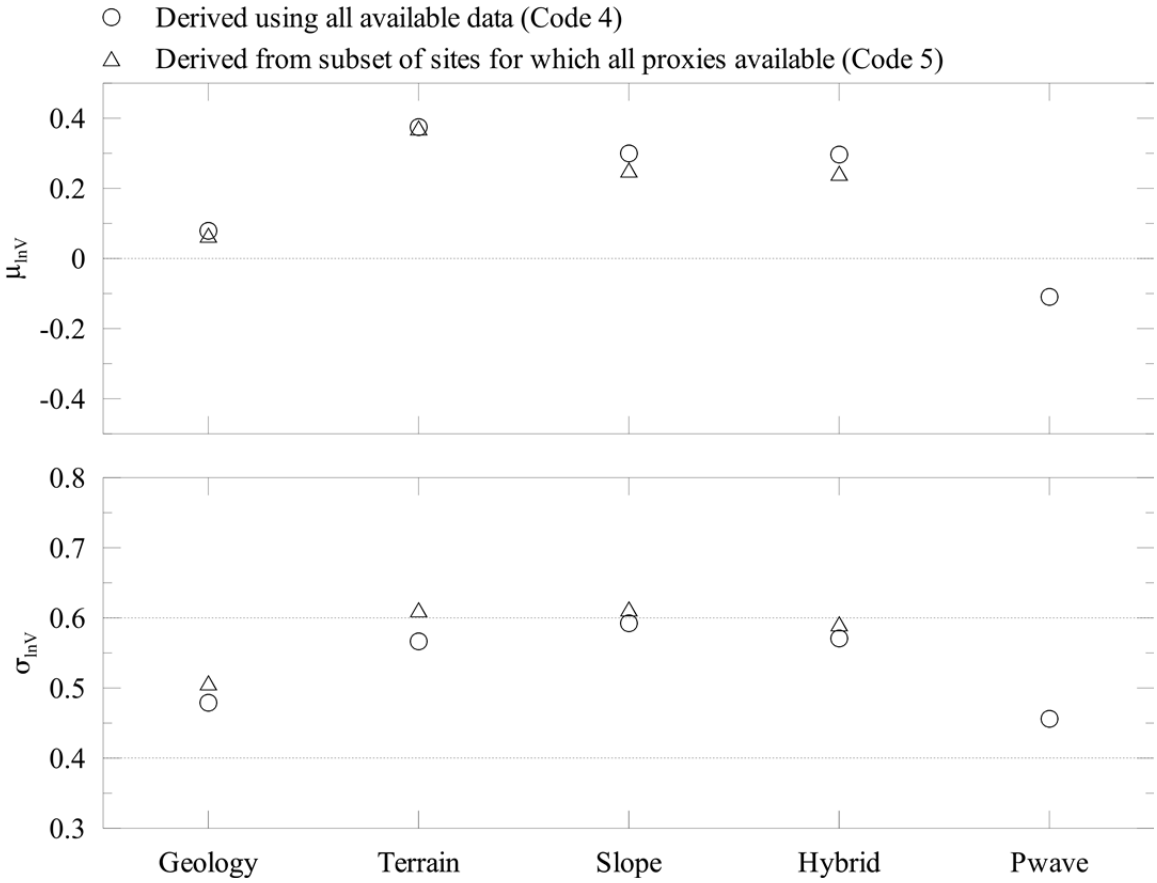

Figure 5.3 **Average residual and standard deviation on the residual for Geology [Kottke et al. 2012], Terrain [Yong et al. 2012], Slope [Wald and Allen 2007], Hybrid [Thompson and Silva 2013] and *P*-wave [Kim et al. 2014], of V_{S30} estimates by proxy at recording stations. Circles represent the residual on the V_{S30} at the 34 recording stations that have estimates of V_{S30} by all proxy methods. Triangles represent the residual on the V_{S30} over all stations where the proxy-based estimate is available.**

5.5 PREFERRED V_{S30} AND ITS UNCERTAINTY

5.5.1 Method of Selecting Preferred V_{S30}

The process by which "preferred" V_{S30} values are assigned in the StDB is as follows (number corresponds to codes in the StDB file):

0. Assign V_{S30} from measurement
1. Assign V_{S30} from known site conditions and geology based on measurements at different location but the same geological condition. This assignment is only used based on a recommendation or site visit from a geologist.

2. Estimate by *P*-wave seismogram method [Kim et al. 2014] for sites having multiple ground motion recordings and corresponding V_{S30} estimates. This code is applied specifically for sites where the estimated $V_{S30} \geq 760$ m/sec.
3. Estimate by hybrid slope-geology [Thompson and Silva 2013]. This code is applied specifically for sites where the estimated $V_{S30} \geq 760$ m/sec.
4. Use weighted average of V_{S30} estimates from all available proxies, including those from the *P*-wave seismogram method when multiple ground motions are available for the *P*-wave estimate.
5. Use weighted average of V_{S30} estimates from all available proxies. This code is used when estimates from the p-wave seismogram method are not available.

The codes are ranked in ascending order of priority for V_{S30}assignment. Code 1 requires knowledge about the placement and location of the specific station in question. As part of the study by Beresnev and Atkinson [1997], some stations in the CENA region had an inferred V_{S30} of 2000 m/sec based on firm rock measurements and site investigations, so for this study, the inferred V_{S30} values were used where available for Code 1 assignment. There were also sites with V_{S30} inferred from known site condition and documented in a series of personal communications between the database developers; see Appendix B. For the use of Code 1, geologic condition is typically verified by site visit by geologist; this is the most common code for firm rock conditions.

Codes 2 and 3 use the estimation of V_{S30} by the *P*-wave seismogram method [Kim et al. 2014] and hybrid slope-geology approach of Thompson and Silva [2013]. Other proxy methods evaluated in this study do not provide fast V_{S30} estimates corresponding to hard-rock site conditions. It is for this reason that special consideration is given to V_{S30}estimates higher that 760 m/sec from these two methods.

The weights of V_{S30} estimates for Codes 4 and 5 are based on the proxy mean and standard deviation of residuals ($\mu_{ln(V)}$ and $\sigma_{ln(V)}$). A relative weight is taken from the inverse of the residual sum of squares of the mean and standard deviation of the proxy as follows:

$$\text{Relative weight for selected proxy} = \frac{1}{\mu^2_{\ln(V)} + \sigma^2_{\ln(V)}} \tag{5.2}$$

This weighting functional form, which is related to the mean square error (MSE), assesses the quality of the proxy methods in terms of both their variation and degree of bias. The actual weight is computed from the relative weights through adjustment to ensure they sum to one. Tables 5.2 and 5.3 show the relative weights and proxy weights for use with Codes 4 and 5 preferred V_{S30} assignment, respectively. If only a subset of proxies is available for V_{S30} assignment, the weights are adjusted to sum to unity for those proxies. For example, if V_{S30}estimates are only available from terrain and geology proxies, the relative weights would be 0.37 and 0.63, respectively.

Figure 5.4 shows the distribution of code assignments for assigning recommended values of V_{S30} at all stations in the StDB. Figure 5.5 shows the distribution of the recommended values.

Table 5.2 **Relative proxy weights by region and applied weights for estimation of V_{S30} when all estimates are available (Code 4).**

Proxy	$\mu_{\ln V}$	$\sigma_{\ln V}$	Count	Relative Weight	Weight
Geology	0.079	0.479	34	4.24	0.27
Terrain	0.375	0.567	34	2.16	0.14
Slope	0.300	0.593	34	2.27	0.15
Hybrid	0.297	0.571	34	2.41	0.15
P-wave	-0.109	0.456	34	4.54	0.29

Table 5.3 **Relative proxy weights by region and applied weights for estimation of V_{S30} when no estimate by *P*-wave proxy is available (Code 5).**

Proxy	$\mu_{\ln V}$	$\sigma_{\ln V}$	Count	Relative Weight
Geology	0.068	0.508	84	3.80
Terrain	0.373	0.612	84	1.94
Slope	0.254	0.613	84	2.27
Hybrid	0.245	0.592	84	2.43

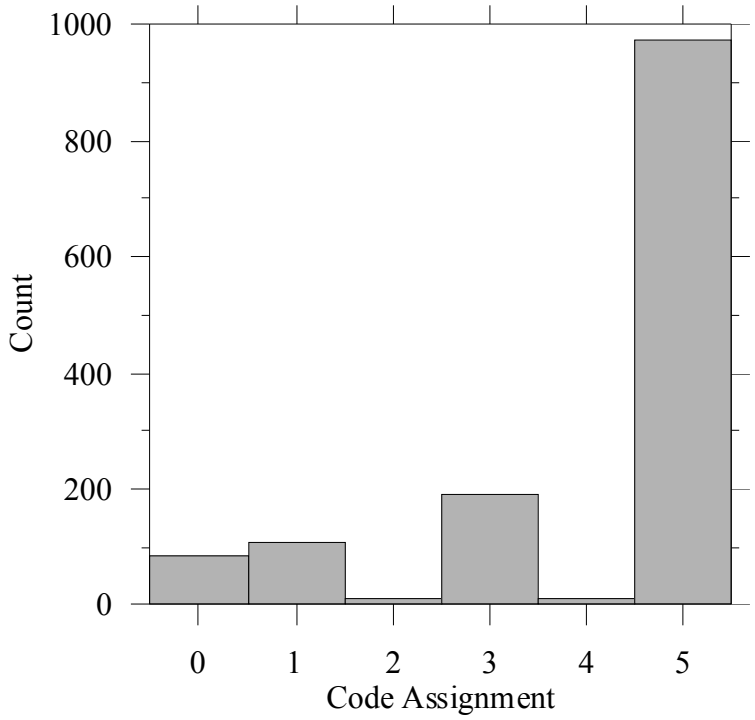

Figure 5.4 **Distribution of code assignment for recommendation of V_{S30}.**

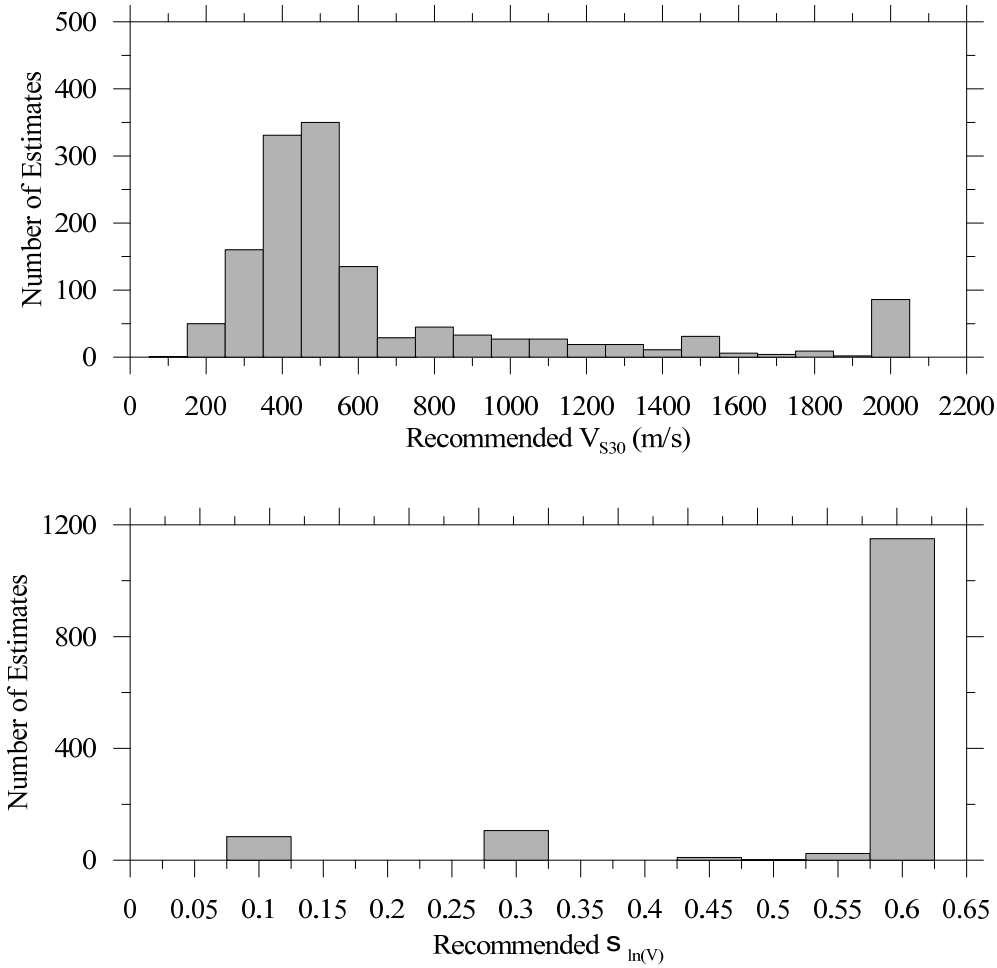

Figure 5.5 Recommended V_{S30} and $\sigma_{\ln V}$ by from Codes 0–5 assignment at all stations.

5.5.2 V_{S30} Uncertainty

The preferred V_{S30} value for a site is taken as the exponent of the mean estimate in natural log units. The assignment of epistemic uncertainty to V_{S30} is dependent on the estimation method, and the dispersion is expressed as a log standard deviation, σ_{lnV}.

5.5.2.1 Code 0 sites (sites with geophysical measurement of V_{S30})

Extensive work was undertaken in the NGA-West2 project to quantify the uncertainty of V_{S30} at locations with multiple V_S profiles [Seyhan et al. 2014]. That study found that for relatively consistent terrain, σ_{lnV} was fairly stable, and not particularly sensitive to site stiffness. For such conditions, a value of $\sigma_{lnV} = 0.1$ was found to reasonably represent the available data. This result is adopted for CENA as well, where we lack data to independently evaluate this dispersion.

5.5.2.2 Code 1 sites

Code 1 depends on inferred site and station condition. The recommended dispersion is $\sigma_{lnV} = 0.3$. This value is based on engineering judgment.

5.5.2.3 Code 2 and 3 sites

We recommend use of the σ_{lnV} values from the residuals analysis in Table 5.2, which are 0.57 for Code 2 and 0.46 for Code 3.

5.5.2.4 Code 4 and 5 sites

For the weighted proxy assignments of V_{S30}, uncertainty is assigned based on the residuals analysis. It is recommended that the site dispersion be calculated by weighting the σ_{lnV} of the site's available proxies by the values listed in Table 5.2 and Table 5.3 for codes 4 and 5, respectively. Figure 5.5 shows the distribution of the recommended values of σ_{lnV}.

6 Database Flatfile and Ground Motion Products

The NGA-East database consists of several complementary products that are linked together by the summary table referred to as the flatfile. The flatfile contains a list of all the selected and processed strong-motion records, metadata information, selected ground-motion intensity measures and the paths to a series of text files for time series, and FAS products. The flatfile is generated using the data collection file developed by CERI (Chapter 2) and by combining selected information from (1) the processing information table (Chapter 3); (2) the earthquake source table (Chapter 4); and (3) the station database (Chapter 5).

The processed acceleration, velocity, and displacement time series are provided for each available component of each recording in a format that is consistent with previous NGA database releases. The processed acceleration time series serve as input in the calculation of numerous ground motion products, including the as-processed PSA for each component, RotD50, and Arias intensity timing information, which are discussed below.

Finally, acceleration Fourier spectra files including both the amplitudes and phases are available for the processing windows described in Chapter 3. For all the intermediate windows only the instrument-corrected unfiltered Fourier spectral information is available. For the complete time series, the corresponding Fourier spectral information is available for the instrument-corrected unfiltered time series as well as for the fully processed time series.

6.1 OVERVIEW OF FLATFILE COMPONENTS AND ORGANIZATION

The flatfile lists all the available records in the database. Each record is assigned a Record Sequence Number (RSN), which is a unique identifier associated to a single instrument-event pair (e.g., record). The RSN refers to all the components of the record. Similarly, each event is assigned an earthquake identifier (EQID), and each station is assigned its own Station ID, as described in Chapters 2, 4, and 5. For NGA-East specifically, RSNs, EQIDs, and Station IDs were assigned at the time the CERI team designed the database. As records were evaluated and processed, some entries were dropped, leading to gaps in the numbering. Some records were also added to the database at a later date, so RSNs and EQIDs do not necessarily follow a natural time progression.

The flatfile information is grouped into the following categories (see Appendix C for complete flatfile fields list and documentation), with each line starting with the RSN:

- SOURCE Metadata: EQID and earthquake event metadata (extracted from the earthquake source table, Chapter 4)
- STATION Metadata: Station ID, station information and site characterization metadata (extracted from the station database, Chapter 5)
- PATH Metadata: Path metadata, including various distance metrics and regionalization information
- RECORD-SPECIFIC Metadata: Record-specific metadata, including paths and file names for time series, time steps, processing corner frequencies and quality flags (extracted from the processing information table, Chapter 3)
- GROUND MOTION INTENSITY MEASURES: intensity measures obtained from the final processed time series such as PSA and Arias Intensity timing.

The flatfile itself, along with a detailed description of each field, is provided in Appendix C. Most of the fields included in the flatfile do not require lengthy explanations, but a short description of selected intensity measures is provided below.

6.2 SUMMARY OF SELECTED INTENSITY MEASURES

The NGA-East project has selected rotated ground motion intensity measure called RotDnn described by Boore [2010b]. RotD50 is the 50th percentile (or median) PSA value computed from two horizontal components, over all non-redundant rotations is the main PSA product considered by NGA-East. The minimum and maximum rotated response spectra, RotD00 and RotD100, were also computed for the project but are not directly used in GMPE development. RotDnn provides an average horizontal PSA measure that is independence of sensor orientation. The NGA-East initial database release is for 5%-damped PSA only. Other ground motion intensity measures provided include the as-recorded three-component spectra and durations relative to the normalized Arias intensity.

6.2.1 Rotdnn

As described in Boore [2010b], the RotDnn spectra are a set of response spectra over all non-redundant rotation angles where 'nn' represents the fractile of the spectra sorted by amplitude. The 'D' indicates that rotation angle will be specific to the period of the oscillator. The RotDnn can be computed from the rotation of the two as-recorded orthogonal horizontal ground motions. For any rotation angle, θ, the rotated time series, a_{ROT}, can be computed from the orthogonal horizontal-component time series, $a_1(t)$ and $a_2(t)$, using Equation (6.1):

$$a_{ROT}(t;\theta) = a_1(t)\cos(\theta) + a_2(t)\sin(\theta) \tag{6.1}$$

The response spectra for the rotated time series are calculated for the non-redundant rotation angles 0–180°. Three fractiles, the minimum (nn = 00), mean (nn = 50), and the maximum (nn = 100) spectral amplitude are considered in the NGA-East project. Further discussion and examples can be found in Boore [2010b].

6.2.2 Duration

Duration of ground shaking can be defined as the time difference between two levels of a normalized plot of cumulative squared acceleration (i.e., Husid plots). For the NGA-East project, 19 durations are provided based on the difference in time of normalized Arias intensity, in 5% increment, from 5% to 100. The 19 different upper bound values ranged from 10 to 100% stepping by 5% increments. A text file reporting the 19 selected durations and their corresponding normalized Arias intensity was created for the horizontal components of records included in the database.

7 REFERENCES

Abrahamson N.A., Silva W.J. (2008). Summary of the Abrahamson & Silva NGA ground-motion relations, *Earthq. Spectra*, 24(1): 67–97.

Aki K. (1969). Analysis of the seismic Coda of local earthquakes as scattered waves, *J. Geophys. Res*., 74: 615–631.

Akkar S., Çağnan Z., Yenier E., Erdoğan Ö., Sandıkkaya M.A., Gülkan P. (2010). The recently compiled Turkish strong-motion database: Preliminary investigation for seismological parameters, *J. Seismol*., 14: 457–479.

Allen T.I., Wald D.J. (2009). On the use of high-resolution topographic data as a proxy for seismic site conditions (V_{S30}), *Bull. Seismol. Soc. Am*., 99: 935–943.

Ancheta T.D., Darragh R.B., Stewart J.P., Seyhan E., Silva W.J., Chiou, B.-S.J., Wooddell K.E., Graves R.W., Kottke A.R., Boore D.M., Kishida T. Donahue J.L. (2013). PEER NGA-West2 Database, *PEER Report 2013/03*, Pacific Earthquake Engineering Research Center, University of California, Berkeley, CA.

Ancheta T.D., Darragh R.B., Stewart J.P., Seyhan E, Silva W.J., Chiou B.S.-J., Wooddell K.E., Graves R.W., Kottke A.R., Boore D.M., Kishida T., Donahue J.L. (2014). NGA-West2 database*, Earthq. Spectra*, 30: 989–1005.

Assatourians, K. (2011). *Personal communication*.

Atkinson G.M., Chen S. (1997). Regional seismograms from historic earthquakes in Southeastern Canada, *Seismol. Res. Lett.*, 68: 797–807.

Baltay A., Hanks T.C., Beroza G.C. (2013). Stable stress-drop measurements and their variability: Implications for ground-prediction, *Bull. Seismol. Soc. Am*., 103(1): 211-222.

Bazzurro P., Sjpberg B., Luco N., Silva W.H., Darragh R.B. (2005). Effects of strong-motion processing procedures on time histories, elastic, and inelastic spectra: Final report, *COSMOS NO. CP-2005/02*, Consortium of Organizations for Strong-Motion Observation Systems, Richmond, CA.

Beresnev I.A., Atkinson G.M. (1997). Shear-wave velocity survey of seismographic sites in eastern Canada: calibration of empirical regression method of estimating site response, *Seismol. Res. Lett.,* 68: 981–987.

Boore D.M. (1983) Stochastic Simulation of High-Frequency Ground Motions based on Seismological Models of the Radiated Spectra, *Bull. Seismol. Soc. Am.*, 73: 1865–1894.

Boore D.M. (2010a). TSPP--A collection of FORTRAN programs for processing and manipulating time series, U.S. Geological Survey *U.S. Geological Survey Open-File Report 2008-1111* (Revision 2.1),, Menlo Park, CA.

Boore D.M. (2010b). Orientation-independent, nongeometric-mean measures of seismic intensity from two horizontal components of motion, *Bull. Seismol. Soc. Am.*, 100(4): 1830–1835.

Boore D.M., Atkinson G.M (1989). Spectral scaling of the 1985-1988 Nahanni, Northwest Territories, earthquakes, *Bull. Seismol. Soc. Am.,* 79: 1736–1761.

Boore, D.M. Atkinson, G.M. (1992). Source spectra for the 1988 Saguenay, Quebec earthquakes, *Bull. Seismol. Soc.Am*., 82: 683–719.

Boore D.M. Akkar S. (2003). Effect of causal and acausal filters on elastic and inelastic response spectra, *Earthq. Eng. Struct. Dyn.*, 32: 1729–1748.

Boore D.M., Atkinson G.M. (2008). Ground-motion prediction equations for the average horizontal component of PGA, PGV, and 5%-damped PSA at spectral periods between 0.01 s and 10.0 s, *Earthq. Spectra*, 24: 99–138.

Boore D.M., Azari Sisi A., Akkar S. (2012). Using pad-stripped acausally filtered strong-motion data, *Bull. Seismol. Soc. Am.*, 102: 751–760.

Boore D.M. Bommer J.J. (2005). Processing of strong-motion accelerograms: needs, options and consequences, *Soil Dyn. Earthq. Eng.*, 25: 93–115.

Brune J.N. (1970). Tectonic stress and the spectra of seismic shear waves from earthquakes, *J. Geophys Res*., 75: 4997–5002.

Campbell K.W., Bozorgnia Y. (2008). NGA ground motion model for the geometric mean horizontal component of PGA, PGV, PGD and 5% damped linear elastic response spectra for periods ranging from 0.01 to 10 s, *Earthq. Spectra*, 24: 139–171.

Chapman M. (2013). *Personal communication*.

Chiou B.S.-J., Makdisi F.I., Youngs R.R. (2000). Style-of-faulting and footwall/hanging wall effects on strong ground motion, FY 1995 *NEHRP Award Number 1434-95-G-2614*, Final Report, 21 pgs.

Chiou B.S.-J., Youngs R.R. (2008). An NGA model for the average horizontal component of peak ground motion and response spectra, *Earthq. Spectra*, 24: 173–216.

Chiou B.-S.J., Darragh R.B., Gregor N., Silva W.J. (2008). NGA project strong-motion database, *Earthq. Spectra*, 24: 23–44.

Cramer C.H. (2008), *Final Report on Initial Database Design for a Database of CEUS Ground Motions*, Final Technical Report to the USGS for first year of Cooperative Agreement 07CRAG0015, 26 pgs., *https://umdrive.memphis.edu/ccramer/public/NGAeast/Documentation/CEUSGMInitialDatabaseDesignFinalRpt.doc*.

Cramer C.H. (2013). *Personal communication.*

Cramer C.H., Kumar A. (2003), 2001 Bhuj, India, earthquake engineering seismoscope recordings and Eastern North America ground-motion attenuation relations, *Bull. Seismol. Soc, Am.,* 93: 1390–1394.

Cramer C.H., Kutliroff J.R., Dangkua D. (2009), *Second Year Final Report on a Database of CEUS Ground Motions*, Final Technical Report to the USGS for Cooperative Agreement 07CRAG0015-Mod1, 12 pgs., *https://umdrive.memphis.edu/ccramer/public/NGAeast/Documentation/SecondYearFinalReportCEUSGMDatabase.doc*.

Cramer C.H., Kutliroff J.R., Dangkua D.T. (2011), *Next Generation Attenuation East Initial Flat Files for Eastern North America*, Report to PEER accompanying NGA-East flat files and time series under subagreement 7140, 4 pgs., *https://umdrive.memphis.edu/ccramer/public/NGAeast/Documentation/NGAEastFinalFlatFilesENA.docx.*

Cramer C.H., Kutliroff J.R., Dangkua D.T., Al Noman M.N. (2013). *Completing the NGA-East CENA/SCR Ground Motion Database*, Final Technical Report to PEER under sub-agreement 7140, April 5, 2013, 18 pgs., *https://umdrive.memphis.edu/ccramer/public/NGAeast/Documentation/NGAEastDbPEERFinalReport.docx.*

Dames and Moore, (1974). GASSAR Seismic Design for General Atomic Company, Site Parameter Study, *Dames & Moore Job No. 2395-001-02*.

EPRI (2004) (2006) (2013). Ground-motion model (GMM) review project: Shear wave velocity measurements at seismic recording stations, Electric Power Research Institute, *EPRI 3002000719*, Palo Alto, CA.

EPRI/DOE/NRC (2012). Central and Eastern United States seismic source characterization for nuclear facilities, U.S. Nuclear Regulatory Commission Report, *NUREG-2115; EPRI Report 1021097*, 6 Volumes, U.S. Department of Energy, Washington, D.C.

Ellsworth W.L. **(**2013). Injection-induced earthquakes, *Science*, 341, doi:10.1126/science.1225942.

Fullerton D., Bush C., Pennell J. (2003). Surficial deposits and materials in the Eastern and Central United States (East of 102 Degrees west longitude), *U.S. Geological Survey Geologic Investigations Series I-2789*.

Fulton R.J. (Compiler) (1986). *Surficial Materials of Canada*, Geological Survey of Canada, Natural Resources Canada. Ottawa. Map 1880A, Scale 1:5 000 000.

Gardner J.K., Knopoff L. (1974). Is the sequence of earthquakes in southern California, with aftershocks removed, Poissonian? *Bull. Seismol. Soc. Am*., 64: 1363–1367.

GSC. Geological Survey of Canada Canadian National Seismograph Network Station book website, *http://www.earthquakescanada.nrcan.gc.ca/stndon/CNSN-RNSC/stnbook-cahierstn/index-eng.php*, last accessed October 20, 2014.

Ghofrani H.G., Atkinson G.M. (2014). Site condition evaluation using morizontal-to-vertical spectral ratios of earthquakes in the NGA-West 2 and Japanese databases, *Soil Dyn. Earthq. Eng*., 67: 30–43, DOI: 10.1016/j.soildyn.2014.08.015.

Goldstein P., Snoke A. (2005). *SAC Availability for the IRIS Community*, Incorporated Institutions for Seismology Data Management Center Electronic Newsletter, *http://www.iris.edu/news/newsletter/vol7no1/page1.htm*.

Goldstein P., Dodge D., Firpo M., Minner L. (2003). SAC2000: Signal processing and analysis tools for seismologists and engineers, in: *The IASPEI International Handbook of Earthquake and Engineering Seismology,* W.H.K. Lee, H. Kanamori, P.C. Jennings, and C. Kisslinger, eds., Academic Press, London.

Hanks T.C.,Kanamori H (1979). A moment magnitude scale, *J. Geophys. Res*., 84(B5): 2348–2350.

Hartzell C., Langer C., Mendoza C. (1994). Rupture histories of eastern North America, *Bull. Seismol. Soc. Am*., 84(6): 1703–1724.

Herrmann R.B., Crossley D.J. (2008). Shear-wave velocity determination for Metropolitan St. Louis focal mechanism, *USGS Grant 05HQGR0046, Final Technical Report.*

Jaume S.C. (2006). Shear-wave velocity profiles via seismic cone penetration test and refraction microtremor techniques at ANSS strong motion sites in Charleston, South Carolina, *Seismol. Res. Lett.*, 77: 771–779.

Kanasewich E.R. (1981). *Time Sequence Analysis in Geophysics,* University of Alberta Press.

Kato K., Aki K., Takemura M. (1995). Site amplification from Coda waves: validation and application to S-wave site response, *Bull. Seismol. Soc. Am*., 85: 467–477.

Kayen R.E., Carkin B.A., Corbett S.C., Zangwill A.S., Lai L., Estevez L. (2014). (in preparation).Seismic-shear wave velocity and ground motion amplification factors for 50 sites affected by the Mineral, Virginia M5.8 earthquake of 23 August 2011, U.S. Geological Survey, *USGS Open-File Report* (in preparation).

Kim B., Hashash Y.M.A., Rathje E.M., Stewart J.P., Ni S., Somerville P.G., Kottke A.R., Silva W.J., Campbell K.W. (2014). Subsurface shear-wave velocity characterization using P-wave seismograms in Central and Eastern North America," *Earthq. Spectra*, (in press).

Konno K., Ohmachi T. (1998). Ground-motion characteristics estimated from spectral ratio between horizontal and vertical components of microtremors, *Bull. Seismol. Soc. Am*., 88(1): 228–241.

Kottke A.R., Hashash Y.M.A., Stewart J.P., Moss C.J., Nikolaou S., Rathje E.M., Silva W.J., Campbell K.W. (2012). Development of geologic site classes for seismic site amplification for Central and Eastern North America, *Proceedings, 15th World Conference in Earthquake Engineering*, Paper 4557, Lisbon, Portugal.

Lin L., Adams J. (2010). Strong motion records of the Val-des-Bois, Québec, earthquake of June 23, 2010. *Canadian Hazard Information Service Internal Report 2010–1.1,* 20 pgs. plus digital Appendix.

Mayne, P. (2011). *Personal communication*.

Novelo-Casanova D.A., Lee W.H.K. (1991). Comparison of techniques that use the single scattering model to compute the quality factor Q from Coda waves, *Pure Appl. Geophys*., 135 77–89.

Odum J.K., Williams R.A., Stephenson W.J., Worley D.M. (2010). Predicted and observed spectral response from collocated shallow, active- and passive-source vs data at five ANSS Sites, Illinois and Indiana, USA, *Seismol. Res. Lett.*, 81: 955–964.

R Development Core Team (2011). *R: A Language and Environment for Statistical Computing,* R Foundation for Statistical Computing, Vienna, Austria. ISBN 3-900051-07-0, *http://www.R-project.org*/.

Read K. El. Naggar H., Eaton D. (2008). Site-response spectra for POLARIS station sites in Southern Ontario and Québec, *Seismol. Res. Lett*., 79: 776–784.

Petersen M.D., Moschetti M.P., Powers M.., Mueller C.S., Haller K.M., Frankel A.D., Zeng Y., Rezaeian S., Harmsen S.C., Boyd O.S., Field E.H., Chen R., Rukstales K.S., Luco N., Wheeler R.L., Williams R.A., Olson A.H. (2014). Documentation for the 2014 Update of the United States National Seismic Hazard Maps, U.S. Geological Survey, *USGS Open-File Report 2014–1091*, Reston, VA.

Phillips S.W., Aki K. (1986). Site amplification of Coda waves from local earthquakes in central California, *Bull. Seismol. Soc. Am*., 76: 627–648.

Saint-Louis University Earthquake Center Network (SLU), *http://www.eas.slu.edu/eqc/*, last accessed October 20, 2014.

Seyhan E, Stewart J.P., Ancheta T.D., Darragh R.B., Graves R.W. (2014). NGA-West 2 site database, *Earthq. Spectra*, 30: 1007–1024.

Silva W.J., Gregor N., Darragh R.B. (1999). Near fault ground motions, A PEARL report to PG&E/CEC/Caltrans, *Award No. SA2193-59652*.

Somerville P.G., Collins N.F., Abrahamson N.A, Graves R.W., Saikia C. (2001). Earthquake source scaling and ground motion attenuation relations for the central and eastern United States, *Final Report to the U.S. Geological Survey, Contract No. 99HQGR0098*.

Spudich P., Fletcher J.B., Hellweg M., Boatwright J., Sullivan C., Joyner W.B., Hanks T.C., Boore D.M., McGarr A., Baker L.M., Lindh A.G. (1996). Earthquake ground motions in extensional tectonic regimes, U.S. Geological Survey, *USGS Open File Report 96-292*.

Thompson E., Silva W.J. (2013) Empirical assessment of site amplification and development of NEHRP factors for CEUS: collaborative research with Pacific Engineering and Tufts University, Report to USGS, *http://earthquake.usgs.gov/research/external/reports/G12AP20003.pdf*.

USGS (2013). United States Geological Survey National Advanced National Seismic System website, *http://earthquake.usgs.gov/monitoring/anss*/, last accessed October 20, 2014.

USGS (2014). United States Geological Survey National Digital Map Database, *http://ngmdb.usgs.gov/ngmdb/ngmdb_home.html*, last accessed October 20, 2014.

Wald D.J. Allen T.I. (2007). Topographic slope as a proxy for seismic site conditions and amplification, *Bull. Seismol. Soc. Am.*, 97: 1379–1395.

Williams R.A., Stephenson W.J., Odum J.K., Worley D.M. (2003). Seismic velocities from high-resolution surface-seismic imaging at six ANSS sites near Memphis, Tennessee, U.S. Geological Survey, *USGS Open-File Report 03–218*, Reston, VA.

Wooddell K.E., Abrahamson N.A. (2014). Classification of main sShocks and aftershocks in the NGA-West2 database, *Earth. Spectra*, 30(3); 1257–1267.

Wong V., Rebollar C.J., Munguia L. (2001). Attenuation of Coda waves at Tres Vírgenes volcanic area, Baja California Sur, México, *Bull. Seismol. Soc. Am.*, 91, 683–693.

Yong A., Hough S.E., Iwahashi J., Braverman A. (2012). A terrain-based site characterization map of California with implications for the contiguous United States, *Bull. Seismol. Soc. Am.*, 102: 114–128.

Appendix A Earthquake Source Table

This appendix provides a link to the latest NGA-East earthquake source table in EXCEL workbook format. The file may be updated periodically, with the last eight digits of the file name indicating the release date in yyyymmdd format. The spreadsheet contains listings for the 96 events in the NGA East ground motion database. Section A.1 presents the basis for selection of the metadata for the individual earthquakes.

http://apps.peer.berkeley.edu/publications/peer_reports/reports_2014/NGA-East_EarthquakeSourceTable_Public.zip

A.1 APPENDIX B SELECTION OF METADATA FOR INDIVIDUAL EARTHQUAKES

This appendix presents the basis for selection of the metadata for the individual earthquakes The metadata are contained in the accompanying MS Excel file linked above. The spreadsheet contains listings for the 96 events in the NGA-East ground motion database.

EQID 01 – Charlevoix, QC, 1925

The primary source of the location and focal mechanism data is Bent [1992]. Johnston [1996] develops an average estimate of $\log(M_o)$, and this value is selected to compute **M**. The standard deviation of **M** is computed as two-thirds of the log of the multiplicative error factor given by Johnston [1996].

EQID 02 – Grand Banks, NL, 1929

The primary source of the location and focal mechanism data is Bent [1995]. Johnston [1996] develops an average estimate of $\log(M_o)$, and this value is selected to compute **M**. The standard deviation of **M** is computed as two-thirds of the log of the multiplicative error factor given by Johnston [1996]. Most catalogs give the earthquake latitude as 44.69˚N, but Engdahl and Villaseñor [2002] relocate the earthquake to latitude 44.539˚N and their location is selected as the preferred location. The Engdahl and Villaseñor [2002] hypocentral depth of 15 km is used, but the CMT depth is kept at the 20 km value found by Bent [1995] from her waver form modelling.

EQID 03 – Timiskaming, QC, 1935

The primary source of the location and focal mechanism data is Bent [1999a]. Johnston [1996] develops an average estimate of log(M_o), and this value is selected to compute **M**. The standard deviation of **M** is computed as two-thirds of the log of the multiplicative error factor given by Johnston [1996]. Most Canadian catalogs list the latitude as 46.78˚N (e.g., Lamontagne et al., [2008]), but several U.S. catalogs list the latitude as 46.87˚N. The Canadian location is selected as the preferred location.

EQID 04 – Cornwall-Massena, ON, 1944

The primary source of the location and focal mechanism data is Bent [1999b]. Johnston [1996] develops an average estimate of log(M_o), and this value is selected to compute **M**. The standard deviation of **M** is computed as two-thirds of the log of the multiplicative error factor given by Johnston [1996].

EQID 05 – Saguenay, QC, 1988

The selected source parameters are those selected for the finite fault ground motion validation exercise for the NGA East project. It should be noted that Johnston [1996] developed an average estimate of log(M_o) that produces **M** 5.85. The standard deviation of **M** is computed as two-thirds of the log of the multiplicative error factor given by Johnston [1996]. Haddon [1992] obtains a much smaller seismic moment but indicated that his value may be an underestimate because of exclusion of significant low frequency signal due to poor signal to noise ratio for periods longer than 2.5 sec.

The finite fault model used in the NGA-East validation exercise is given below. Note that the moment magnitude is slightly lower than the average value taken from Johnston [1996]. The finite fault model was used to compute the distances to the recording stations.

NGA-East Finite Fault Model for Saguenay, 1988.

Latitude*	Longitude*	Depth*	Strike	Dip	Rake	RL	RW	Mo	**M**
48.098	-71.208	21.47	320	65	78	6.48	6.48	5.85E+24	5.81

*Location of center point of the top of the rupture plane

EQID 06 – La Malbaie, QC, August 1997

The parameters for this earthquake are taken from NUREG-2115. The value of **M** is estimated from M_N. No focal mechanism is available. The earthquake is assumed to be reverse based on the predominant focal mechanisms in the area.

EQID 07 – La Malbaie, QC, October 1997

The parameters for this earthquake are taken from Du et al. [2003] except for the more precise location given in the NRCAN catalog. Boatwright [2014] also reports **M** 4.29 based on regional spectral analysis (RSA). A nominal uncertainty of 0.1 is assigned to **M** based on typical values.

EQID 08 – Cap-Rouge, QC, November 1997

The parameters for this earthquake are taken from four sources. Three sources report very similar seismic moments and focal mechanisms and the fourth [Boatwight 2014] reports a very similar value of **M**. A fifth source [Bent 2014] reports a significantly larger seismic moment (~0.5 units larger **M**) and a significantly different focal mechanism. Given the large difference between the values from Bent [2014] and the other sources, and the consistency of the other estimates, the values from Bent [2014] were not used to derive the average values of **M** and depth. The preferred focal mechanism was taken from Ma and Adams [2002] as it is intermediate between the solutions of SLU and Du et al. [2003]. The more precise epicentral location given in the NRCAN catalog is used.

EQID 09 – Cote-Nord, QC, March 1999

The parameters for this earthquake are taken from a number of sources. Four reported values of M_o and Boatwright's [2014] RSA **M** are used to compute an average value of **M**. It should be noted that the value of M_o provided by Bent [2014] are consistent with the other estimates, as is her focal mechanism. The reported focal mechanisms are all similar and the one from Lamont was used as the preferred value for simulating ruptures. The selected depth is an average of the reported depths.

EQID 10 – Kipawa, QC, January 2000

The parameters for this earthquake are taken from a number of sources that report similar results. The focal mechanism is taken from the Bent et al. [2002] study if this event. It is similar to other estimates.

EQID 11 – La Malbaie, QC, June 2000

The location is taken from the NRCAN catalog and the estimate of **M** from Atkinson [2004a; 2004b]. A nominal uncertainty in **M** of 0.1 is assigned. No focal mechanism is available. The earthquake is assumed to be reverse based on the predominant focal mechanisms in the area.

EQID 12 – Laurentide, QC, July 2000

The location is taken from the NRCAN catalog and the estimate of **M** from Atkinson [2004a; 2004b]. A nominal uncertainty in **M** of 0.1 is assigned. The focal mechanism is taken from Bent et al. [2003].

EQID 13 – Laurentide, QC, July 2000 (second event)

The location is taken from the NRCAN catalog and the estimate of **M** from Atkinson [2004a; 2004b]. A nominal uncertainty in **M** of 0.1 is assigned. No focal mechanism is available. The earthquake is assumed to be reverse based on the predominant focal mechanisms in the area.

EQID 14 – Ashtabula, OH, January 2001

The location and depth are taken from the Seeber et al. [2004] study of this event. The value of **M** is averaged from the available assessments and the focal mechanism is taken from Du et al. [2003].

EQID 15 – Enolal, AR, July 2001

The location is taken from the more precise value in NUREG-2115. The depth, value of **M** and focal mechanism are taken from the SLU website. A nominal uncertainty in **M** of 0.1 is assigned.

EQID 16 – Au Sable Forks, NY, April 2002

The location and focal mechanism are taken from the Kim and Seeber [2003] study of this event. The value of **M** and the depth are averages of the reported values.

EQID 17 – Lac Laratelle, QC, June 2002

The more precise location is taken from the NRCAN catalog. The focal mechanism and depth are taken from the SLU website. Bent [2014] reports a depth of 23 km, but indicates that it is poorly constrained. The reported values of **M** are averaged.

EQID 18 – Carbon, IN, June 2002

The more precise location is taken from the SLU website along with the focal mechanism. The depth and value of **M** are averages of the two reported values.

EQID 19 – Boyd, NE, November 2002

The more precise location is taken from NUREG-2115. The depth, **M**, and focal mechanism are taken from the SLU website. A nominal uncertainty in **M** of 0.1 is assigned.

EQID 20 – Charleston, SC, November 2002

The more precise location is taken from NUREG-2115. The depth, **M**, and focal mechanism are taken from the SLU website. A nominal uncertainty in **M** of 0.1 is assigned.

EQID 21 – Ft Payne, AL, April 2003

The more precise location is taken from ANSS. The depth, **M**, and focal mechanism are taken from the SLU website. A nominal uncertainty in **M** of 0.1 is assigned.

EQID 22 – Blytheville, AR, April 2003

The location and values of **M** and $\sigma_{\mathbf{M}}$ estimated from other magnitude measures are taken from NUREG-2115.

EQID 23 – Bardwell, KY, June 2003

The location and focal mechanism are taken from the SLU web site. The values of **M** and source depth are averages of the SLU and LNSN assessments.

EQID 24 – La Malbaie, QC, June 2003

The location is taken from the NRCAN catalog. The focal mechanism is taken from the SLU website. The depth is taken as the average of the source depths from SLU and Atkinson [2004]. The depth from Bent [2014] is not used as she indicates that it is poorly constrained. The reported values of **M** are averaged to produce the selected value.

EQID 25 – Bark Lake, QC, October 2003

The location is taken from the NRCAN catalog. The values of **M** and $\sigma_{\mathbf{M}}$ estimated from other magnitude measures are taken from NUREG-2115. No focal mechanism is available. The earthquake is assumed to be reverse based on the predominant focal mechanisms in the area.

EQID 26 – Jefferson, VA, December 2003

The parameters for this earthquake are taken from Kim and Chapman [2003].

EQID 27 – St. Teresa, Mexico, April 2004

This earthquake is not investigated in this report.

EQID 28 – La Baie, QC, May 2004

The location is taken from the NRCAN catalog. The values of **M** and $\sigma_{\mathbf{M}}$ estimated from other magnitude measures are taken from NUREG-2115. No focal mechanism is available. The earthquake is assumed to be reverse based on the predominant focal mechanisms in the area.

EQID 29 – Prairie Center, IL, June 2004

The location and focal mechanism are taken from the SLU web site. The values of **M** and source depth are averages of the SLU and LNSN assessments.

EQID 30 – Port Hope, ON, August 2004

The location and focal mechanism are taken from Kim et al. [2006], a study if this event. The values of **M** and source depth are averages of the available assessments.

EQID 31 – Milligan Ridge, AR, February 2005

The location, focal mechanism, and value of **M** are taken from the SLU web site. A nominal uncertainty in **M** of 0.1 is assigned.

EQID 32 – Riviere du Loup, QC, March 2005

The selected source parameters are those selected for the finite fault ground motion validation exercise for the NGA East project. Note that the average of the reported values of **M** is 4.67, instead of the value of **M** of 4.60 used in the validation exercise.

The finite fault model used in the NGA-East validation exercise is given below. The finite fault model was used to compute the distances to the recording stations.

NGA-East Finite Fault Model for Riviere du Loup, March 2005.

Latitude*	Longitude*	Depth*	Strike	Dip	Rake	RL	RW	Mo	**M**
47.751	-69.724	12.3	170	60	80	1.6	1.6	9.02E+22	4.60

*Location of center point of the top of the rupture plane

EQID 33 – Shady Grove, AR, May 2005

The location, focal mechanism, and value of **M** are taken from the SLU web site. A nominal uncertainty in **M** of 0.1 is assigned.

EQID 34 – Miston, TN, June 2005

The location, focal mechanism, and value of **M** are taken from the SLU web site. A nominal uncertainty in **M** of 0.1 is assigned.

EQID 35 – Thurso, ON, February 2006

The location and focal mechanism are taken from the SLU web site. The location matched the NRCAN location. The value of **M** is averaged from the reported values and the source depth is an average, excluding the estimate of Bent [2014] as she indicated hers is poorly constrained.

EQID 36 – Hawkesbury ON, February 2006

The location is taken from NRCAN and the value of **M** is estimated from other size measures in NUREG-2115. No focal mechanism is available. The earthquake is assumed to be reverse based on the predominant focal mechanisms in the area.

EQID 37 – Baie Saint Paul QC, April 2006

The location and focal mechanism are taken from the SLU website. The value of **M** is an average of the available estimates.

EQID 38 – Ridgley, TN, September 2006

The location and estimate of **M** (based on other size measures) are taken from NUREG-2115. No focal mechanism is available. The earthquake is assumed to be strike slip based on the predominant focal mechanisms in the area.

EQID 39 – Gulf of Mexico, September 2006

This earthquake is not investigated in this report.

EQID 40 – Acadia, ME, October 2006

The more precise location is taken from the Weston Observatory catalog. The depth, value of **M,** and focal mechanism are taken from the SLU website. A nominal uncertainty in **M** of 0.1 is assigned.

EQID 41 – Marston, MO, October 2006

The location and estimate of **M** (based on other size measures) are taken from NUREG-2115. No focal mechanism is available. The earthquake is assumed to be strike slip based on the predominant focal mechanisms in the area.

EQID 42 – Marvin, VA, November 2006

This event is a mine collapse [Chapman, *Personal communication*].

EQID 43 – Skeggs, VA, November 2006

This event is a mine collapse [Chapman, *Personal communication*].

EQID 44 – Cobourg ON, July 2007

The location is taken from NRCAN and the value of **M** is estimated from other size measures in NUREG-2115. No focal mechanism is available. The earthquake is assumed to be reverse based on the predominant focal mechanisms in the area.

EQID 45 – Baie Saint Paul, QC, January 2008

The location is taken from NRCAN and the value of **M** is estimated from other size measures in NUREG-2115. No focal mechanism is available. The earthquake is assumed to be reverse based on the predominant focal mechanisms in the area.

EQID 46 – Mt Carmel, IL, April 2008

The location and focal mechanism are taken from the SLU web site. The values of **M** and source depth are averages of the SLU and USGS assessments.

EQID 47 – Mt Carmel, IL, April 2008, aftershock

The location, focal mechanism, and value of **M** are taken from the SLU web site. A nominal uncertainty in **M** of 0.1 is assigned.

EQID 48 – Mt Carmel, IL, April 2008, aftershock

The location, focal mechanism, and value of **M** are taken from the SLU web site. A nominal uncertainty in **M** of 0.1 is assigned.

EQID 49 – Mt Carmel, IL, April 2008, aftershock

The location, focal mechanism, and value of **M** are taken from the SLU web site. A nominal uncertainty in **M** of 0.1 is assigned.

EQID 50 – Buckingham, QC, June 2008

The location is taken from NRCAN and the value of **M** is estimated from other size measures in NUREG-2115. No focal mechanism is available. The earthquake is assumed to be reverse based on the predominant focal mechanisms in the area.

EQID 51 – Riviere du Loup, QC, November 2008, aftershock

The location is taken from NRCAN and the value of **M** is the average reported values. The source depth and focal mechanism are taken from the SLU website.

EQID 52 – Pine Forest, SC, December 2008

The location and estimate of **M** (based on other size measures) are taken from NUREG-2115. No focal mechanism is available. The earthquake is assumed to be strike slip based on the predominant focal mechanisms in the area.

EQID 53 – Rosehill, SC, January 2009

The location is taken from ANSS and the value of **M** is estimated from m_D using the relationships in NUREG-2115. No focal mechanism is available. The earthquake is assumed to be strike slip based on the predominant focal mechanisms in the area.

EQID 54 – Palmetto, SC, May 2009

The location is taken from ANSS and the value of **M** is estimated from m_{bLg} using the relationships in NUREG-2115. No focal mechanism is available. The earthquake is assumed to be strike slip based on the predominant focal mechanisms in the area.

EQID 55 – Constance Bay, ON, May 2009

The location is taken from NRCAN and the value of **M** is estimated from M_N using the relationships in NUREG-2115. No focal mechanism is available. The earthquake is assumed to be reverse based on the predominant focal mechanisms in the area.

EQID 56 – Jones, OK, January 2010

The location, focal mechanism, and value of **M** are taken from the SLU web site. A nominal uncertainty in **M** of 0.1 is assigned.

EQID 57 – Lincoln, OK, February 2010

The more precise location is taken from ANSS, the focal mechanism, source depth, and value of **M** are taken from the SLU web site. A nominal uncertainty in **M** of 0.1 is assigned.

EQID 58 – Whiting, MO, March 2010

The location, focal mechanism, and value of **M** are taken from the SLU web site. A nominal uncertainty in **M** of 0.1 is assigned.

EQID 59 – Lebanon, IL, May 2010

The location is taken from ANSS and the value of **M** is estimated from m_D using the relationships in NUREG-2115. No focal mechanism is available. The earthquake is assumed to be strike slip based on the predominant focal mechanisms in the area.

EQID 60 – Val-des-Bois QC, June 2010

The location and focal mechanism are taken from the SLU web site. The value of **M** and source depth are averages of the reported values.

EQID 61 – St Flavien QC, July 2010

The more precise location is taken from NRCAN, the source depth, value of **M**, and focal mechanism are taken from Lamontagne et al. [2013]. As discussed in that paper, a depth of 19–20 km (average of 19.5 used) based on wave form modelling is preferred over the 13 km depth obtained from the moment tensor solution.

EQID 62 – Bhuj, India, January, 2011

This earthquake is not investigated in this report.

EQID 63 – Mt. Laurier QC, October 1990

The more precise location is taken from NRCAN, the source depth, value of **M**, and focal mechanism are taken from Lamontagne et al. [1994]. Lamontagne et al. [1994] show two focal planes, but the steep dip is consistent with the aftershock distribution they show. Therefore, only use steeply dipping plane.

EQID 64 – Montgomery, MD, July 2010

The location, focal mechanism, and value of **M** are taken from the SLU web site. A nominal uncertainty in **M** of 0.1 is assigned.

EQID 65 – Gazli, USSR, May 1976

Information for this event was taken from the NGA West 2 database.

EQID 66 – Slaughterville, OK, October 2010

The location, focal mechanism, and value of **M** are taken from the SLU web site. A nominal uncertainty in **M** of 0.1 is assigned.

EQID 67 – Guy, AR, October 2010

The location, focal mechanism, and value of **M** are taken from the SLU web site. A nominal uncertainty in **M** of 0.1 is assigned.

EQID 68 – Concord, NH, September 2010

The location is taken from ANSS and the value of **M** is estimated from m_{bLg} and m_C using the relationships in NUREG-2115. No focal mechanism is available. The earthquake is assumed to be reverse based on the predominant focal mechanisms in the area.

EQID 69 – Nahani, NWT, November 1985 Foreshock

Information for this event was taken from the initial NGA East Event File [Cramer et al. 2013].

EQID 70 – Nahani, NWT, December 1985 Second Mainshock

Information for this event was taken from the NGA West 2 database.

EQID 71 – Nahani, NWT, December 1985 Aftershock

Information for this event was taken from the initial NGA East Event File [Cramer et al. 2013].

EQID 72 – Nahani, NWT, December 1985 Aftershock

Location and **M** taken from Boore and Atkinson [1989]. Focal mechanism from Horner et al. [1990].

EQID 73 – Arcadia, OK, November 2010

The location, focal mechanism, and value of **M** are taken from the SLU web site. A nominal uncertainty in **M** of 0.1 is assigned.

EQID 74 – Bethel Acres, OK, December 2010

The location, focal mechanism, and value of **M** are taken from the SLU web site. A nominal uncertainty in **M** of 0.1 is assigned.

EQID 75 – Greenstown, IN, December 2010

The location, focal mechanism, and value of **M** are taken from the SLU web site. A nominal uncertainty in **M** of 0.1 is assigned.

EQID 76 – Guy, AR, November 2010

The location, focal mechanism, and value of **M** are taken from the SLU web site. A nominal uncertainty in **M** of 0.1 is assigned.

EQID 77 – Greenbrier, AR, February 2011

The location, focal mechanism, and value of **M** are taken from the SLU web site. A nominal uncertainty in **M** of 0.1 is assigned.

EQID 78 – Greenbrier, AR, February 2011

The location, focal mechanism, and value of **M** are taken from the SLU web site. A nominal uncertainty in **M** of 0.1 is assigned.

EQID 79 – Greenbrier, AR, February 2011

The location, focal mechanism, and value of **M** are taken from the SLU web site. A nominal uncertainty in **M** of 0.1 is assigned.

EQID 80 – Greenbrier, AR, February 2011

The location, focal mechanism, and value of **M** are taken from the SLU web site. A nominal uncertainty in **M** of 0.1 is assigned.

EQID 81 – Sullivan, MO, June 2011

The location, focal mechanism, and value of **M** are taken from the SLU web site. A nominal uncertainty in **M** of 0.1 is assigned.

EQID 82 – Eagle Lake, ME, July 2006

The more precise location is taken from the Weston catalog. The source depth and focal mechanism are taken from the SLU website. The value of **M** is an average of the SLU and Boatwight [2014] values.

EQID 83 – Val-des-Bois, QC, June 2010, Aftershock

The location is taken from NRCAN and the value of **M** is estimated from M_N using the relationships in NUREG-2115. No focal mechanism is available. The earthquake is assumed to be reverse based on the predominant focal mechanisms in the area.

EQID 84 – Val-des-Bois, QC, July 2010, Aftershock

The location is taken from NRCAN and the value of **M** is estimated from M_N using the relationships in NUREG-2115. No focal mechanism is available. The earthquake is assumed to be reverse based on the predominant focal mechanisms in the area.

EQID 85 – Hawkesbury ON, March 2011

The location is taken from NRCAN. The focal mechanism is taken from the SLU website. The values of **M** and source depth are averaged from the reported values.

EQID 86 – Charlevoix, QC, May 2001

The location is taken from NRCAN and the value of **M** is taken from Atkinson [2004a; 2004b]. A nominal uncertainty in **M** of 0.1 is assigned. No focal mechanism is available. The earthquake is assumed to be reverse based on the predominant focal mechanisms in the area.

EQID 87 – Baie Saint Paul, QC, August 2002

The location is taken from NRCAN and the value of **M** is taken from Atkinson [2004a; 2004b]. A nominal uncertainty in **M** of 0.1 is assigned. No focal mechanism is available. The earthquake is assumed to be reverse based on the predominant focal mechanisms in the area.

EQID 88 – Mineral, VA, August 2011

The selected source parameters are based primarily on Chapman [2013]. The average of the reported values of **M** is 5.74, which is larger than the value used in the validation exercise. The preferred SLU solution is the strike of 175˚ while Chapman [2013] and Motazedian and Ma [2014] prefer a strike of 29˚.

The finite fault model used in the NGA-East validation exercise is given below. The finite fault model was used to compute the distances to the recording stations.

NGA-East Finite Fault Model for Mineral, VA, August 2011

Latitude*	Longitude*	Depth*	Strike	Dip	Rake	RL	RW	Mo	M
37.929	-77.981	5.84	29	51	113	5.56	5.56	3.72E+24	5.68

*Location of center point of the top of the rupture plane

EQID 89 – Mineral, VA, August 2011, Aftershock

The location, focal mechanism, and value of **M** are taken from the SLU web site. A nominal uncertainty in **M** of 0.1 is assigned.

EQID 90 – Sparks, OK, November 2011, Foreshock

The location, focal mechanism, and value of **M** are taken from the SLU web site. A nominal uncertainty in **M** of 0.1 is assigned.

EQID 91 – Sparks, OK, November 2011, Mainshock

The location and focal mechanism are taken from the SLU web site. The values of **M** and source depth are averages of the reported values.

EQID 92 – Cormel, TX, October 2011

The location and focal mechanism are taken from the SLU web site. The values of **M** and source depth are averages of the reported values.

EQID 93 – Miramichi, NB, March 1982, Aftershock

The location and focal mechanism are taken from Wetmiller et al. [1984]. The value of **M** is an average of the Atkinson [2004a; 2004b] and Shin and Herrmann [1989] values.

EQID 94 – Miramichi, NB, May 1982, Aftershock

The location and focal mechanism are taken from Wetmiller et al. [1984]. The value of **M** is an average of the Atkinson [2004a; 2004b] and Shin and Herrmann [1989] values.

EQID 116 – Saguenay, QB, November 1988, Foreshock

The location and value of **M** are taken from Boore and Atkinson [1992]. The focal mechanism is taken from North et al. [1990]. A nominal uncertainty in **M** of 0.1 is assigned.

EQID 117 – Saguenay, QB, November 1988, Aftershock

The location and value of **M** are taken from Boore and Atkinson [1992]. The focal mechanism is taken from North et al. [1990]. A nominal uncertainty in **M** of 0.1 is assigned.

A.2 REFERENCES

Ancheta T.D., Darragh R.B., Stewart J.P., Seyhan E., Silva W.J., Chiou B.S.-J., Wooddell K.E., Graves R.W., Kottke A.R., Boore D.M., Kishida T., Donahue J.L. (2013). PEER NGAWest2 database, *PEER Report No. 2013/03*, Pacific Earthquake Engineering Research Center, University of California, Berkeley, CA.

ANSS – http://earthquake.usgs.gov/earthquakes/search/ accessed June 2014.

Atkinson G.M. (2004a). Empirical attenuation of ground-motion spectral amplitudes in southeastern Canada and the northeastern United States, *Bull Seismol. Soc. Am*., 94: 1079–1095.

Atkinson G.M. (2004b). ERRATUM - Empirical attenuation of ground-motion spectral amplitudes in southeastern Canada and the northeastern United States, *Bull Seismol. Soc. Am*., 94: 2419–2423.

Bent A.L. (1992). A re-examination of the 1925 Charlevoix, Quebec earthquake, *Bull Seismol. Soc. Am*., 82: 2097–2113.

Bent, A.L. (1995) A complex double-couple source mechanism for the MS 7.2 1929 Grand Banks earthquake, *Bull Seismol. Soc. Am*., 85: 1003–1020.

Bent A.L. (1996a). An improved source mechanism for the 1935 Timiskaming, Quebec earthquake from regional waveforms, *Pageoph*, 146: 5–20.

Bent A.L. (1996b). Source parameters of the damaging Cornwall-Massena earthquake of 1944 from regional waveforms, *Bull Seismol. Soc. Am*., 86: 489–497.

Bent A.L. (2014). *Written communication*.

Bent A.L., Drysdale J., Perry H.K.C. (2003). Focal mechanisms for eastern Canadian earthquakes, 1994–2000, *Seismol. Res. Lett*., 74: 452–468.

Bent A.L., Lamontagne M., Adams J., Woodgold C.R.D., Halchuk S., Drysdale J., Wetmiller R.J., Ma S. (2002). The Kipawa, Quebec, "Millennium" earthquake, *Seismol. Res. Lett*., 73(2): 285–297.

Boatwright, J. (2014). *Written communication.*Boore D.M., Atkinson G.M. (1989). Spectral scaling of the 1985 to 1988 Nahanni, Northwest Territories, earthquakes, *Bull Seismol. Soc. Am*., 79: 1736–1761.

Boore D.M., Atkinson G.M. (1992). Source spectra for the 1988 Saguenay, Quebec, earthquakes, *Bull Seismol. Soc. Am*., 82: 683–719.

Boore D.M., Campbell K.W., Atkinson G.M. (2010). Determination of stress parameters for eight well-recorded earthquakes in eastern North America, *Bull Seismol. Soc. Am*., 100: 1632–1645.

Chapman M.C. (2013). On the rupture process of the 23 August 2011 Virginia earthquake, *Bull Seismol. Soc. Am*., 103(2A): 613–628.

Chiou B.S.-J., Youngs R.R. (2008). NGA model for average horizontal component of peak ground motion and response spectra, *PEER Report 2008/09*, Pacific Earthquake Engineering Research Center, University of California, Berkeley, CA.

Cramer C.H., Kutliroff J.R., Dangkua D.T., Al Noman, M.N. (2013). Completing the NGA East ENA/SCR Ground Motion Database, Report prepared for the Pacific Earthquake Engineering Research Center by the Center for Earthquake Research and Information, *University of Memphis under Subagreement 7140, https://umdrive.memphis.edu/ccramer/public/NGAeast/Documentation/NGAEastDbPEERFinalReport.docx*.

Dewey J.W., Gordon D.W. (1984). Map showing recomputed hypocenters of earthquakes in the eastern and central United States and adjacent Canada, 1925 to 1980, Dept. of the Interior, *U.S. Geological Survey, Misc. Field Studies, Map MF-1699*, 39 pgs.

Du W.-X., Kim, W.-Y., Sykes, L.R. (2003). Earthquake source parameters and state of stress for the northeastern United States and southeastern Canada from analysis of regional seismograms, *Bull Seismol. Soc. Am*., 93(4): 1633–1648.

Engdahl E.R., Villaseñor A. (2002). Global Seismicity: 1900–1999, in *International Handbook of Earthquake and Engineering Seismology*, W.H.K. Lee, H. Kanamori, P.C. Jennings, and C. Kisslinger (eds.), Part A, Chapter 41, pp. 665–690, Academic Press.

EPRI/USDOE/USNRC, 2012, Central and Eastern United States Seismic Source Characterization for Nuclear Facilities, U.S. Nuclear Regulatory Commission Report, *NUREG-2115; EPRI Report 1021097*, 6 Volumes; DOE Report# DOE/NE-0140.

Haddon, R. A. W., 1992, Waveform modeling of strong-motion data for the Saguenay earthquake of 25 November 1988, *Bull Seismol. Soc. Am*., 82, no. 2, pp. 720–754.

Haddon R.A.W., Adams J. (1997). Anatomy of a small intraplate earthquake: a dissection of its rupture characteristics using regional data, *Geophys. J. Int*., 129: 235–251.

Hanks T.C., Kanamori, H. (1979). A moment magnitude scale: *J. Geophys. Res*., 84(B5): 2348–2350.

Hartzell S., Mendoza C., Zeng Y. (2013). Rupture model of the 2011 Mineral, Virginia, earthquake from teleseismic and regional waveforms, *Geophys. Res. Lett*., 40: 1–6.

Horner R.B., Wetmiller R.J., Lamontagne M., Plouffe M. (1990). A fault model for the Nahanni earthquakes from aftershock studies, *Bull Seismol. Soc. Am*., 80: 1553–1570.

Johnston A.C. (1996). Seismic moment assessment of earthquakes in stable continental regions – I: Instrumental seismicity, *Geophys. J. Int*., 124: 381–414.

Kim W.-Y. (2003). The 18 June 2002 Caborn, Indiana, earthquake: Reactivation of ancient rift in the Wabash Valley seismic zone? *Bull Seismol. Soc. Am*., 93: 2201–2211.

Kim W.-Y., Chapman M. (2005). The 9 December 2003 central Virginia earthquake sequence: A compound earthquake in the Central Virginia seismic zone, *Bull Seismol. Soc. Am*., 95: 2428–2445.

Kim W.-Y, Dineva S., Ma S., Eaton, D. (2006) The 4 August 2004, Lake Ontario, earthquake, *Seismol. Res. Lett.*, 77(1): 65–73.

Kim W.-Y., Seeber L. (2003) Source characteristics and hazard implications of the April 20, 2002, Mw 5, Plattsburgh, NY, earthquake sequence, *Final Technical Report Award Number: 03HQGR0007*.

Lamontagne M., Bent A.L., Woodgold C.R.D., Ma S., Peci V. (2004) The 16 March 1999 mN 5.1 Cote-Nord earthquake: the largest earthquake ever recorded in the lower St. Lawrence seismic zone, Canada, *Seismol. Res. Lett.*, 75: 299–316.

Lamontagne M., Halchuk S., Cassidy J.F., Rogers G.C. (2008). Significant Canadian earthquakes of the period 1600–2006, *Seismol. Res. Lett.*, 79: 211–223.

Lamontagne, M., Hasegawa H.S., Forsyth D.A., Buchbinder G.G.R., Cajka M., 1994, The Mont-Laurier, Quebec earthquake of 19 October 1990 and its seismotectonic environment, *Bull Seismol. Soc. Am*., 84: 1506–1522.

Lamontagne M., Keating P., Bent A.L., Peci V., Drysdale J. (2013). The 23 July 2010 mN 4.1 Laurier-Station, Quebec, earthquake: A midcrustal tectonic earthquake occurrence unrelated to nearby underground natural gas storage, *Seismol. Res. Lett.*, 83: 921–932.

Ma S., Adams J. (2002). Moment tensor solutions by surface waveform modeling and related studies for moderate earthquakes in eastern Canada and its vicinity, *Geological Survey of Canada, Draft Open File Report* (reformatted June 2014).

Ma, S., and Eaton, D.W., 2007, Western Quebec Seismic Zone (Canada): Clustered, Midcrustal seismicity along a Mesozoic hot spot track: Journal of Geophysical Research, v. 112, B06305.

Motazedian D., Ma S. (2014). A review study of the source parameters of the 23 August 2011 Mw 5.7 Virginia earthquake, *Bull Seismol. Soc. Am*., 104: 2611–2618.

NRCAN – Natural Resources Canada, Earthquakes Canada, *http://www.earthquakescanada.nrcan.gc.ca/stndon/NEDB-BNDS/bull-eng.php*, accessed June, 2014.

North R.G., Wetmiller R.J., Adams J., Anglin F.M., Hasegawa H.S., Lamontagne M., Du Berger R., Seeber L., Armbruster J. (1989). Preliminary results from the November 25, 1988 Saguenay (Quebec) earthquake, *Seismol. Res. Lett.*, 60: 89–93.

SLU (2014). North America Moment Tensor, Saint Louis University, *http://www.eas.slu.edu/eqc/eqc_mt/MECH.NA/*, accessed June, 2014.

Seeber L., Armbruster J.G., Kim W.-Y. (2004). A fluid-injection-triggered earthquake sequence in Ashtabula, Ohio: implications for seismogenesis in stable continental regions, Bull Seismol. Soc. Am., 94: 76–87.

Shin T.-C., Herrmann R.B. (1987). Lg attenuation and source studies using 1982 Miramichi data, *Bull Seismol. Soc. Am.,* 77: 384–397.

Somerville P.G., McLaren J., Saikia C., Helmberger D. (1990). The Nov. 25, 1988 Saguenay, Quebec earthquake: source parameters and the attenuation of strong ground motion, *Bull Seismol. Soc. Am.,* 80: 1118–1143.

Wetmiller R.J., Adams J., Anglin F.M., Hasegawa H.S, Stevens A.E. (1984) Aftershock sequences of the 1982 Miramichi, New Brunswick earthquakes, *Bull Seismol. Soc. Am.,* 74: 621–653.

Appendix B Station Database

This appendix provides a link to the NGA-East Station Database in EXCEL workbook format. The file may be updated periodically, with the last eight digits of the file name indicating the release date in yyyymmdd format. The field explanations and references are included in separate sheets of the workbook.

http://apps.peer.berkeley.edu/publications/peer_reports/reports_2014/NGA-East_StationDatabase_Public.zip

Appendix C Flatfile for 5%-Damped PSA

This appendix provides a link to the latest NGA-East flatfile in EXCEL workbook format. The file may be updated periodically, with the last eight digits of the file name indicating the release date in yyyymmdd format. Section C.1 provides the explanation of the different fields (columns) contained in the flatfile. Supplemental information on regionalization fields is provided in Section C.2.

http://apps.peer.berkeley.edu/publications/peer_reports/reports_2014/NGA-East_Flatfile_Public.zip

C.1 EXPLANATION OF FLATFILE FIELDS

The NGA-East flatfile is provided as an EXCEL workbook format with each row containing information for a specific record and each column constituting a different field (Table C.1). The different fields are grouped into four main categories:

- columns B-V: earthquake event information, mostly borrowed from Appendix A.
- columns W-AJ: recording station information, mostly borrowed from Appendix B.
- columns AK- AQ: propagation and path information including regionalization as documented in Appendix C.2.
- columns AR-SW: record-specific information including processing information and ground motion intensity measures, as defined in Chapter 3.

All numerical fields are set to "-999" when the metric does not exist, is not defined or is not available at the time of the flatfile release. All text fields are set to "NA" for the same reasons.

Table C.1 NGA-East flatfile fields.

Column	Column Name	Description
A	Record Sequence Number	A unique number assigned to each strong-motion record in the flatfile for identification.
B	EQID	A unique number assigned to each earthquake for identification.
C	Earthquake Name	Unique name composed of the common earthquake name, followed by year, month and day of the event. The naming usually includes the name of the general area or country where the earthquake occurred.
D	Earthquake Location	General earthquake location. Can be used as a shorter alternative for earthquake name.
E	Year	Year of earthquake.
F	Month	Month of earthquake.
G	Day	Day of earthquake.
H	Hour	Origin time of earthquake (hour).
I	Minute	Origin time of earthquake (minute).
J	Earthquake Magnitude	Magnitude of earthquake. When there are multiple reliable estimates of earthquake magnitude, the average value of the reliable estimates is used. See Report Appendix A.
K	Magnitude Uncertainty: Statistical	Magnitude uncertainty is taken as either the standard deviation of the reliable magnitude estimates or as the statistical uncertainty on the conversion relationship. If only one magnitude is reported, a nominal uncertainty of 0.1 is assigned. See Report Appendix A.
L	Epicenter Latitude (deg)	As defined in Report Appendix A.
M	Epicenter Longitude (deg)	As defined in Report Appendix A.
N	Hypocenter Depth (km)	As defined in Report Appendix A.
O	CMT Depth (km)	Depth defined from centroid moment tensor inversion (CMT). As defined in Report Appendix A.
P	Depth Used (km)	Depth used for distance computations, see Report Section 4.4.
Q	Strike (deg)	Strike angle of the fault plane used to approximate the causative fault surface. 0^o <= Strike <= 360^o. Convention of fault strike, dip, and rake follows that described in Aki and Richards [1980].
R	Dip (deg)	Dip angle of the fault plane. 0^o <= Dip <= 90^o. (see note above)
S	Rake (deg)	Rake is the angle measured on the fault plane counterclockwise from the reference strike direction to the average slip direction (see Report Figure 4.1 for schematic) -180^o <= Rake <= 180^o

Column	Column Name	Description
T	Finite Rupture Model: 1=Yes; 0=No	See Report Section 4.2 and Appendix A.
U	Mechanism Based on Rake Angle	Mechanism Class / Rake Angles Unknown -999 --- Strike - Slip 0: -180 ≤ Rake < -150; -30 ≤ Rake ≤ 30; 150 < Rake ≤ 180 --- Normal 1: -120 ≤ Rake < -60 --- Reverse 2: 60 < Rake ≤ 120 --- Reverse - Oblique 3: 30 < Rake ≤ 60; 120 < Rake ≤ 150 --- Normal - Oblique 4: -150 ≤ Rake < -120; -60 ≤ Rake < -30
V	USGS Potentially Induced Event (PIE) Flag	Flag=1 (PIE), Flag=0 (non PIE or tectonic), see Report Section 4.6.
W	Station Sequence Number	An arbitrary unique sequence number assigned to a location at which one or more recording instrument(s) exist(s).
X	Network.Station Code (pref.)	Preferred station code (various data providers have different names for a given station). The station name follows the IRIS convention: NN.SSS.II.O.AA.where NN is the network identifier (see Report Table 2.2) SSS is a 3-5 character unique station id for that network II is a two-letter code for the instrument type. O is the instrument orientation (generally E, N, or Z for East, North, and Vertical) AA is a two-character designator among different instruments at the same station (which is sometimes optional)
Y	Network.Station Code (alt.1)	Alternate station code 1 (see description above).
Z	Network.Station Code (alt.2)	Alternate station code 2 (see description above).
AA	Network.Station Code (alt. 3)	Alternate station code 3 (see description above).
AB	Network.Station Code (alt. 4)	Alternate station code 4 (see description above).
AC	Station name	The name of the station, as retrieved from data providers' documentation. It usually corresponds to a location.
AD	Station Latitude (deg)	As defined in Report Appendix B.
AE	Station Longitude (deg)	As defined in Report Appendix B.
AF	Station Elevation (m)	As defined in Report Appendix B.

Column	Column Name	Description
AG	Preferred V_{S30} assignment Code	This column identifies the source of the preferred V_{S30} (see Report Section 5.5).
AH	Preferred V_{S30} (m/sec)	V_{S30} assignment (see Report Section 5.5).
AI	Standard deviation of V_{S30} (in natural log units)	Uncertainty of V_{S30}. Sigma (standard deviation) values are estimated based on the source of the preferred V_{S30} value (see Report Section 5.5).
AJ	NEHRP Classification Based on Preferred V_{S30}	The NEHRP site class was determined based on the preferred V_{S30} values. Class V_{S30} range (m/sec) A > 1500 B 760 - 1500 C 360– 760 D 180 – 360 E < 180 F (special study soils) can't be identified based on V_{S30} alone.
AK	EpiD (km)	Distance from the recording site to the epicenter. Same as R_{epi}.
AL	HypD (km)	Distance from the recording site to the hypocenter. Same as R_{hypo}.
AM	ClstD (km)	Closest distance from the recording site to the ruptured fault area. Same as R_{RUP}.
AN	Joyner-Boore Dist. (km)	Shortest horizontal distance from the recording site to the vertical projection of the rupture on the surface. Same as R_{JB}.
AO	Event Region Number	CENA region in which the epicenter is located. See Report Section C.2.
AP	Station Region Number	CENA region in which the recording station is located. See Report Section C.2.
AQ	Path Region Number	CENA region in which the path from the epicenter to the recording station is located. See Report Section C.2.
AR	File Name (Horizontal 1)	Directory name and file name of time series data files.
AS	File Name (Horizontal 2)	Directory name and file name of time series data files.
AT	File Name (Vertical)	Directory name and file name of time series data files.
AU	H1 component azimuth (degrees)	
AV	H2 component azimuth (degrees)	
AW	Instrument Type	'A' for acceleration time series, 'V' for a velocity time series.
AX	Sampling time step, dt (sec)	
AY	Nyquist Frequency (Hz)	Highest resolvable frequency= 1/(2*dt).

Column	Column Name	Description
AZ	HP-H1 (Hz)	Corner frequency of the high-pass filter of component H1. 1. When component unavailable, corner frequency is -999. 2. If filter was not applied, corner frequency is 0
BA	HP-H2 (Hz)	Corner frequency of the high-pass filter of component H2. (see note for HP-H1)
BB	HP-V (Hz)	Corner frequency of the high-pass filter of the vertical component. (see note for HP-H1)
BC	LP-H1 (Hz)	Corner frequency of the low-pass filter of component H1. (see note for HP-H1)
BD	LP-H2 (Hz)	Corner frequency of the low-pass filter of component H2. (see note for HP-H1)
BE	LP-V (Hz)	Corner frequency of the low-pass filter of the vertical component. (see note for HP-H1)
BF	Microseism Lower-bound - H1 (Hz)	Lower frequency limit of microseism window for component H1. -999 for no microseism observed. See Report Section 3.4.6.
BG	Microseism Lower-bound - H2 (Hz)	Lower frequency limit of microseism window for component H2. -999 for no microseism observed. See Report Section 3.4.6.
BH	Microseism Lower-bound - HV (Hz)	Lower frequency limit of microseism window for the vertical component. -999 for no microseism observed. See Report Section 3.4.6.
BI	Microseism Upper-bound - H1 (Hz)	Upper frequency limit of microseism window for component H1. -999 for no microseism observed. See Report Section 3.4.6.
BJ	Microseism Upper-bound - H2 (Hz)	Upper frequency limit of microseism window for component H2. -999 for no microseism observed. See Report Section 3.4.6.
BK	Microseism Upper-bound - HV (Hz)	Upper frequency limit of microseism window for the vertical component. -999 for no microseism observed. See Report Section 3.4.6.
BL	High-pass factor	This HP factor is the ratio of the lowest usable frequency ("LUF") to the corner frequency ("HP") of the high-pass filter. The recommended lowest usable frequency is the frequency above which spectra from high-pass filtered data are relatively unaffected by the filter.
BM	Low-pass factor	This LP factor is the ratio of the lowest usable frequency ("HUF") to the corner frequency ("LP") of the low-pass filter. If no HP was selevcted for the component, it is taken as the Nyquist frequency to define the HUF. The recommended HUF is the frequency below which spectra from high-pass filtered data are relatively unaffected by the filter.
BN	Lowest Usable Freq. - H1 (Hz)	This column ("LUF") is the product of "HP-H1" and "High-pass Factor", except when "HP-H1" is -999 or 0. When "HP-H1" is -999, "LUF" is again -999.
BO	Lowest Usable Freq. - H2 (Hz)	Same as above, for component H2.
BP	Lowest Usable Freq. - V (Hz)	Same as above, for the vertical component.

Column	Column Name	Description
BQ	Highest Usable Freq. - H1 (Hz)	This column ("HUF") is the product of "LP-H1" and "Low-pass Factor", except when "LP-H1" is -999, in which case the Nyquist is used in place of the LP-H1.
BR	Highest Usable Freq. - H2 (Hz)	Same as above, for component H2.
BS	Highest Usable Freq. - V (Hz)	Same as above, for the vertical component.
BT	Lowest Usable Freq. - Ave. Component (Hz)	This column is the recommended lowest usable frequency for the average horizontal component. It is taken as the larger of the LUF for H1 and H2.
BU	Highest Usable Freq. - Ave. Component (Hz)	This column is the recommended highest usable frequency for the average horizontal component. It is taken as the smallest of the HUF for H1 and H2.
BV	Usable Freq. Bandwidth - Ave. Component (Hz)	Difference between HUF and LUF in Hz.
BW	Lowest Usable Period - Ave. Component (sec)	This column ("LUP") is the recommended lowest usable period for RotDnn. It is taken as the inverse of the Highest Usable Freq. - Ave. Component (Hz)
BX	Highest Usable Period - Ave. Component (sec)	This column ("HUP") is the recommended highest usable period for RotDnn. It is taken as the inverse of Lowest Usable Freq. - Ave. Component (Hz)
BY	Usable Period Bandwidth - Ave. Component (sec)	Difference between HUP and LUP in sec.
BZ	Quality Flag Based on Ground Motions Residuals	Quality Flag for PGA, PGV, PSA(0.05sec) residuals relative to AB11 (140 and 300 bars): 0: all residuals within +/-4sigma 1: one or two residuals outside +/-4sigma 2: all residuals outside +/-4sigma
CA	Column intentionally left empty (“NA”)	
CB	Column intentionally left empty (“NA”)	
CC	Noise Window Flag	See Report Section 3.4.2 for window length definitions.0: full pre-event noise window available. 1: pre-event noise window shorter than preferred value. 2: pre-event noise window non-existent; may be due to data already processed or may be due to late P-wave trigger.
CD	SLg Window Flag	See Report Section 3.4.2 for window length definitions. 0: full SLg window NGA-East preferred length available. 1: SLg window shorter than preferred length, but at least as long as Chapman (2013). Shorter length may be due to data already processed or to record stopping early. 2: SLg window shorter than length defined in Chapman (2013). This *may* involve truncation of S-waves and may be due to data already processed or to record stopping early.
CE	Coda Window Flag	See Report Section 3.4.2 for window length definitions. 0: full Coda window available. 1: Coda window shorter than preferred value. 2: Coda window non-existent; may be due to data already processed or may be due to record stopping early.

Column	Column Name	Description
CF	RotDnn fractile	nn is the fractile for RotD PSA metric. See Report Section 6.2.
CG	Damping (%)	Damping ratio for oscillator response used in PSA (RotDnn).
CH	PGA -H RotDnn (g)	Peak ground acceleration (*g*) for RotDnn.
CI	PGV -H RotDnn (cm/s)	Peak ground velocity (cm/sec) for RotDnn.
CJ	PGD -H RotDnn (cm)	Peak ground displacement (cm) for RotDnn.
CK-SW	T0.0067s-T10.0s	RotDnn PSA values for oscillator period in header (sec), in units of *g*.

C.2 REGIONALIZATION FIELDS

A separate task in NGA-East was to regionalize CENA on the basis of systematic differences in simulated ground motions. From this task four distinct regions were defined [Dreiling et al. 2014]. The four regions are:

1. Mississippi Embayment/Gulf Coast region (MEM)
2. Central North America (CNA)
3. The Appalachian Province (APP)
4. The Atlantic Coastal Plain (ACP)

These four regions are shown in Figure C.1 with the numbering used in the NGA-East flatfile.

The NGA-East flatfile includes three separate fields for regionalization. The first two, columns AU and AV, correspond to the Event and Station Region Number, respectively. For these two fields, the number directly corresponds to the region containing the epicenter (Event field) and the station (Station field). If the epicenter or the station is outside these four regions, the flag is set to -999.

The third and last regionalization field (column AW) is called Path Region Number and aims to define a region containing the full propagation path (from the epicenter to the Station). If the full path in contained within any of the four regions above, the field is populated with the region number directly (Figures C.2–C.5). If any or both of the Event or Station Region Number is outside the four regions (at least one of the fields is -999), then the Event-Station field is also -999.

The regionalization task also demonstrated that the four regions could be aggregated into two distinct attenuation groups:

GROUP 1: Central North America, Appalachians, Atlantic Coastal Plain

GROUP 2: Mississippi Embayment/Gulf Coast

Two new regions were created to accommodate this grouping of regions. Region 5 includes paths that cross any or many of the regions' 2, 3 and 4 boundaries. To fully populate the attenuation Group 1 from above, one would have to combine data with Path Region numbers 2, 3, 4 and 5. Region 6 allows for paths crossing between any sub-region of Group 1 into region 1 (MEM). Figures C.2–C.8 illustrate the various paths included in the NGA-East database.

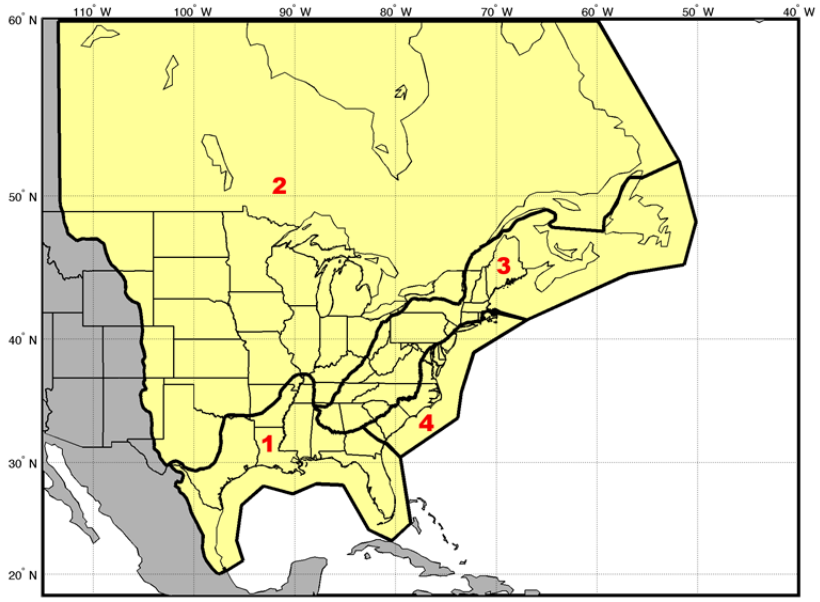

Figure C.1 **Four regions defined for Central and Eastern North America (CENA). The regions have been numbered as follows for the NGA-East database: (1) Mississippi Embayment/Gulf Coast region; (2) Central North America; (3) the Appalachian Province; and (4) the Atlantic Coastal Plain.**

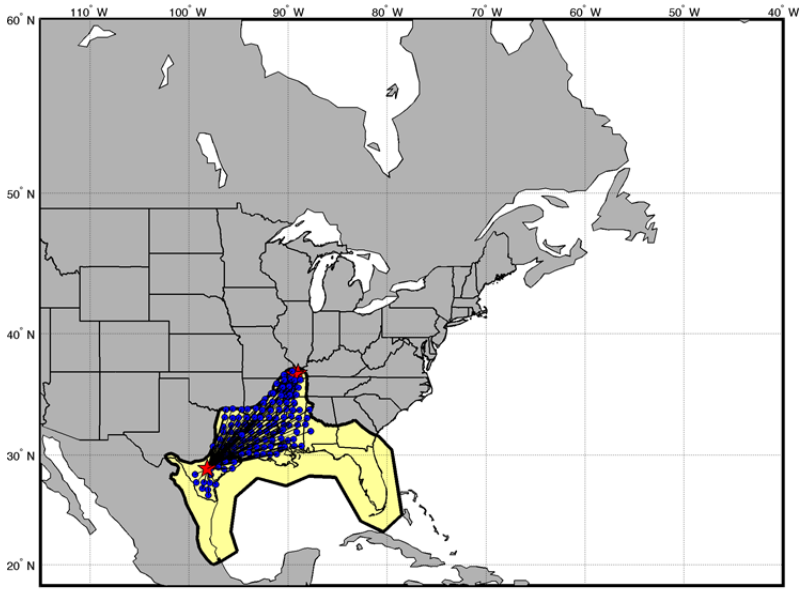

Figure C.2 **Paths contained within region 1: Mississippi Embayment/Gulf Coast.**

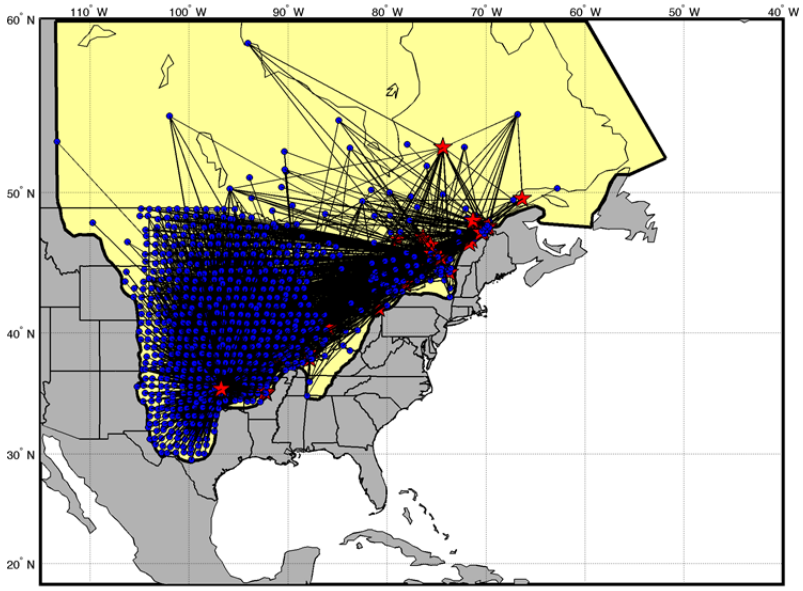

Figure C.3 **Paths contained within region 2: Central North America.**

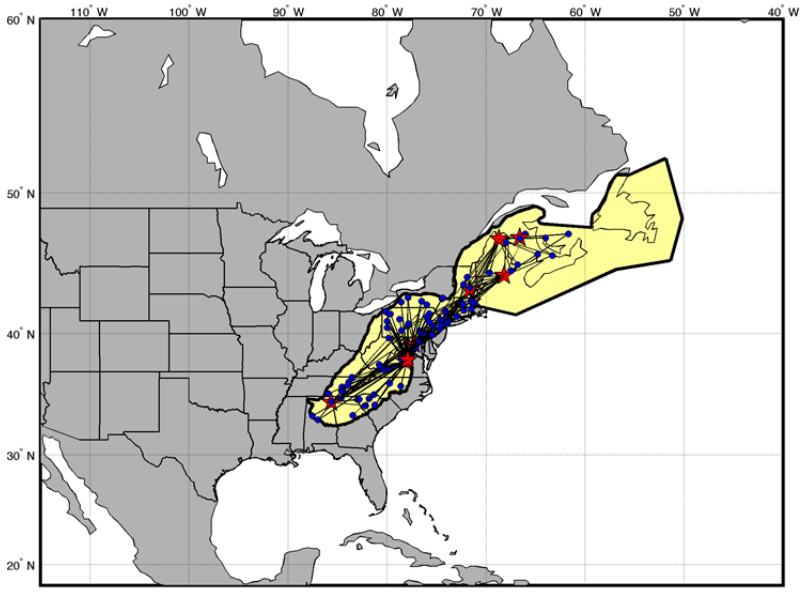

Figure C.4 Paths contained within region 3: Appalachian Province.

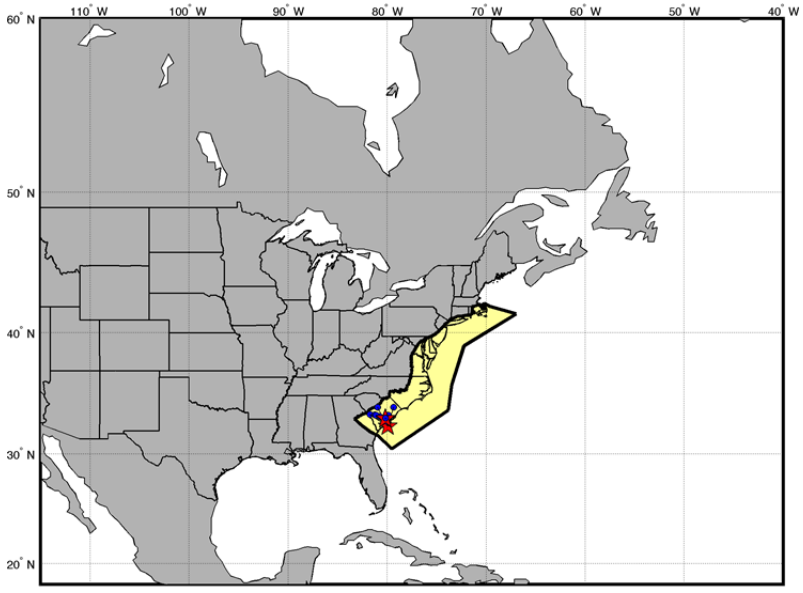

Figure C.5 Paths contained within region 4: Atlantic Coastal Plain.

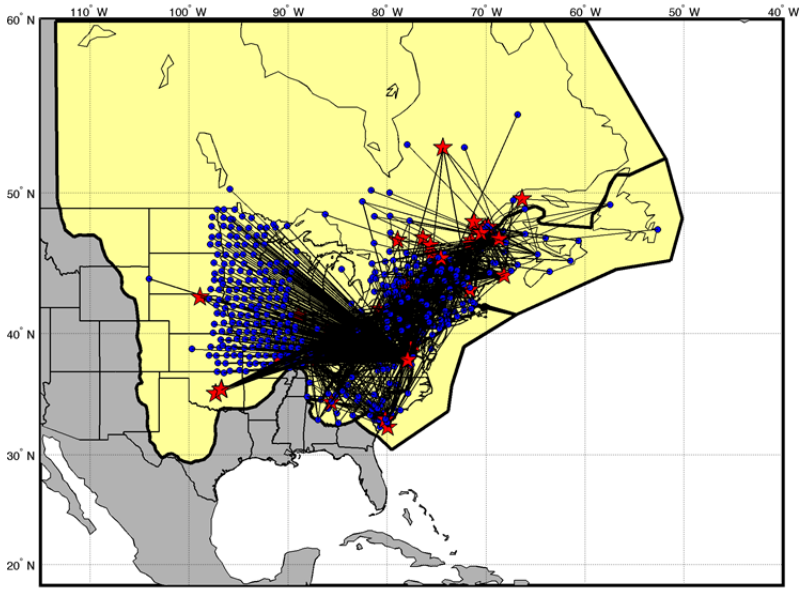

Figure C.6 **Path region 5: crossings between CENA regions (excluding the Mississippi Embayment/Gulf Coast region).**

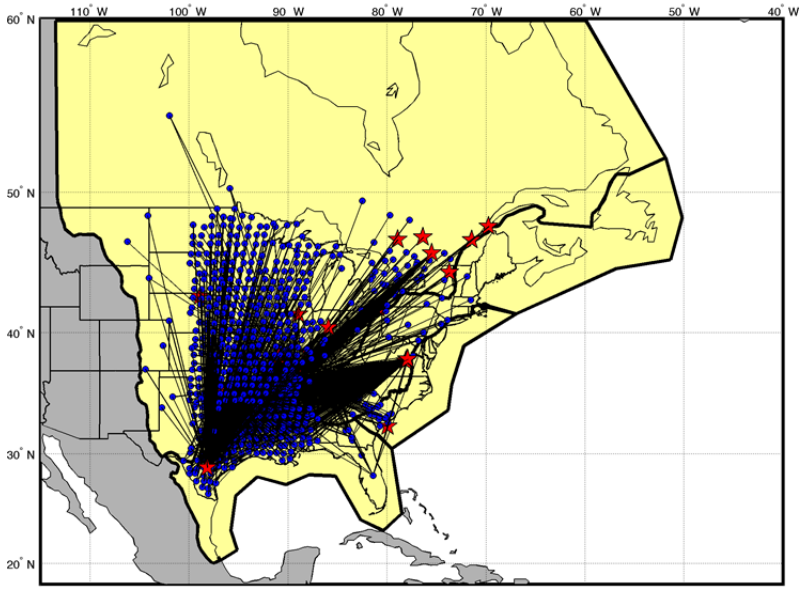

Figure C.7 **Paths region 6: paths crossings between CENA regions 2, 3 and/or 4 and the Mississippi Embayment/Gulf Coast region.**

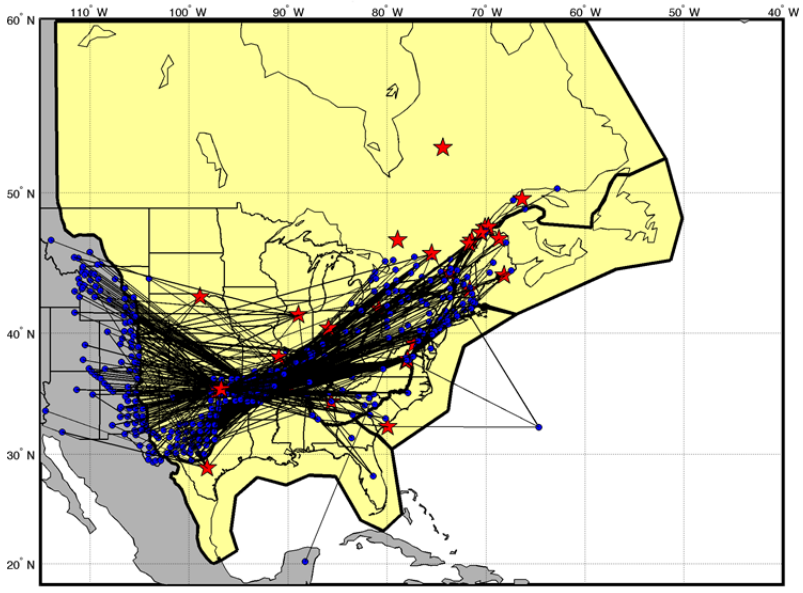

Figure C.8. Paths extending beyond the defined CENA regions (Path region = -999).

C.3 REFERENCES

Aki, K., Richards P.G. (1980). *Quantitative Seismology and Methods*, W.H. Freeman and Co., San Francisco, CA.

BSSC (2001). NEHRP Recommended Provisions for Seismic Regulations for New Buildings and Other Structures, Part 1: Provisions and Part 2: Commentary, Building Seismic Safety Council, Federal Emergency Management Agency, *FEMA-368 and FEMA-369*, Washington D.C.

Dreiling J., Isken M.P., Mooney W.D., Chapman M.C., Godbee R. W. (2014). NGA-East regionalization report: comparison of four crustal regions within Central and Eastern North America using waveform modeling and 5%-damped pseudo-spectral acceleration response, *PEER Report No. 2014/15*, Pacific Earthquake Engineering Research Center, University of California, Berkeley, CA.

PEER REPORTS

PEER reports are available as a free PDF download from http://peer.berkeley.edu/publications/peer_reports_complete.html. Printed hard copies of PEER reports can be ordered directly from our printer by following the instructions at http://peer.berkeley.edu/publications/peer_reports.html. For other related questions about the PEER Report Series, contact the Pacific Earthquake Engineering Research Center, 325 Davis Hall mail code 1792, Berkeley, CA 94720. Tel.: (510) 642-3437; Fax: (510) 665-1655; Email: peer_editor@berkeley.edu

PEER 2014/17 *PEER NGA-East Database.* Christine A. Goulet, Tadahiro Kishida, Timothy D. Ancheta, Chris H. Cramer, Robert B. Darragh, Walter J. Silva, Youssef M.A. Hashash, Joseph Harmon, Jonathan P. Stewart, Katie E. Wooddell, and Robert R. Youngs. October 2014.

PEER 2014/15 *NGA-East Regionalization Report: Comparison of Four Crustal Regions within Central and Eastern North America using Waveform Modeling and 5%-Damped Pseudo-Spectral Acceleration Response.* Jennifer Dreiling, Marius P. Isken, Walter D. Mooney, Martin C. Chapman, and Richard W. Godbee. October 2014.

PEER 2014/14 *Scaling Relations between Seismic Moment and Rupture Area of Earthquakes in Stable Continental Regions*. Paul Somerville. August 2014.

PEER 2014/13 *PEER Preliminary Notes and Observations on the August 24, 2014, South Napa Earthquake*. Grace S. Kang (Editor), Stephen A. Mahin (Editors). September 2014.

PEER 2014/12 *Reference-Rock Site Conditions for Central and Eastern North America: Part II – Attenuation (Kappa) Definition*. Kenneth W. Campbell, Youssef M.A. Hashash, Byungmin Kim, Albert R. Kottke, Ellen M. Rathje, Walter J. Silva, and Jonathan P. Stewart. August 2014.

PEER 2014/11 *Reference-Rock Site Conditions for Central and Eastern North America: Part I - Velocity Definition*. Youssef M.A. Hashash, Albert R. Kottke, Jonathan P. Stewart, Kenneth W. Campbell, Byungmin Kim, Ellen M. Rathje, Walter J. Silva, Sissy Nikolaou, and Cheryl Moss. August 2014.

PEER 2014/10 *Evaluation of Collapse and Non-Collapse of Parallel Bridges Affected by Liquefaction and Lateral Spreading*. Benjamin Turner, Scott J. Brandenberg, and Jonathan P. Stewart. August 2014.

PEER 2014/09 *PEER Arizona Strong-Motion Database and GMPEs Evaluation*. Tadahiro Kishida, Robert E. Kayen, Olga-Joan Ktenidou, Walter J. Silva, Robert B. Darragh, and Jennie Watson-Lamprey. June 2014.

PEER 2014/08 *Unbonded Pretensioned Bridge Columns with Rocking Detail*. Jeffrey A. Schaefer, Bryan Kennedy, Marc O. Eberhard, John F. Stanton. June 2014.

PEER 2014/07 *Northridge 20 Symposium Summary Report: Impacts, Outcomes, and Next Steps*. May 2014.

PEER 2014/06 *Report of the Tenth Planning Meeting of NEES/E-Defense Collaborative Research on Earthquake Engineering*. December 2013.

PEER 2014/05 *Seismic Velocity Site Characterization of Thirty-One Chilean Seismometer Stations by Spectral Analysis of Surface Wave Dispersion*. Robert Kayen, Brad D. Carkin, Skye Corbet, Camilo Pinilla, Allan Ng, Edward Gorbis, and Christine Truong. April 2014.

PEER 2014/04 *Effect of Vertical Acceleration on Shear Strength of Reinforced Concrete Columns.* Hyerin Lee and Khalid M. Mosalam. April 2014.

PEER 2014/03 *Retest of Thirty-Year-Old Neoprene Isolation Bearings.* James M. Kelly and Niel C. Van Engelen. March 2014.

PEER 2014/02 *Theoretical Development of Hybrid Simulation Applied to Plate Structures.* Ahmed A. Bakhaty, Khalid M. Mosalam, and Sanjay Govindjee. January 2014.

PEER 2014/01 *Performance-Based Seismic Assessment of Skewed Bridges.* Peyman Kaviani, Farzin Zareian, and Ertugrul Taciroglu. January 2014.

PEER 2013/26 *Urban Earthquake Engineering. Proceedings of the U.S.-Iran Seismic Workshop.* December 2013.

PEER 2013/25 *Earthquake Engineering for Resilient Communities: 2013 PEER Internship Program Research Report Collection.* Heidi Tremayne (Editor), Stephen A. Mahin (Editor), Jorge Archbold Monterossa, Matt Brosman, Shelly Dean, Katherine deLaveaga, Curtis Fong, Donovan Holder, Rakeeb Khan, Elizabeth Jachens, David Lam, Daniela Martinez Lopez, Mara Minner, Geffen Oren, Julia Pavicic, Melissa Quinonez, Lorena Rodriguez, Sean Salazar, Kelli Slaven, Vivian Steyert, Jenny Taing, and Salvador Tena. December 2013.

PEER 2013/24 *NGA-West2 Ground Motion Prediction Equations for Vertical Ground Motions.* September 2013.

PEER 2013/23 *Coordinated Planning and Preparedness for Fire Following Major Earthquakes.* Charles Scawthorn. November 2013.

PEER 2013/22 *GEM-PEER Task 3 Project: Selection of a Global Set of Ground Motion Prediction Equations.* Jonathan P. Stewart, John Douglas, Mohammad B. Javanbarg, Carola Di Alessandro, Yousef Bozorgnia, Norman A. Abrahamson, David M. Boore, Kenneth W. Campbell, Elise Delavaud, Mustafa Erdik and Peter J. Stafford. December 2013.

PEER 2013/21 *Seismic Design and Performance of Bridges with Columns on Rocking Foundations.* Grigorios Antonellis and Marios Panagiotou. September 2013.

PEER 2013/20 *Experimental and Analytical Studies on the Seismic Behavior of Conventional and Hybrid Braced Frames.* Jiun-Wei Lai and Stephen A. Mahin. September 2013.

PEER 2013/19 *Toward Resilient Communities: A Performance-Based Engineering Framework for Design and Evaluation of the Built Environment.* Michael William Mieler, Bozidar Stojadinovic, Robert J. Budnitz, Stephen A. Mahin and Mary C. Comerio. September 2013.

PEER 2013/18 *Identification of Site Parameters that Improve Predictions of Site Amplification.* Ellen M. Rathje and Sara Navidi. July 2013.

PEER 2013/17 *Response Spectrum Analysis of Concrete Gravity Dams Including Dam-Water-Foundation Interaction.* Arnkjell Løkke and Anil K. Chopra. July 2013.

PEER 2013/16 *Effect of hoop reinforcement spacing on the cyclic response of large reinforced concrete special moment frame beams.* Marios Panagiotou, Tea Visnjic, Grigorios Antonellis, Panagiotis Galanis, and Jack P. Moehle. June 2013.

PEER 2013/15 *A Probabilistic Framework to Include the Effects of Near-Fault Directivity in Seismic Hazard Assessment.* Shrey Kumar Shahi, Jack W. Baker. October 2013.

PEER 2013/14 *Hanging-Wall Scaling using Finite-Fault Simulations.* Jennifer L. Donahue and Norman A. Abrahamson. September 2013.

PEER 2013/13 *Semi-Empirical Nonlinear Site Amplification and its Application in NEHRP Site Factors.* Jonathan P. Stewart and Emel Seyhan. November 2013.

PEER 2013/12 *Nonlinear Horizontal Site Response for the NGA-West2 Project.* Ronnie Kamai, Norman A. Abramson, Walter J. Silva. May 2013.

PEER 2013/11 *Epistemic Uncertainty for NGA-West2 Models.* Linda Al Atik and Robert R. Youngs. May 2013.

PEER 2013/10 *NGA-West 2 Models for Ground-Motion Directionality.* Shrey K. Shahi and Jack W. Baker. May 2013.

PEER 2013/09 *Final Report of the NGA-West2 Directivity Working Group.* Paul Spudich, Jeffrey R. Bayless, Jack W. Baker, Brian S.J. Chiou, Badie Rowshandel, Shrey Shahi, and Paul Somerville. May 2013.

PEER 2013/08 *NGA-West2 Model for Estimating Average Horizontal Values of Pseudo-Absolute Spectral Accelerations Generated by Crustal Earthquakes.* I. M. Idriss. May 2013.

PEER 2013/07 *Update of the Chiou and Youngs NGA Ground Motion Model for Average Horizontal Component of Peak Ground Motion and Response Spectra.* Brian Chiou and Robert Youngs. May 2013.

PEER 2013/06 *NGA-West2 Campbell-Bozorgnia Ground Motion Model for the Horizontal Components of PGA, PGV, and 5%-Damped Elastic Pseudo-Acceleration Response Spectra for Periods Ranging from 0.01 to 10 sec.* Kenneth W. Campbell and Yousef Bozorgnia. May 2013.

PEER 2013/05 *NGA-West 2 Equations for Predicting Response Spectral Accelerations for Shallow Crustal Earthquakes.* David M. Boore, Jonathan P. Stewart, Emel Seyhan, Gail M. Atkinson. May 2013.

PEER 2013/04 *Update of the AS08 Ground-Motion Prediction Equations Based on the NGA-West2 Data Set.* Norman Abrahamson, Walter Silva, and Ronnie Kamai. May 2013.

PEER 2013/03 *PEER NGA-West2 Database.* Timothy D. Ancheta, Robert B. Darragh, Jonathan P. Stewart, Emel Seyhan, Walter J. Silva, Brian S.J. Chiou, Katie E. Wooddell, Robert W. Graves, Albert R. Kottke, David M. Boore, Tadahiro Kishida, and Jennifer L. Donahue. May 2013.

PEER 2013/02 *Hybrid Simulation of the Seismic Response of Squat Reinforced Concrete Shear Walls.* Catherine A. Whyte and Bozidar Stojadinovic. May 2013.

PEER 2013/01 *Housing Recovery in Chile: A Qualitative Mid-program Review.* Mary C. Comerio. February 2013.

PEER 2012/08 *Guidelines for Estimation of Shear Wave Velocity.* Bernard R. Wair, Jason T. DeJong, and Thomas Shantz. December 2012.

PEER 2012/07 *Earthquake Engineering for Resilient Communities: 2012 PEER Internship Program Research Report Collection.* Heidi Tremayne (Editor), Stephen A. Mahin (Editor), Collin Anderson, Dustin Cook, Michael Erceg, Carlos

Esparza, Jose Jimenez, Dorian Krausz, Andrew Lo, Stephanie Lopez, Nicole McCurdy, Paul Shipman, Alexander Strum, Eduardo Vega. December 2012.

PEER 2012/06 *Fragilities for Precarious Rocks at Yucca Mountain.* Matthew D. Purvance, Rasool Anooshehpoor, and James N. Brune. December 2012.

PEER 2012/05 *Development of Simplified Analysis Procedure for Piles in Laterally Spreading Layered Soils.* Christopher R. McGann, Pedro Arduino, and Peter Mackenzie–Helnwein. December 2012.

PEER 2012/04 *Unbonded Pre-Tensioned Columns for Bridges in Seismic Regions.* Phillip M. Davis, Todd M. Janes, Marc O. Eberhard, and John F. Stanton. December 2012.

PEER 2012/03 *Experimental and Analytical Studies on Reinforced Concrete Buildings with Seismically Vulnerable Beam-Column Joints.* Sangjoon Park and Khalid M. Mosalam. October 2012.

PEER 2012/02 *Seismic Performance of Reinforced Concrete Bridges Allowed to Uplift during Multi-Directional Excitation.* Andres Oscar Espinoza and Stephen A. Mahin. July 2012.

PEER 2012/01 *Spectral Damping Scaling Factors for Shallow Crustal Earthquakes in Active Tectonic Regions.* Sanaz Rezaeian, Yousef Bozorgnia, I. M. Idriss, Kenneth Campbell, Norman Abrahamson, and Walter Silva. July 2012.

PEER 2011/10 *Earthquake Engineering for Resilient Communities: 2011 PEER Internship Program Research Report Collection.* Eds. Heidi Faison and Stephen A. Mahin. December 2011.

PEER 2011/09 *Calibration of Semi-Stochastic Procedure for Simulating High-Frequency Ground Motions.* Jonathan P. Stewart, Emel Seyhan, and Robert W. Graves. December 2011.

PEER 2011/08 *Water Supply in regard to Fire Following Earthquake.* Charles Scawthorn. November 2011.

PEER 2011/07 *Seismic Risk Management in Urban Areas. Proceedings of a U.S.-Iran-Turkey Seismic Workshop.* September 2011.

PEER 2011/06 *The Use of Base Isolation Systems to Achieve Complex Seismic Performance Objectives.* Troy A. Morgan and Stephen A. Mahin. July 2011.

PEER 2011/05 *Case Studies of the Seismic Performance of Tall Buildings Designed by Alternative Means.* Task 12 Report for the Tall Buildings Initiative. Jack Moehle, Yousef Bozorgnia, Nirmal Jayaram, Pierson Jones, Mohsen Rahnama, Nilesh Shome, Zeynep Tuna, John Wallace, Tony Yang, and Farzin Zareian. July 2011.

PEER 2011/04 *Recommended Design Practice for Pile Foundations in Laterally Spreading Ground.* Scott A. Ashford, Ross W. Boulanger, and Scott J. Brandenberg. June 2011.

PEER 2011/03 *New Ground Motion Selection Procedures and Selected Motions for the PEER Transportation Research Program.* Jack W. Baker, Ting Lin, Shrey K. Shahi, and Nirmal Jayaram. March 2011.

PEER 2011/02 *A Bayesian Network Methodology for Infrastructure Seismic Risk Assessment and Decision Support.* Michelle T. Bensi, Armen Der Kiureghian, and Daniel Straub. March 2011.

PEER 2011/01 *Demand Fragility Surfaces for Bridges in Liquefied and Laterally Spreading Ground.* Scott J. Brandenberg, Jian Zhang, Pirooz Kashighandi, Yili Huo, and Minxing Zhao. March 2011.

PEER 2010/05 *Guidelines for Performance-Based Seismic Design of Tall Buildings.* Developed by the Tall Buildings Initiative. November 2010.

PEER 2010/04 *Application Guide for the Design of Flexible and Rigid Bus Connections between Substation Equipment Subjected to Earthquakes.* Jean-Bernard Dastous and Armen Der Kiureghian. September 2010.

PEER 2010/03 *Shear Wave Velocity as a Statistical Function of Standard Penetration Test Resistance and Vertical Effective Stress at Caltrans Bridge Sites.* Scott J. Brandenberg, Naresh Bellana, and Thomas Shantz. June 2010.

PEER 2010/02 *Stochastic Modeling and Simulation of Ground Motions for Performance-Based Earthquake Engineering.* Sanaz Rezaeian and Armen Der Kiureghian. June 2010.

PEER 2010/01 *Structural Response and Cost Characterization of Bridge Construction Using Seismic Performance Enhancement Strategies.* Ady Aviram, Božidar Stojadinović, Gustavo J. Parra-Montesinos, and Kevin R. Mackie. March 2010.

PEER 2009/03 *The Integration of Experimental and Simulation Data in the Study of Reinforced Concrete Bridge Systems Including Soil-Foundation-Structure Interaction.* Matthew Dryden and Gregory L. Fenves. November 2009.

PEER 2009/02 *Improving Earthquake Mitigation through Innovations and Applications in Seismic Science, Engineering, Communication, and Response. Proceedings of a U.S.-Iran Seismic Workshop.* October 2009.

PEER 2009/01 *Evaluation of Ground Motion Selection and Modification Methods: Predicting Median Interstory Drift Response of Buildings.* Curt B. Haselton, Ed. June 2009.

PEER 2008/10 *Technical Manual for Strata.* Albert R. Kottke and Ellen M. Rathje. February 2009.

PEER 2008/09 *NGA Model for Average Horizontal Component of Peak Ground Motion and Response Spectra.* Brian S.-J. Chiou and Robert R. Youngs. November 2008.

PEER 2008/08 *Toward Earthquake-Resistant Design of Concentrically Braced Steel Structures.* Patxi Uriz and Stephen A. Mahin. November 2008.

PEER 2008/07 *Using OpenSees for Performance-Based Evaluation of Bridges on Liquefiable Soils.* Stephen L. Kramer, Pedro Arduino, and HyungSuk Shin. November 2008.

PEER 2008/06 *Shaking Table Tests and Numerical Investigation of Self-Centering Reinforced Concrete Bridge Columns.* Hyung IL Jeong, Junichi Sakai, and Stephen A. Mahin. September 2008.

PEER 2008/05 *Performance-Based Earthquake Engineering Design Evaluation Procedure for Bridge Foundations Undergoing Liquefaction-Induced Lateral Ground Displacement.* Christian A. Ledezma and Jonathan D. Bray. August 2008.

PEER 2008/04 *Benchmarking of Nonlinear Geotechnical Ground Response Analysis Procedures.* Jonathan P. Stewart, Annie On-Lei Kwok, Yousseff M. A. Hashash, Neven Matasovic, Robert Pyke, Zhiliang Wang, and Zhaohui Yang. August 2008.

PEER 2008/03 *Guidelines for Nonlinear Analysis of Bridge Structures in California.* Ady Aviram, Kevin R. Mackie, and Božidar Stojadinović. August 2008.

PEER 2008/02 *Treatment of Uncertainties in Seismic-Risk Analysis of Transportation Systems.* Evangelos Stergiou and Anne S. Kiremidjian. July 2008.

PEER 2008/01 *Seismic Performance Objectives for Tall Buildings.* William T. Holmes, Charles Kircher, William Petak, and Nabih Youssef. August 2008.

PEER 2007/12 *An Assessment to Benchmark the Seismic Performance of a Code-Conforming Reinforced Concrete Moment-Frame Building.* Curt Haselton, Christine A. Goulet, Judith Mitrani-Reiser, James L. Beck, Gregory G. Deierlein, Keith A. Porter, Jonathan P. Stewart, and Ertugrul Taciroglu. August 2008.

PEER 2007/11 *Bar Buckling in Reinforced Concrete Bridge Columns.* Wayne A. Brown, Dawn E. Lehman, and John F. Stanton. February 2008.

PEER 2007/10 *Computational Modeling of Progressive Collapse in Reinforced Concrete Frame Structures.* Mohamed M. Talaat and Khalid M. Mosalam. May 2008.

PEER 2007/09 *Integrated Probabilistic Performance-Based Evaluation of Benchmark Reinforced Concrete Bridges.* Kevin R. Mackie, John-Michael Wong, and Božidar Stojadinović. January 2008.

PEER 2007/08 *Assessing Seismic Collapse Safety of Modern Reinforced Concrete Moment-Frame Buildings.* Curt B. Haselton and Gregory G. Deierlein. February 2008.

PEER 2007/07 *Performance Modeling Strategies for Modern Reinforced Concrete Bridge Columns.* Michael P. Berry and Marc O. Eberhard. April 2008.

PEER 2007/06 *Development of Improved Procedures for Seismic Design of Buried and Partially Buried Structures.* Linda Al Atik and Nicholas Sitar. June 2007.

PEER 2007/05 *Uncertainty and Correlation in Seismic Risk Assessment of Transportation Systems.* Renee G. Lee and Anne S. Kiremidjian. July 2007.

PEER 2007/04 *Numerical Models for Analysis and Performance-Based Design of Shallow Foundations Subjected to Seismic Loading.* Sivapalan Gajan, Tara C. Hutchinson, Bruce L. Kutter, Prishati Raychowdhury, José A. Ugalde, and Jonathan P. Stewart. May 2008.

PEER 2007/03 *Beam-Column Element Model Calibrated for Predicting Flexural Response Leading to Global Collapse of RC Frame Buildings.* Curt B. Haselton, Abbie B. Liel, Sarah Taylor Lange, and Gregory G. Deierlein. May 2008.

PEER 2007/02 *Campbell-Bozorgnia NGA Ground Motion Relations for the Geometric Mean Horizontal Component of Peak and Spectral Ground Motion Parameters.* Kenneth W. Campbell and Yousef Bozorgnia. May 2007.

PEER 2007/01 *Boore-Atkinson NGA Ground Motion Relations for the Geometric Mean Horizontal Component of Peak and Spectral Ground Motion Parameters.* David M. Boore and Gail M. Atkinson. May. May 2007.

PEER 2006/12 *Societal Implications of Performance-Based Earthquake Engineering.* Peter J. May. May 2007.

PEER 2006/11 *Probabilistic Seismic Demand Analysis Using Advanced Ground Motion Intensity Measures, Attenuation Relationships, and Near-Fault Effects.* Polsak Tothong and C. Allin Cornell. March 2007.

PEER 2006/10 *Application of the PEER PBEE Methodology to the I-880 Viaduct.* Sashi Kunnath. February 2007.

PEER 2006/09 *Quantifying Economic Losses from Travel Forgone Following a Large Metropolitan Earthquake.* James Moore, Sungbin Cho, Yue Yue Fan, and Stuart Werner. November 2006.

PEER 2006/08 *Vector-Valued Ground Motion Intensity Measures for Probabilistic Seismic Demand Analysis*. Jack W. Baker and C. Allin Cornell. October 2006.

PEER 2006/07 *Analytical Modeling of Reinforced Concrete Walls for Predicting Flexural and Coupled–Shear-Flexural Responses*. Kutay Orakcal, Leonardo M. Massone, and John W. Wallace. October 2006.

PEER 2006/06 *Nonlinear Analysis of a Soil-Drilled Pier System under Static and Dynamic Axial Loading.* Gang Wang and Nicholas Sitar. November 2006.

PEER 2006/05 *Advanced Seismic Assessment Guidelines.* Paolo Bazzurro, C. Allin Cornell, Charles Menun, Maziar Motahari, and Nicolas Luco. September 2006.

PEER 2006/04 *Probabilistic Seismic Evaluation of Reinforced Concrete Structural Components and Systems.* Tae Hyung Lee and Khalid M. Mosalam. August 2006.

PEER 2006/03 *Performance of Lifelines Subjected to Lateral Spreading*. Scott A. Ashford and Teerawut Juirnarongrit. July 2006.

PEER 2006/02 *Pacific Earthquake Engineering Research Center Highway Demonstration Project.* Anne Kiremidjian, James Moore, Yue Yue Fan, Nesrin Basoz, Ozgur Yazali, and Meredith Williams. April 2006.

PEER 2006/01 *Bracing Berkeley. A Guide to Seismic Safety on the UC Berkeley Campus.* Mary C. Comerio, Stephen Tobriner, and Ariane Fehrenkamp. January 2006.

PEER 2005/16 *Seismic Response and Reliability of Electrical Substation Equipment and Systems.* Junho Song, Armen Der Kiureghian, and Jerome L. Sackman. April 2006.

PEER 2005/15 *CPT-Based Probabilistic Assessment of Seismic Soil Liquefaction Initiation.* R. E. S. Moss, R. B. Seed, R. E. Kayen, J. P. Stewart, and A. Der Kiureghian. April 2006.

PEER 2005/14 *Workshop on Modeling of Nonlinear Cyclic Load-Deformation Behavior of Shallow Foundations.* Bruce L. Kutter, Geoffrey Martin, Tara Hutchinson, Chad Harden, Sivapalan Gajan, and Justin Phalen. March 2006.

PEER 2005/13 *Stochastic Characterization and Decision Bases under Time-Dependent Aftershock Risk in Performance-Based Earthquake Engineering.* Gee Liek Yeo and C. Allin Cornell. July 2005.

PEER 2005/12 *PEER Testbed Study on a Laboratory Building: Exercising Seismic Performance Assessment*. Mary C. Comerio, editor. November 2005.

PEER 2005/11 *Van Nuys Hotel Building Testbed Report: Exercising Seismic Performance Assessment.* Helmut Krawinkler, editor. October 2005.

PEER 2005/10 *First NEES/E-Defense Workshop on Collapse Simulation of Reinforced Concrete Building Structures.* September 2005.

PEER 2005/09 *Test Applications of Advanced Seismic Assessment Guidelines.* Joe Maffei, Karl Telleen, Danya Mohr, William Holmes, and Yuki Nakayama. August 2006.

PEER 2005/08 *Damage Accumulation in Lightly Confined Reinforced Concrete Bridge Columns.* R. Tyler Ranf, Jared M. Nelson, Zach Price, Marc O. Eberhard, and John F. Stanton. April 2006.

PEER 2005/07 *Experimental and Analytical Studies on the Seismic Response of Freestanding and Anchored Laboratory Equipment.* Dimitrios Konstantinidis and Nicos Makris. January 2005.

PEER 2005/06 *Global Collapse of Frame Structures under Seismic Excitations*. Luis F. Ibarra and Helmut Krawinkler. September 2005.

PEER 2005//05 *Performance Characterization of Bench- and Shelf-Mounted Equipment.* Samit Ray Chaudhuri and Tara C. Hutchinson. May 2006.

PEER 2005/04 *Numerical Modeling of the Nonlinear Cyclic Response of Shallow Foundations.* Chad Harden, Tara Hutchinson, Geoffrey R. Martin, and Bruce L. Kutter. August 2005.

PEER 2005/03 *A Taxonomy of Building Components for Performance-Based Earthquake Engineering.* Keith A. Porter. September 2005.

PEER 2005/02 *Fragility Basis for California Highway Overpass Bridge Seismic Decision Making*. Kevin R. Mackie and Božidar Stojadinović. June 2005.

PEER 2005/01 *Empirical Characterization of Site Conditions on Strong Ground Motion.* Jonathan P. Stewart, Yoojoong Choi, and Robert W. Graves. June 2005.

PEER 2004/09 *Electrical Substation Equipment Interaction: Experimental Rigid Conductor Studies.* Christopher Stearns and André Filiatrault. February 2005.

PEER 2004/08 *Seismic Qualification and Fragility Testing of Line Break 550-kV Disconnect Switches.* Shakhzod M. Takhirov, Gregory L. Fenves, and Eric Fujisaki. January 2005.

PEER 2004/07 *Ground Motions for Earthquake Simulator Qualification of Electrical Substation Equipment.* Shakhzod M. Takhirov, Gregory L. Fenves, Eric Fujisaki, and Don Clyde. January 2005.

PEER 2004/06 *Performance-Based Regulation and Regulatory Regimes.* Peter J. May and Chris Koski. September 2004.

PEER 2004/05 *Performance-Based Seismic Design Concepts and Implementation: Proceedings of an International Workshop.* Peter Fajfar and Helmut Krawinkler, editors. September 2004.

PEER 2004/04 *Seismic Performance of an Instrumented Tilt-up Wall Building.* James C. Anderson and Vitelmo V. Bertero. July 2004.

PEER 2004/03 *Evaluation and Application of Concrete Tilt-up Assessment Methodologies.* Timothy Graf and James O. Malley. October 2004.

PEER 2004/02 *Analytical Investigations of New Methods for Reducing Residual Displacements of Reinforced Concrete Bridge Columns.* Junichi Sakai and Stephen A. Mahin. August 2004.

PEER 2004/01 *Seismic Performance of Masonry Buildings and Design Implications.* Kerri Anne Taeko Tokoro, James C. Anderson, and Vitelmo V. Bertero. February 2004.

PEER 2003/18 *Performance Models for Flexural Damage in Reinforced Concrete Columns.* Michael Berry and Marc Eberhard. August 2003.

PEER 2003/17 *Predicting Earthquake Damage in Older Reinforced Concrete Beam-Column Joints.* Catherine Pagni and Laura Lowes. October 2004.

PEER 2003/16 *Seismic Demands for Performance-Based Design of Bridges.* Kevin Mackie and Božidar Stojadinović. August 2003.

PEER 2003/15 *Seismic Demands for Nondeteriorating Frame Structures and Their Dependence on Ground Motions.* Ricardo Antonio Medina and Helmut Krawinkler. May 2004.

PEER 2003/14 *Finite Element Reliability and Sensitivity Methods for Performance-Based Earthquake Engineering.* Terje Haukaas and Armen Der Kiureghian. April 2004.

PEER 2003/13 *Effects of Connection Hysteretic Degradation on the Seismic Behavior of Steel Moment-Resisting Frames.* Janise E. Rodgers and Stephen A. Mahin. March 2004.

PEER 2003/12 *Implementation Manual for the Seismic Protection of Laboratory Contents: Format and Case Studies.* William T. Holmes and Mary C. Comerio. October 2003.

PEER 2003/11 *Fifth U.S.-Japan Workshop on Performance-Based Earthquake Engineering Methodology for Reinforced Concrete Building Structures.* February 2004.

PEER 2003/10 *A Beam-Column Joint Model for Simulating the Earthquake Response of Reinforced Concrete Frames.* Laura N. Lowes, Nilanjan Mitra, and Arash Altoontash. February 2004.

PEER 2003/09 *Sequencing Repairs after an Earthquake: An Economic Approach.* Marco Casari and Simon J. Wilkie. April 2004.

PEER 2003/08 *A Technical Framework for Probability-Based Demand and Capacity Factor Design (DCFD) Seismic Formats*. Fatemeh Jalayer and C. Allin Cornell. November 2003.

PEER 2003/07 *Uncertainty Specification and Propagation for Loss Estimation Using FOSM Methods.* Jack W. Baker and C. Allin Cornell. September 2003.

PEER 2003/06 *Performance of Circular Reinforced Concrete Bridge Columns under Bidirectional Earthquake Loading*. Mahmoud M. Hachem, Stephen A. Mahin, and Jack P. Moehle. February 2003.

PEER 2003/05 *Response Assessment for Building-Specific Loss Estimation.* Eduardo Miranda and Shahram Taghavi. September 2003.

PEER 2003/04 *Experimental Assessment of Columns with Short Lap Splices Subjected to Cyclic Loads*. Murat Melek, John W. Wallace, and Joel Conte. April 2003.

PEER 2003/03 *Probabilistic Response Assessment for Building-Specific Loss Estimation.* Eduardo Miranda and Hesameddin Aslani. September 2003.

PEER 2003/02 *Software Framework for Collaborative Development of Nonlinear Dynamic Analysis Program.* Jun Peng and Kincho H. Law. September 2003.

PEER 2003/01 *Shake Table Tests and Analytical Studies on the Gravity Load Collapse of Reinforced Concrete Frames.* Kenneth John Elwood and Jack P. Moehle. November 2003.

PEER 2002/24 *Performance of Beam to Column Bridge Joints Subjected to a Large Velocity Pulse.* Natalie Gibson, André Filiatrault, and Scott A. Ashford. April 2002.

PEER 2002/23 *Effects of Large Velocity Pulses on Reinforced Concrete Bridge Columns.* Greg L. Orozco and Scott A. Ashford. April 2002.

PEER 2002/22 *Characterization of Large Velocity Pulses for Laboratory Testing.* Kenneth E. Cox and Scott A. Ashford. April 2002.

PEER 2002/21 *Fourth U.S.-Japan Workshop on Performance-Based Earthquake Engineering Methodology for Reinforced Concrete Building Structures*. December 2002.

PEER 2002/20 *Barriers to Adoption and Implementation of PBEE Innovations.* Peter J. May. August 2002.

PEER 2002/19 *Economic-Engineered Integrated Models for Earthquakes: Socioeconomic Impacts.* Peter Gordon, James E. Moore II, and Harry W. Richardson. July 2002.

PEER 2002/18 *Assessment of Reinforced Concrete Building Exterior Joints with Substandard Details*. Chris P. Pantelides, Jon Hansen, Justin Nadauld, and Lawrence D. Reaveley. May 2002.

PEER 2002/17 *Structural Characterization and Seismic Response Analysis of a Highway Overcrossing Equipped with Elastomeric Bearings and Fluid Dampers: A Case Study*. Nicos Makris and Jian Zhang. November 2002.

PEER 2002/16 *Estimation of Uncertainty in Geotechnical Properties for Performance-Based Earthquake Engineering*. Allen L. Jones, Steven L. Kramer, and Pedro Arduino. December 2002.

PEER 2002/15 *Seismic Behavior of Bridge Columns Subjected to Various Loading Patterns.* Asadollah Esmaeily-Gh. and Yan Xiao. December 2002.

PEER 2002/14 *Inelastic Seismic Response of Extended Pile Shaft Supported Bridge Structures.* T.C. Hutchinson, R.W. Boulanger, Y.H. Chai, and I.M. Idriss. December 2002.

PEER 2002/13 *Probabilistic Models and Fragility Estimates for Bridge Components and Systems.* Paolo Gardoni, Armen Der Kiureghian, and Khalid M. Mosalam. June 2002.

PEER 2002/12 *Effects of Fault Dip and Slip Rake on Near-Source Ground Motions: Why Chi-Chi Was a Relatively Mild M7.6 Earthquake.* Brad T. Aagaard, John F. Hall, and Thomas H. Heaton. December 2002.

PEER 2002/11 *Analytical and Experimental Study of Fiber-Reinforced Strip Isolators*. James M. Kelly and Shakhzod M. Takhirov. September 2002.

PEER 2002/10 *Centrifuge Modeling of Settlement and Lateral Spreading with Comparisons to Numerical Analyses***.** Sivapalan Gajan and Bruce L. Kutter. January 2003.

PEER 2002/09 *Documentation and Analysis of Field Case Histories of Seismic Compression during the 1994 Northridge, California, Earthquake.* Jonathan P. Stewart, Patrick M. Smith, Daniel H. Whang, and Jonathan D. Bray. October 2002.

PEER 2002/08 *Component Testing, Stability Analysis and Characterization of Buckling-Restrained Unbonded Braces™*. Cameron Black, Nicos Makris, and Ian Aiken. September 2002.

PEER 2002/07 *Seismic Performance of Pile-Wharf Connections*. Charles W. Roeder, Robert Graff, Jennifer Soderstrom, and Jun Han Yoo. December 2001.

PEER 2002/06 *The Use of Benefit-Cost Analysis for Evaluation of Performance-Based Earthquake Engineering Decisions*. Richard O. Zerbe and Anthony Falit-Baiamonte. September 2001.

PEER 2002/05 *Guidelines, Specifications, and Seismic Performance Characterization of Nonstructural Building Components and Equipment*. André Filiatrault, Constantin Christopoulos, and Christopher Stearns. September 2001.

PEER 2002/04 *Consortium of Organizations for Strong-Motion Observation Systems and the Pacific Earthquake Engineering Research Center Lifelines Program: Invited Workshop on Archiving and Web Dissemination of Geotechnical Data, 4–5 October 2001*. September 2002.

PEER 2002/03 *Investigation of Sensitivity of Building Loss Estimates to Major Uncertain Variables for the Van Nuys Testbed.* Keith A. Porter, James L. Beck, and Rustem V. Shaikhutdinov. August 2002.

PEER 2002/02 *The Third U.S.-Japan Workshop on Performance-Based Earthquake Engineering Methodology for Reinforced Concrete Building Structures*. July 2002.

PEER 2002/01 *Nonstructural Loss Estimation: The UC Berkeley Case Study*. Mary C. Comerio and John C. Stallmeyer. December 2001.

PEER 2001/16 *Statistics of SDF-System Estimate of Roof Displacement for Pushover Analysis of Buildings.* Anil K. Chopra, Rakesh K. Goel, and Chatpan Chintanapakdee. December 2001.

PEER 2001/15 *Damage to Bridges during the 2001 Nisqually Earthquake.* R. Tyler Ranf, Marc O. Eberhard, and Michael P. Berry. November 2001.

PEER 2001/14 *Rocking Response of Equipment Anchored to a Base Foundation.* Nicos Makris and Cameron J. Black. September 2001.

PEER 2001/13 *Modeling Soil Liquefaction Hazards for Performance-Based Earthquake Engineering.* Steven L. Kramer and Ahmed-W. Elgamal. February 2001.

PEER 2001/12 *Development of Geotechnical Capabilities in OpenSees.* Boris Jeremić. September 2001.

PEER 2001/11 *Analytical and Experimental Study of Fiber-Reinforced Elastomeric Isolators*. James M. Kelly and Shakhzod M. Takhirov. September 2001.

PEER 2001/10 *Amplification Factors for Spectral Acceleration in Active Regions.* Jonathan P. Stewart, Andrew H. Liu, Yoojoong Choi, and Mehmet B. Baturay. December 2001.

PEER 2001/09 *Ground Motion Evaluation Procedures for Performance-Based Design.* Jonathan P. Stewart, Shyh-Jeng Chiou, Jonathan D. Bray, Robert W. Graves, Paul G. Somerville, and Norman A. Abrahamson. September 2001.

PEER 2001/08 *Experimental and Computational Evaluation of Reinforced Concrete Bridge Beam-Column Connections for Seismic Performance*. Clay J. Naito, Jack P. Moehle, and Khalid M. Mosalam. November 2001.

PEER 2001/07 *The Rocking Spectrum and the Shortcomings of Design Guidelines.* Nicos Makris and Dimitrios Konstantinidis. August 2001.

PEER 2001/06 *Development of an Electrical Substation Equipment Performance Database for Evaluation of Equipment Fragilities*. Thalia Agnanos. April 1999.

PEER 2001/05 *Stiffness Analysis of Fiber-Reinforced Elastomeric Isolators.* Hsiang-Chuan Tsai and James M. Kelly. May 2001.

PEER 2001/04 *Organizational and Societal Considerations for Performance-Based Earthquake Engineering.* Peter J. May. April 2001.

PEER 2001/03 *A Modal Pushover Analysis Procedure to Estimate Seismic Demands for Buildings: Theory and Preliminary Evaluation.* Anil K. Chopra and Rakesh K. Goel. January 2001.

PEER 2001/02 *Seismic Response Analysis of Highway Overcrossings Including Soil-Structure Interaction.* Jian Zhang and Nicos Makris. March 2001.

PEER 2001/01 *Experimental Study of Large Seismic Steel Beam-to-Column Connections.* Egor P. Popov and Shakhzod M. Takhirov. November 2000.

PEER 2000/10 *The Second U.S.-Japan Workshop on Performance-Based Earthquake Engineering Methodology for Reinforced Concrete Building Structures.* March 2000.

PEER 2000/09 *Structural Engineering Reconnaissance of the August 17, 1999 Earthquake: Kocaeli (Izmit), Turkey*. Halil Sezen, Kenneth J. Elwood, Andrew S. Whittaker, Khalid Mosalam, John J. Wallace, and John F. Stanton. December 2000.

PEER 2000/08 *Behavior of Reinforced Concrete Bridge Columns Having Varying Aspect Ratios and Varying Lengths of Confinement.* Anthony J. Calderone, Dawn E. Lehman, and Jack P. Moehle. January 2001.

PEER 2000/07 *Cover-Plate and Flange-Plate Reinforced Steel Moment-Resisting Connections.* Taejin Kim, Andrew S. Whittaker, Amir S. Gilani, Vitelmo V. Bertero, and Shakhzod M. Takhirov. September 2000.

PEER 2000/06 *Seismic Evaluation and Analysis of 230-kV Disconnect Switches.* Amir S. J. Gilani, Andrew S. Whittaker, Gregory L. Fenves, Chun-Hao Chen, Henry Ho, and Eric Fujisaki. July 2000.

PEER 2000/05 *Performance-Based Evaluation of Exterior Reinforced Concrete Building Joints for Seismic Excitation.* Chandra Clyde, Chris P. Pantelides, and Lawrence D. Reaveley. July 2000.

PEER 2000/04 *An Evaluation of Seismic Energy Demand: An Attenuation Approach.* Chung-Che Chou and Chia-Ming Uang. July 1999.

PEER 2000/03 *Framing Earthquake Retrofitting Decisions: The Case of Hillside Homes in Los Angeles*. Detlof von Winterfeldt, Nels Roselund, and Alicia Kitsuse. March 2000.

PEER 2000/02 *U.S.-Japan Workshop on the Effects of Near-Field Earthquake Shaking.* Andrew Whittaker, ed. July 2000.

PEER 2000/01 *Further Studies on Seismic Interaction in Interconnected Electrical Substation Equipment.* Armen Der Kiureghian, Kee-Jeung Hong, and Jerome L. Sackman. November 1999.

PEER 1999/14 *Seismic Evaluation and Retrofit of 230-kV Porcelain Transformer Bushings*. Amir S. Gilani, Andrew S. Whittaker, Gregory L. Fenves, and Eric Fujisaki. December 1999.

PEER 1999/13 *Building Vulnerability Studies: Modeling and Evaluation of Tilt-up and Steel Reinforced Concrete Buildings.* John W. Wallace, Jonathan P. Stewart, and Andrew S. Whittaker, editors. December 1999.

PEER 1999/12 *Rehabilitation of Nonductile RC Frame Building Using Encasement Plates and Energy-Dissipating Devices.* Mehrdad Sasani, Vitelmo V. Bertero, James C. Anderson. December 1999.

PEER 1999/11 *Performance Evaluation Database for Concrete Bridge Components and Systems under Simulated Seismic Loads.* Yael D. Hose and Frieder Seible. November 1999.

PEER 1999/10 *U.S.-Japan Workshop on Performance-Based Earthquake Engineering Methodology for Reinforced Concrete Building Structures.* December 1999.

PEER 1999/09 *Performance Improvement of Long Period Building Structures Subjected to Severe Pulse-Type Ground Motions.* James C. Anderson, Vitelmo V. Bertero, and Raul Bertero. October 1999.

PEER 1999/08 *Envelopes for Seismic Response Vectors.* Charles Menun and Armen Der Kiureghian. July 1999.

PEER 1999/07 *Documentation of Strengths and Weaknesses of Current Computer Analysis Methods for Seismic Performance of Reinforced Concrete Members.* William F. Cofer. November 1999.

PEER 1999/06 *Rocking Response and Overturning of Anchored Equipment under Seismic Excitations.* Nicos Makris and Jian Zhang. November 1999.

PEER 1999/05 *Seismic Evaluation of 550 kV Porcelain Transformer Bushings.* Amir S. Gilani, Andrew S. Whittaker, Gregory L. Fenves, and Eric Fujisaki. October 1999.

PEER 1999/04 *Adoption and Enforcement of Earthquake Risk-Reduction Measures.* Peter J. May, Raymond J. Burby, T. Jens Feeley, and Robert Wood.

PEER 1999/03 *Task 3 Characterization of Site Response General Site Categories.* Adrian Rodriguez-Marek, Jonathan D. Bray, and Norman Abrahamson. February 1999.

PEER 1999/02 *Capacity-Demand-Diagram Methods for Estimating Seismic Deformation of Inelastic Structures: SDF Systems.* Anil K. Chopra and Rakesh Goel. April 1999.

PEER 1999/01 *Interaction in Interconnected Electrical Substation Equipment Subjected to Earthquake Ground Motions.* Armen Der Kiureghian, Jerome L. Sackman, and Kee-Jeung Hong. February 1999.

PEER 1998/08 *Behavior and Failure Analysis of a Multiple-Frame Highway Bridge in the 1994 Northridge Earthquake.* Gregory L. Fenves and Michael Ellery. December 1998.

PEER 1998/07 *Empirical Evaluation of Inertial Soil-Structure Interaction Effects.* Jonathan P. Stewart, Raymond B. Seed, and Gregory L. Fenves. November 1998.

PEER 1998/06 *Effect of Damping Mechanisms on the Response of Seismic Isolated Structures.* Nicos Makris and Shih-Po Chang. November 1998.

PEER 1998/05 *Rocking Response and Overturning of Equipment under Horizontal Pulse-Type Motions.* Nicos Makris and Yiannis Roussos. October 1998.

PEER 1998/04 *Pacific Earthquake Engineering Research Invitational Workshop Proceedings, May 14–15, 1998: Defining the Links between Planning, Policy Analysis, Economics and Earthquake Engineering.* Mary Comerio and Peter Gordon. September 1998.

PEER 1998/03 *Repair/Upgrade Procedures for Welded Beam to Column Connections.* James C. Anderson and Xiaojing Duan. May 1998.

PEER 1998/02 *Seismic Evaluation of 196 kV Porcelain Transformer Bushings.* Amir S. Gilani, Juan W. Chavez, Gregory L. Fenves, and Andrew S. Whittaker. May 1998.

PEER 1998/01 *Seismic Performance of Well-Confined Concrete Bridge Columns.* Dawn E. Lehman and Jack P. Moehle. December 2000.

ONLINE PEER REPORTS

The following PEER reports are available by Internet only at http://peer.berkeley.edu/publications/peer_reports_complete.html.

PEER 2012/103 *Performance-Based Seismic Demand Assessment of Concentrically Braced Steel Frame Buildings.* Chui-Hsin Chen and Stephen A. Mahin. December 2012.

PEER 2012/102 *Procedure to Restart an Interrupted Hybrid Simulation: Addendum to PEER Report 2010/103.* Vesna Terzic and Bozidar Stojadinovic. October 2012.

PEER 2012/101 *Mechanics of Fiber Reinforced Bearings.* James M. Kelly and Andrea Calabrese. February 2012.

PEER 2011/107 *Nonlinear Site Response and Seismic Compression at Vertical Array Strongly Shaken by 2007 Niigata-ken Chuetsu-oki Earthquake.* Eric Yee, Jonathan P. Stewart, and Kohji Tokimatsu. December 2011.

PEER 2011/106 *Self Compacting Hybrid Fiber Reinforced Concrete Composites for Bridge Columns.* Pardeep Kumar, Gabriel Jen, William Trono, Marios Panagiotou, and Claudia Ostertag. September 2011.

PEER 2011/105 *Stochastic Dynamic Analysis of Bridges Subjected to Spacially Varying Ground Motions.* Katerina Konakli and Armen Der Kiureghian. August 2011.

PEER 2011/104 *Design and Instrumentation of the 2010 E-Defense Four-Story Reinforced Concrete and Post-Tensioned Concrete Buildings.* Takuya Nagae, Kenichi Tahara, Taizo Matsumori, Hitoshi Shiohara, Toshimi Kabeyasawa, Susumu Kono, Minehiro Nishiyama (Japanese Research Team) and John Wallace, Wassim Ghannoum, Jack Moehle, Richard Sause, Wesley Keller, Zeynep Tuna (U.S. Research Team). June 2011.

PEER 2011/103 *In-Situ Monitoring of the Force Output of Fluid Dampers: Experimental Investigation.* Dimitrios Konstantinidis, James M. Kelly, and Nicos Makris. April 2011.

PEER 2011/102 *Ground-motion prediction equations 1964 - 2010.* John Douglas. April 2011.

PEER 2011/101 *Report of the Eighth Planning Meeting of NEES/E-Defense Collaborative Research on Earthquake Engineering.* Convened by the Hyogo Earthquake Engineering Research Center (NIED), NEES Consortium, Inc. February 2011.

PEER 2010/111 *Modeling and Acceptance Criteria for Seismic Design and Analysis of Tall Buildings.* Task 7 Report for the Tall Buildings Initiative - Published jointly by the Applied Technology Council. October 2010.

PEER 2010/110 *Seismic Performance Assessment and Probabilistic Repair Cost Analysis of Precast Concrete Cladding Systems for Multistory Buildlings.* Jeffrey P. Hunt and Božidar Stojadinovic. November 2010.

PEER 2010/109 *Report of the Seventh Joint Planning Meeting of NEES/E-Defense Collaboration on Earthquake Engineering. Held at the E-Defense, Miki, and Shin-Kobe, Japan, September 18–19, 2009.* August 2010.

PEER 2010/108 *Probabilistic Tsunami Hazard in California.* Hong Kie Thio, Paul Somerville, and Jascha Polet, preparers. October 2010.

PEER 2010/107 *Performance and Reliability of Exposed Column Base Plate Connections for Steel Moment-Resisting Frames.* Ady Aviram, Božidar Stojadinovic, and Armen Der Kiureghian. August 2010.

PEER 2010/106 *Verification of Probabilistic Seismic Hazard Analysis Computer Programs.* Patricia Thomas, Ivan Wong, and Norman Abrahamson. May 2010.

PEER 2010/105 *Structural Engineering Reconnaissance of the April 6, 2009, Abruzzo, Italy, Earthquake, and Lessons Learned.* M. Selim Günay and Khalid M. Mosalam. April 2010.

PEER 2010/104 *Simulating the Inelastic Seismic Behavior of Steel Braced Frames, Including the Effects of Low-Cycle Fatigue.* Yuli Huang and Stephen A. Mahin. April 2010.

PEER 2010/103 *Post-Earthquake Traffic Capacity of Modern Bridges in California.* Vesna Terzic and Božidar Stojadinović. March 2010.

PEER 2010/102 *Analysis of Cumulative Absolute Velocity (CAV) and JMA Instrumental Seismic Intensity (I_{JMA}) Using the PEER–NGA Strong Motion Database.* Kenneth W. Campbell and Yousef Bozorgnia. February 2010.

PEER 2010/101 *Rocking Response of Bridges on Shallow Foundations.* Jose A. Ugalde, Bruce L. Kutter, and Boris Jeremic. April 2010.

PEER 2009/109 *Simulation and Performance-Based Earthquake Engineering Assessment of Self-Centering Post-Tensioned Concrete Bridge Systems.* Won K. Lee and Sarah L. Billington. December 2009.

PEER 2009/108 *PEER Lifelines Geotechnical Virtual Data Center.* J. Carl Stepp, Daniel J. Ponti, Loren L. Turner, Jennifer N. Swift, Sean Devlin, Yang Zhu, Jean Benoit, and John Bobbitt. September 2009.

PEER 2009/107 *Experimental and Computational Evaluation of Current and Innovative In-Span Hinge Details in Reinforced Concrete Box-Girder Bridges: Part 2: Post-Test Analysis and Design Recommendations.* Matias A. Hube and Khalid M. Mosalam. December 2009.

PEER 2009/106 *Shear Strength Models of Exterior Beam-Column Joints without Transverse Reinforcement.* Sangjoon Park and Khalid M. Mosalam. November 2009.

PEER 2009/105 *Reduced Uncertainty of Ground Motion Prediction Equations through Bayesian Variance Analysis.* Robb Eric S. Moss. November 2009.

PEER 2009/104 *Advanced Implementation of Hybrid Simulation.* Andreas H. Schellenberg, Stephen A. Mahin, Gregory L. Fenves. November 2009.

PEER 2009/103 *Performance Evaluation of Innovative Steel Braced Frames.* T. Y. Yang, Jack P. Moehle, and Božidar Stojadinovic. August 2009.

PEER 2009/102 *Reinvestigation of Liquefaction and Nonliquefaction Case Histories from the 1976 Tangshan Earthquake.* Robb Eric Moss, Robert E. Kayen, Liyuan Tong, Songyu Liu, Guojun Cai, and Jiaer Wu. August 2009.

PEER 2009/101 *Report of the First Joint Planning Meeting for the Second Phase of NEES/E-Defense Collaborative Research on Earthquake Engineering.* Stephen A. Mahin et al. July 2009.

PEER 2008/104 *Experimental and Analytical Study of the Seismic Performance of Retaining Structures.* Linda Al Atik and Nicholas Sitar. January 2009.

PEER 2008/103 *Experimental and Computational Evaluation of Current and Innovative In-Span Hinge Details in Reinforced Concrete Box-Girder Bridges. Part 1: Experimental Findings and Pre-Test Analysis.* Matias A. Hube and Khalid M. Mosalam. January 2009.

PEER 2008/102 *Modeling of Unreinforced Masonry Infill Walls Considering In-Plane and Out-of-Plane Interaction.* Stephen Kadysiewski and Khalid M. Mosalam. January 2009.

PEER 2008/101 *Seismic Performance Objectives for Tall Buildings.* William T. Holmes, Charles Kircher, William Petak, and Nabih Youssef. August 2008.

PEER 2007/101 *Generalized Hybrid Simulation Framework for Structural Systems Subjected to Seismic Loading.* Tarek Elkhoraibi and Khalid M. Mosalam. July 2007.

PEER 2007/100 *Seismic Evaluation of Reinforced Concrete Buildings Including Effects of Masonry Infill Walls.* Alidad Hashemi and Khalid M. Mosalam. July 2007.

The Pacific Earthquake Engineering Research Center (PEER) is a multi-institutional research and education center with headquarters at the University of California, Berkeley. Investigators from over 20 universities, several consulting companies, and researchers at various state and federal government agencies contribute to research programs focused on performance-based earthquake engineering.

These research programs aim to identify and reduce the risks from major earthquakes to life safety and to the economy by including research in a wide variety of disciplines including structural and geotechnical engineering, geology/seismology, lifelines, transportation, architecture, economics, risk management, and public policy.

PEER is supported by federal, state, local, and regional agencies, together with industry partners.

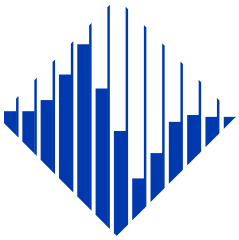

PEER Core Institutions:
University of California, Berkeley (Lead Institution)
California Institute of Technology
Oregon State University
Stanford University
University of California, Davis
University of California, Irvine
University of California, Los Angeles
University of California, San Diego
University of Southern California
University of Washington

PEER reports can be ordered at http://peer.berkeley.edu/publications/peer_reports.html or by contacting

Pacific Earthquake Engineering Research Center
University of California, Berkeley
325 Davis Hall, mail code 1792
Berkeley, CA 94720-1792
Tel: 510-642-3437
Fax: 510-642-1655
Email: peer_editor@berkeley.edu

ISSN 1547-0587X